INSTITUTO POTOSINO DE INVESTIGACIÓN CIENTÍFICA Y TECNOLÓGICA, A.C.

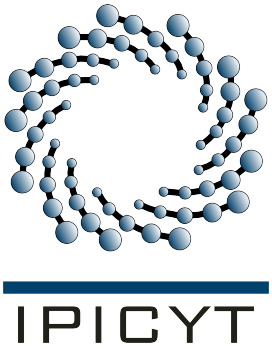

POSGRADO EN CONTROL Y SISTEMAS DINÁMICOS

Synchronization Phenomena in Memristive Neural Networks: A Study of Generalized Synchronization

Tesis que presenta:

Illiani Carro Pérez

Para obtener el grado de:

Doctora En Control Y Sistemas Dinámicos

Director de tesis

Dr. Juan Gonzalo Barajas Ramírez

San Luis Potosí, S.L.P., 15 Mayo de 2026

Constancia de Aprobación de Tesis

La tesis *Synchronization Phenomena in Memristive Neural Networks: A Study of Generalized Synchronization* presentada para obtener el Grado de Doctora en Control y Sistemas Dinámicos fue elaborada por Illiani Carro Pérez y aprobada el 15 Mayo 2026 por los suscritos, designados por el Colegio de Profesores de la División de Control y Sistemas Dinámicos del Instituto Potosino de Investigación Científica y Tecnológica, A.C.

Dr. Juan Gonzalo Barajas Ramírez (Director de la Tesis)	Dr. César Octavio Maldonado Ahumada (Sinodal)
Dr. Eric Campos Cantón (Sinodal)	Dr. Luis Javier Ontañón García Pimentel (Sinodal)

Créditos Institucionales

Esta tesis fue elaborada en la División de Control y Sistemas Dinámicos del Instituto Potosino de Investigación Científica y Tecnológica, A.C., bajo la dirección del Dr. Juan Gonzalo Barajas Ramírez.
Durante la realización del trabajo, el autor recibió una beca académica de la Secretaría de Ciencia, Humanidades, Tecnología e Innovación (SECIHTI), número 968050, y del Instituto Potosino de Investigación Científica y Tecnológica, A. C.

Dedicado mi niña interior por que siempre mantuvo la motivaciön de aprender y no rendirse en los momentos mas dificiles

A mis padres César Carro Gutiërrez y María de los Ángeles Pérez Venegas.

A mi hermano Antonio Carro Pérez.

A mi amiga Ana Nolasco Reyes que en los momentos cruciales, me motivó para terminar el escrito de tesis.

Agradecimientos

Agradezco a Dios por darme fortaleza y salud para culminar esta etapa de mi vida academica.
Agradezco a mi familia y amigos por su apoyo incondicional.

Resumen

En los últimos años, se han propuesto circuitos basados en memristores para emular el comportamiento de neuronas y sinapsis biológicas. Los memristores son dispositivos eléctricos no lineales cuya resistencia depende del historial de voltaje o corriente que se les aplica, lo que los hace adecuados para modelar la memoria y los procesos de aprendizaje en sistemas neuronales. Al incorporarse a modelos neuronales y sinápticos, estos dispositivos dan lugar a redes neuronales memristivas (MNN), que han atraído gran atención por sus posibles aplicaciones en el ámbito de la computación neuromórfica.

El objetivo de esta tesis es analizar el comportamiento dinámico de las redes neuronales memristivas, con especial énfasis en la estabilidad de los puntos de equilibrio y los fenómenos de sincronización. En primer lugar, se investiga la existencia y estabilidad de los puntos de equilibrio en una clase de redes neuronales memristivas de integración y disparo con acoplamiento variable en el tiempo. Se derivan condiciones suficientes para garantizar la existencia de un único punto de equilibrio estable para cada condición inicial. En segundo lugar, se estudia el comportamiento de sincronización de dos neuronas Hindmarsh-Rose acopladas bidireccionalmente a través de un memristor ideal. Mediante el análisis de estabilidad de Lyapunov, se demuestra que se produce una sincronización idéntica cuando la memductancia supera un valor umbral determinado y los estados del memristor convergen a valores constantes.

Finalmente, se investiga numéricamente la sincronización generalizada de dos neuronas Hindmarsh-Rose acopladas a través de sinapsis memristivas activas idénticas. El análisis muestra que la sincronización generalizada surge cuando el parámetro de intensidad del memristor supera un valor crítico, mientras que otros regímenes de sincronización, como la sincronización idéntica, de fase y de retardo, no aparecen. Además, las variaciones en el coeficiente de intensidad del memristor afectan significativamente las características temporales de los patrones de activación neuronal.

Estos resultados contribuyen a la comprensión de cómo los dispositivos memristivos influyen en las propiedades dinámicas de las redes neuronales y proporcionan información sobre el papel del acoplamiento memristivo en el comportamiento neuronal colectivo.

Abstract

In recent years, memristor-based circuits have been proposed to emulate the behavior of biological neurons and synapses. Memristors are nonlinear electrical devices whose resistance depends on the history of the voltage or current applied to them, making them suitable for modeling memory and learning processes in neural systems. When incorporated into neuronal and synaptic models, these devices give rise to memristive neural networks (MNNs), which have attracted significant attention due to their potential applications in areas such as pattern recognition, associative memory, and neuromorphic computing.

The objective of this thesis is to analyze the dynamical behavior of memristive neural networks, with particular emphasis on the stability of equilibrium points and synchronization phenomena. First, the existence and stability of equilibrium points are investigated in a class of memristive integrate-and-fire neural networks with time-varying coupling. Sufficient conditions are derived to guarantee the existence of a unique stable equilibrium point for each initial condition.

Second, the synchronization behavior of two Hindmarsh–Rose neurons bidirectionally coupled through an ideal memristor is studied. Using Lyapunov stability analysis, it is shown that identical synchronization occurs when the memductance exceeds a certain threshold value, and the memristor states converge to constant values.

Finally, the generalized synchronization of two Hindmarsh–Rose neurons coupled through identical active memristive synapses is investigated numerically. The analysis shows that generalized synchronization emerges when the memristor strength parameter exceeds a critical value, while other synchronization regimes such as identical, phase, and lag synchronization do not appear. Additionally, variations in the memristor strength coefficient significantly affect the temporal characteristics of the neuronal firing patterns.

These results contribute to the understanding of how memristive devices influence the dynamical properties of neural networks and provide insight into the role of memristive coupling in collective neuronal behavior.

Contents

Chapter 1

Introduction

Neural systems exhibit complex dynamical behaviors arising from interactions among interconnected neurons. The analysis of such behaviors in neural systems has been a central topic in nonlinear science and computational neuroscience. Mathematical models of neurons and their interconnections provide a framework for understanding complex phenomena such as oscillations, synchronization, and pattern formation in neural networks.

In recent years, memristive devices have emerged as promising elements for modeling neuronal and synaptic dynamics due to their inherent memory properties. These devices enable the development of memristive neural networks (MNN), which extend classical neural models by incorporating a state-dependent coupling mechanism.

The inclusion of memristive elements in neural models has led to the observation of rich dynamical behaviors, including stable equilibrium states [1], as well as synchronization phenomena such as identical synchronization [2], and exponential synchronization [3]. Understanding the conditions under which these behaviors emerge requires analyzing the influence of memristor parameters and network topology.

1.1 State of the Art

The electrical behavior of the neuron has been of interest since the beginning of Louis Galvani's experiments, who studied the stimulation of muscular nerves in amphibians. In 1840, Emil du Bois-Reymond provided experimental evidence that nerve activity is associated with electrical signals. Later in 1888, Nernst showed that the fluids inside and outside the neuron contain ions that flow through the cell membrane, which is proposed to be selectively permeable. The differences in ion concentration generate an electric potential.

Building on these experimental and theoretical developments, Lapicque proposed in 1907 one of the first mathematical models of the neuronal membrane, capturing the integration of incoming stimuli and the generation of spikes via a threshold mechanism. In this model, the insulating properties of the cell membrane are represented by a capacitor, capturing its ability to store electrical charge. At the same time, the semi-permeable nature of the membrane allows a continuous flow of ions across it. This passive transport is commonly represented

as a leakage current, modeled as a linear conductance in the neuron's electrical equivalent circuit, while the current source represents the external stimulus applied to the neuron. When this stimulus is applied, the membrane accumulates or integrates the incoming current over time. This mathematical model is described by a differential equation. When the membrane potential reaches a threshold, the neuron emits a spike, called an action potential, which is a discrete event.

Since then, numerous models have been developed to describe neuronal behavior and their interactions within networks. A major milestone was achieved in 1952, when Hodgkin and Huxley proposed a dynamical model that accounts for the ionic mechanisms underlying action potential generation in the giant squid's membrane. Later, Hindmarsh and Rose proposed a dynamical model that captures the electrical activity of other invertebrates, [4] [5]. This model, referred to as the Hindmarsh-Rose neuron model (HR), considers only two state variables [6] and characterizes bursting activity as rapid, successive spikes in the neuronal membrane voltage driven by a depolarizing current pulse. These models have made it possible to study complex dynamical phenomena such as oscillations, pattern formation, and synchronization.

From the biological point of view, an action potential propagates from neuron to neuron through a specialized site called a synapse, which is a site where a neuron's dendrite is aligned with another neuron's axon terminal. There are two types of biological synapses, electrical and chemical. An electrical synapse occurs when two axon terminals are connected by gap junctions, allowing ions to flow directly between cells. This type of synapse enables the rapid and bidirectional flow of ions. In contrast, a chemical synapse involves the release of neurotransmitters from the presynaptic neuron into the synaptic cleft, which then bind to receptors on the postsynaptic neuron. This process is slow and unidirectional.

In recent years, the incorporation of memristive elements into neural models and synapses has attracted significant attention. A memristor, an acronym for *memory resistor*, is a theoretical device proposed in 1971. It is described by a constitutive relation of the charge and magnetic flux, which means that the behavior of the device is determined by a functional relationship between these variables. Depending on how this relationship is expressed, the memristor can be classified as charge-controlled or flux-controlled. In the case of a flux-controlled memristor, the memductance depends on the magnetic flux, which is the time integral of the input voltage. This dependence on past input signals endows the memristor with memory, distinguishing it from classical resistive elements. Furthermore, a memristor exhibiting negative memristance is referred to as an active memristor, otherwise is passive [7].

Memristive behavior has also been identified in neuronal dynamics. In 1976 [7], it is proposed that the opening and closing dynamics of ion channels depend not only on the instantaneous membrane potential but also on its past activity, indicating the presence of memory effects. In this sense, such mechanisms can be modeled using memristive elements. The Leaky-Integrate and Fire neuron model, which captures the passive electrical properties of the neuron membrane, also admits a memristive description. In this formulation, the memristive element captures the adaptive behavior associated with the opening and closing behavior of ion channels, leading to the so-called Memristive Integrate-and-Fire neuron model [1].

Memristive synapses have been proposed to model the coupling element between neu-

rons; also, memristors have been proposed to model synaptic properties. In particular, the difference in membrane potential between nearby neurons can induce changes in the electromagnetic field, leading to current responses that exhibit memristive behavior [3].

Memristive Neural Networks (MNN) are dynamical models in which a memristor characterizes the behavior of a neuron or synapse. Memristive dynamics have led to the observation of rich behaviors, including stable equilibrium states and different forms of synchronization. These advances have motivated the study of the memristor definition influence the emergence of collective dynamics, particularly in complex, time-varying systems.

1.2 Problem description

The introduction of memristive devices into synaptic and neuronal modeling has opened new possibilities for capturing complex network behaviors. Further simplified memristive neuron models, such as the memristive integrate-and-fire neuron, capture history-dependent voltage dynamics associated with ion-channel activity while maintaining the simplicity of classical integrate-and-fire formulations. Such as the memristive integrate-and-fire neuron, has a continuum of equilibria, where each stable equilibrium corresponds to a memory state determined by the system's initial conditions [1]. Although conditions for the global asymptotic stability of the memory state in memristive integrate-and-fire neural networks (MIFNN) have been established in [1], the case of time-varying coupling has not been fully addressed. In particular, sufficient conditions for the existence and stability of the memory state in an MIFNN with time-varying interconnections remain an open problem.

Beyond memristive neuron models, significant attention has been given to the modeling of synaptic interactions using memristive devices to represent synaptic couplings whose conductance depends on an internal state variable [3]. Several studies have investigated the synchronization and firing patterns of two HR neurons, or of purely Hindmarsh–Rose systems, coupled via memristive synapses, revealing rich memory-dependent dynamics. In reference [2], two HR neurons achieved synchronization when the electromagnetic induction coefficient is set above a certain value. In [3], exponential synchronization in an MNN consisting of two HR neurons coupled through a locally active memristor is proved analytically under appropriate memristor coupling coefficient and memristor initial state. In [8], a MNN model is described that includes an equal number of neurons and memristors. The model shows a transition from non-synchronization to synchronization, while random and small-world networks reach a partially coherent state during this process. While memristive neuron and synapse models have been extensively studied at the level of pairwise couplings [9]– [8], analytical results on synchronization remain limited. In particular, only [3] provides analytical results on the synchronization of Hindmarsh–Rose neurons coupled through a locally active memristor. This limitation highlights the need to investigate the conditions for identical synchronization in Hindmarsh–Rose neurons coupled by passive memristive elements with alternative descriptions of memristance function. Moreover, the influence of active memristor parameters on the temporal characteristics of firing patterns in such systems remains an open problem. Finally, the role of active memristive coupling in the emergence of synchronization regimes beyond identical synchronization, such as generalized synchronization, remains unexplored in the current literature.

This thesis focuses on the analysis of equilibrium solutions and synchronization regimes in memristive neural networks, with particular emphasis on understanding how memristive coupling influences collective dynamics.

Three main problems are investigated. The first concerns the derivation of sufficient conditions for the existence and stability of the memory state in a Memristive Integrate-and-Fire Neural network with time-varying interconnections. The second addresses sufficient conditions for identical synchronization in Hindmarsh–Rose neurons coupled by a passive memristor. The third focuses on the numerical investigation of the emergence of generalized synchronization in Hindmarsh–Rose neurons coupled through an active memristive synapse.

1.3 Objectives

Analyze the stability of dynamic behaviors in memristive neural networks (MNN), particularly the stability of equilibrium points and synchronized behavior.

- Determine sufficient conditions for the existence and stability of the memory state in a Memristive Integrate-and-Fire neural network with time-varying interconnections
- Derive sufficient conditions for identical synchronization in Hindmarsh–Rose neurons coupled by a passive memristor.
- Numerically investigate the emergence of generalized synchronization in Hindmarsh–Rose neurons coupled through an active memristive synapse.

1.4 Document description

This thesis is organized as follows. Chapter 2 presents the theoretical framework used throughout this work, including fundamental concepts of stability theory, synchronization in dynamical systems, and basic notions of complex network theory. Chapter 3 introduces the memristive neural network models considered in this study formulates the corresponding dynamical systems and the main results on the analysis of equilibrium points, stability and synchronization properties of the proposed models of this thesis. Finally chapter 4 summarizes the main conclusions and discusses possible directions for future research.

1.5 Published results

The following publications have been produced as a result of the research presented in this thesis:

Journal Articles

[**J.1**] Carro-Pérez, I., Barajas-Ramírez, J.G. (2025). **Generalized Synchronization of Hindmarsh–Rose Neurons with Memristive Couplings**. *Dynamics*, Vol. 5, Issue 4, pp. 50. DOI: 10.3390/dynamics5040050

Conference Proceedings

[**C.1**] Carro-Perez, I, Barajas-Ramirez, J.G. (2020). **Stability of the Memory State of a Time-Varying Memristive Neural Network Model**. In *Congreso Nacional de Control Automático*, pp. 1-5, ISSN: 2594-24

[**C.2**] Carro-Perez, I, Barajas-Ramirez, J.G.(2022). **Synchronization of memristor based bidirectionally coupled Hindmarsh-Rose neurons**. In *Congreso Nacional de Control Automático*, pp. 516-521. October, ISSN: 2594-2492.

Chapter

[**C.3**] Anzo-Hernández, A., Carro-Pérez, I., Bonilla-Capilla, B., Barajas-Ramírez, J.G. (2024). **Synchronization of Memristive Hindmarsh–Rose Neurons Connected by Memristive Synapses**. In *Complex Systems and Their Applications*, EDIESCA 2023, Campos-Cantón, E., Huerta-Cuellar, G., Zambrano-Serrano, E., Tlelo-Cuautle, E. (eds), Springer, Cham. DOI: 10.1007/978-3-031-51224-7_8

Chapter 2

Preliminaries

This chapter presents the theoretical framework used throughout this thesis. First, the mathematical models of neurons and synapses are introduced. The discussion begins with the physical structure of the neuron, followed by electrical representations of the neuronal membrane, culminating in the Hodgkin–Huxley model.

Next, memristors are introduced as suitable devices for modeling neuronal and synaptic dynamics. Their fundamental properties are discussed, along with simple examples illustrating their behavior. Based on these concepts, memristive neuron models are presented, followed by an overview of memristive neural network (MNN) models relevant to this work.

Finally, the theoretical tools required for the analysis of memristive neural networks are introduced. In particular, fundamental concepts of Lyapunov stability are presented, providing sufficient conditions for the stability of equilibrium points and synchronization manifolds in coupled dynamical systems. These concepts form the basis for analyzing the stability of synchronized motion in the memristive neural networks considered in this thesis.

The discussion begins with fundamental concepts of Lyapunov stability, which provide sufficient conditions for the stability of equilibrium points and, more generally, for the stability of synchronization manifolds in coupled dynamical systems. These concepts are fundamental for understanding current approaches to the stability of synchronized motion in memristive neural networks. For instance, in [3], two memristive HR neurons are connected via a memristive synapse without an external current, and it is demonstrated that exponential synchronization can be achieved using the Lyapunov direct method. Similarly, for other memristive neural network models composed of memristive integrate-and-fire neurons interconnected via resistive elements, sufficient conditions for global asymptotic stability of the network equilibrium have been established.

Synchronization theory is an essential part of the theoretical framework developed in this chapter, providing fundamental tools for analyzing collective dynamics in memristive neural networks. Various synchronization phenomena have been investigated in memristive neural networks. In addition to identical synchronization, which has attracted significant attention [10], other collective behaviors such as phase synchronization and spatiotemporal patterns have also been reported [9, 11]. Moreover, coexisting firing patterns have been observed in memristive neural networks with non-identical neurons coupled through memristive synapses

[12, 13].

In addition, network theory plays a central role in the analysis of large-scale memristive neural networks, as the collective dynamics strongly depend on the underlying interconnection topology. Recent studies have highlighted the influence of network structure on the synchronization of MNN [8]. In particular, different topologies such as fully connected, small-world, and random networks have been considered, motivating the need for a theoretical framework that captures the effects of connectivity patterns on network dynamics.

2.1 Neuronal models

2.1.1 Historical notes

The brain is an organ that has been of interest to the research community in the search for answers about its function and structure. Inquiries about its function date back to the classical era. The philosopher Aristotle claimed that the brain was a secondary organ that served as a cooling source of the heart, as opposed to the heart, which was attributed to being the center of sensation and movement. The physician Galen hypothesized that the brain was the site of termination of all senses and was responsible for cognition and conscious actions [14].

One of the significant milestones in the brain structure was achieved in 1888 by Santiago Ramon y Cajal, revealing that the nervous system is composed of individual cells called *neurons*, which are separate from each other. The slight separation between them was a communication site. Among different shapes of neurons observed through his experiments, it was identified that the neuron cell body extended to a long slender cable called *axon*. A representation of the neuron obtained from [**?**] is depicted in Figure 2.1, where the main parts of the neuron are observed. Since the neuron is a biological cell, it has a membrane separating its interior from its environment.

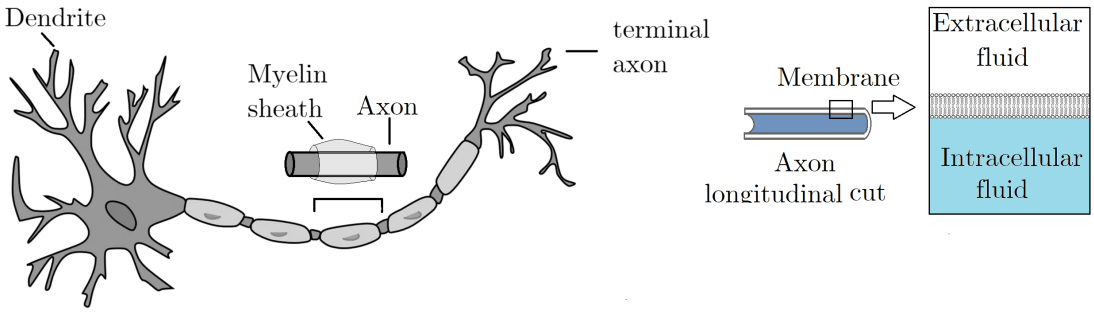

Figure 2.1: Neuron (a) Classic structure (b) approximation of its membrane

Regarding brain function, at the end of XVIII century, experiments had been initiated to discover the electrical properties of the nervous system. Galvani performed experiments in which the sciatic nerve of a frog was electrically stimulated, and he observed the contraction

of the animal muscle. This led him to hypothesize that nerves conduct electricity and are generated inside the animal body [15]. Later, in 1841, Emil du Bois-Reymond provided new evidence that confirmed the existence of a constant electric potential in striated muscle during its contraction; this phenomenon was coined the name of *action potential* [16].

The physicochemical mechanisms of electrical nerve stimulation remained unclear until 1888 [17] was pointed out that the nerve, as an organic tissue, is composed of a semi-permeable membrane, which, in the presence of an electrolytic solution and a current applied, causes ions movement by diffusion force. Also, given that the membrane is semipermeable, ions with one type of charge are stopped on one side of the membrane; this causes its polarization, where the net charge at the membrane results from two forces interacting: electrostatic and diffusive. Following this insight and the interest in the electrical characterization of nerve membrane, Lapique [18] obtains a first approximation of its equivalent circuit and its associated mathematical model characterizing the electrical polarization of nerve membrane under external stimulus. This model is presented in the next section.

2.1.2 Lapicque model

Lapicque characterizes the electrical polarization of nerve membranes as the one of a capacitor; he adds the effect of leakage inherent to this electrical element.

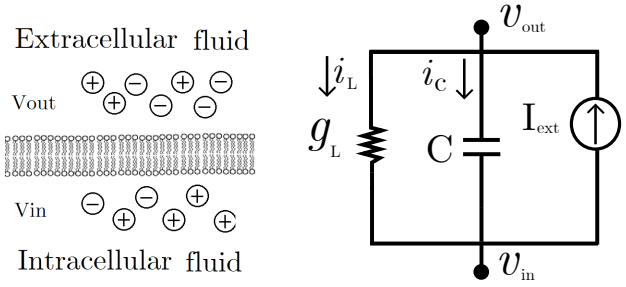

(a) Neuron membrane

(b) Integrate-and-fire neuron circuit

Figure 2.2

The circuit associated with membrane electrical behavior is represented in 2.2b, where v_{out}, v_{in} is the voltage inside and outside the membrane, respectively. Therefore, the membrane voltage:

$$E = v_{in} - v_{out} \tag{2.1}$$

i_c is the capacitor's current, i_L is the leakage current, C is the capacitance, g_L is the leakage conductance, I_{ext} is an external constant current.

The current i_c associated with the membrane capacitance is proportional to the rate of change of the voltage across the capacitor, that is:

$$i_c = C\dot{E} \tag{2.2}$$

the current in the conductance g_c is given by $i_L = g_L v$. Therefore, the dynamic model associated with the circuit in Figure 2.2b is obtained through Kirchhoff's Current Law (LKC):

$$C\dot{E} = -g_L E + I_{ext} \tag{2.3}$$

$$\tau\dot{E} = -E + \frac{I_{ext}}{g_L} \tag{2.4}$$

where $\tau = C/g_L$. Equation (2.4) corresponds to the classical leaky integrate-and-fire (LIF) model, originally introduced by Lapicque, which describes the membrane potential as a leaky integrator driven by an external current.

Nonetheless, the relation between nerve stimulation and action potential generation was unknown. In 1949 [19], a technique was developed to measure ion concentrations through the membranes of excitable cells. Hodgkin and Huxley applied this technique to the squid giant axon and subsequently proposed the first dynamical model describing the electrical behavior of neurons, now known as the Hodgkin–Huxley (HH) model, which incorporates the contribution of ionic currents to action potential generation.

2.1.3 Hodgkin and Huxley neuron model

Neuron membrane is a complex structure consisting of two layers of lipids, where specialized structures are embedded —known as ion channels—, through which ions move from one side to the other [20]. Electrical properties are inherited from membrane composition. The lipid layer insulates the neuron's interior from the exterior; its permeability can be affected by several factors, such as temperature and the types of solutes present. This is why the feature of semi-permeability is attributed to it. An illustration of the membrane and *ion channels* is illustrated in figure 2.3. Ion channels can be classified according to their activation mechanism; voltage-gated types are opened and closed depending on the membrane potential, which is associated with an electrochemical gradient. Hodgkin and Huxley found three different ions that influence the membrane voltage: chlorine Cl^-, potassium K^+, and sodium Na^+. The concentration of such ions at resting state inside and outside the membrane (in mM):

$$\begin{array}{rclrcl} [Cl^-]_{in} & \approx & 329.45, & [Cl^-]_{out} & \approx & 40 \\ [K^+]_{in} & \approx & 400, & [K^+]_{out} & \approx & 20 \\ [Na^+]_{in} & \approx & 50, & [Na^+]_{out} & \approx & 440 \end{array} \tag{2.5}$$

When channels of a specific ion (positive or negative) are activated, the net flux of ions results from two opposing forces: diffusion and electrostatic. When the external stimulus is applied, ions with specific charge start to move across the membrane by diffusion force through the voltage-gated channels; this causes the accumulation of (positive or negative) charges on one side of the membrane, whereby ions start to move by the electrostatic force, attracting ions oppositely charged and repulsing equally charged. This makes it possible to have different amounts of electrical charges inside and outside the cell. Nernst [21] found that

when these forces are balanced, the net flux of ions is null. Thus, the membrane is said to be at electrochemical equilibrium, and its corresponding electric potential v_{ion} can be calculated through:

$$E_{ion} = \frac{kT}{qz} \ln\left(\frac{c_{out}}{c_{in}}\right) \tag{2.6}$$

where E_{ion} is the Nernst potential of the specific *ion*, k(Joule/°K) Boltzmann constant, T temperature in °K, q(Coulomb) is the electric charge of the ion, c_{out} and c_{in} is the ion concentration outside and inside the membrane respectively. See Appendix A for a more detailed description of Nernst's potential derivation.

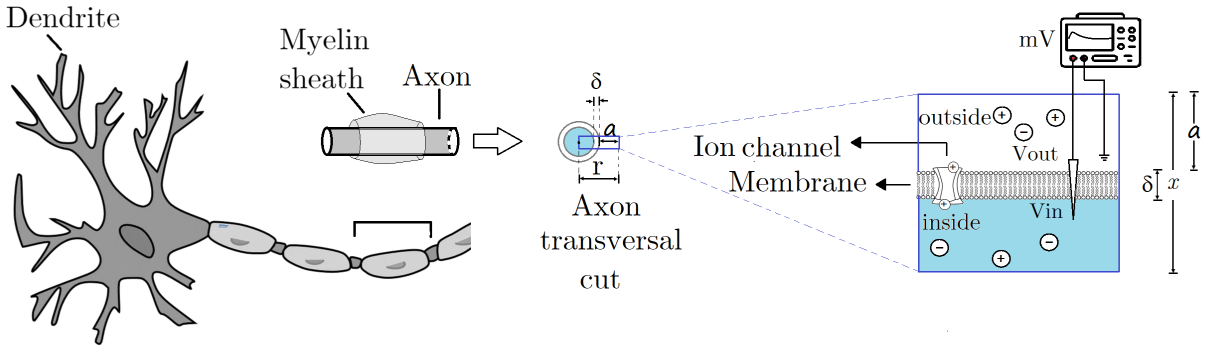

Figure 2.3: Multiscale representation of a neuron, showing its morphology, axonal cross-section, and the ion-channel mechanisms responsible for the generation of membrane potential

From the Nernst equation, it is obtained $\frac{kT}{q} = 25.8\text{mV}$ [22]. The equilibrium potential for Cl^-, it is calculated considering $z = -1$, $E_{Cl^-} = -54.4\text{mV}$. For cations K^+ and Na^+, the equilibrium potential is calculated using $z = 1$, as a result $E_K = -77\text{mV}$ and $E_{Na} = 50\text{mV}$. In [23], the membrane potential, potassium, sodium, and chlorine equilibrium potentials are expressed with respect to membrane resting potential E_r, that is:

$$\begin{aligned} v &= E - E_r \\ v_{Na} &= E_{Na} - E_r \\ v_K &= E_K - E_r \\ v_{Cl} &= E_{Cl} - E_r \end{aligned} \tag{2.7}$$

Where v represents the shifted membrane potential and v_{Na}, v_K, v_{Cl} are shifted equilibrium potentials of the corresponding sodium, potassium, and chlorine ions. Considering $E_r = -65\text{mV}$, it is obtained $v_{Na} = 115\text{mV}$, $v_K = -12\text{mV}$, $v_{Cl} = 10.6\text{mV}$.

Membrane electrical properties are inherited from its physical composition. The first is related to the fact that it is a dielectric layer separating two conductors (the inside and the outside of the cell). Positive charges accumulate on one side of the insulator, while negative charges are on the opposite side through the application of the external stimulus. Therefore, the membrane has the capacitance property. A second electrical characteristic is related to the flow of ions through their corresponding channels at a specific rate; this induces an electrical current and its associated conductance.

The circuit associated with neuron membrane electrical behavior proposed by Hodgkin and Huxley is represented in Figure 2.4.

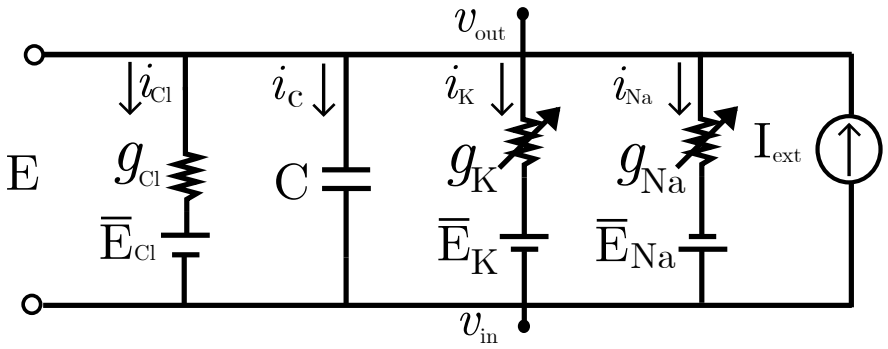

Figure 2.4: Circuit representation of the Hodgkin–Huxley (HH) neuron model

The electrical representation of potassium and sodium conductances in [23] are considered to be non-linear resistors and considered to be built through active elements. In contrast, the conductance of the chlorine channel is modeled through a resistor. The external current is represented by I_{ext} whose units are $\mu A{\cdot}\text{cm}^2$.

The capacitance C of the membrane is characterized through its properties such as thickness δ and dielectric constant ϵ:

$$C = \frac{\epsilon \text{A}}{\delta} \tag{2.8}$$

where A is the cross-sectional area. If $\epsilon = 1 \times 10^{-12}\text{F/cm}$ and $\delta = 10\text{nm}$, the capacitance per unit area is $C = 1\mu\text{F/cm}^2$.

The conductivity of the chlorine channel is modeled as a passive element:

$$g_{Cl} = \frac{1}{\rho_{Cl}\delta} \tag{2.9}$$

where ρ_{Cl} is bulk membrane resistivity ($\Omega{\cdot}\text{cm}$), which is $\rho_{Cl} = \frac{1}{3}\Omega{\cdot}\text{cm}$. As a result $g_{Cl} = 0.3\text{mS/cm}^2$. This is also called leakage conductance, given that ions flow constantly. The current associated with the chlorine ion channel is:

$$i_{Cl} = g_{Cl}(E - E_{Cl}) \tag{2.10}$$

the units of i_{Cl} are $\mu A/\text{cm}^2$. For convenience chlorine current (2.10) is rewritten in the form:

$$i_{Cl} = g_{Cl}(v - v_{Cl}) \tag{2.11}$$

Hodgkin and Huxley performed experiments to characterize the sodium and potassium conductances. The electrical characterization was performed by measuring the ionic current of interest —which was not influenced by other currents— and simultaneously fixing the membrane voltage to a constant value —known as membrane voltage-clamp — so that the current necessary to maintain this potential was recorded. Their recordings showed that sodium and potassium conductance behavior is not constant over time. Furthermore, potassium conductance grew monotonically in time to a steady level and stayed at that value

during the membrane voltage-clamp polarization. This rise in conductance is called the activation of K^+ channel. The potassium conductance curves were observed to correspond to a first-order system with a delay. Hodgkin and Huxley proposed the potassium conductance to be modeled as:

$$g_K = \bar{g}_K n^{p_n} \tag{2.12}$$

where p_n is constant representing the probability that K^+ channel opens, $\bar{g}_K$ is the maximum conductance of potassium channels and n represents the fraction of opened potassium channels —a dimensionless state variable, *i.e.* $n \in [0, 1]$—. The differential equation of the rate of change of n is:

$$\dot{n} = \frac{n_\infty(v) - n}{\tau_n(v)} \tag{2.13}$$

where the functionals $n_\infty(v)$ and $\tau_n(v)$ depend on $\alpha_n(v)$ and $\beta_n(v)$ defined by:

$$\tau_n(v) = \frac{1}{\alpha_n(v) + \beta_n(v)} \tag{2.14a}$$

$$n_\infty(v) = \alpha_n(v)\tau_n(v) \tag{2.14b}$$

where $n_\infty(v)$ is the limiting fraction of opened K^+ channels if the membrane potential is steady as $t \to \infty$, $\tau_n(v)$ is the time constant of approach to the steady state. Where $\alpha_n(v)$ and $\beta_v(n)$ are defined by:

$$\alpha_n(v) = \frac{0.01(10 - v)}{e^{\{\frac{10-v}{10}\}} - 1} \tag{2.15a}$$

$$\beta_n(v) = 0.125e^{\{\frac{-v}{80}\}} \tag{2.15b}$$

Substituting (2.14) in (2.13) is obtained:

$$\dot{n} = \alpha_n(v) - n(\alpha_n(v) + \beta_n(v)) \tag{2.16}$$

rewriting (2.16) is obtained:

$$\dot{n} = \alpha_n(v)(1 - n) - \beta_n(v)n \tag{2.17}$$

From the equation (2.17), it is shown that $1 - n$ is the fraction of closed K^+ channels, then $\alpha_n(v)$ and $\beta_n(v)$ are functions representing the rate of opening and closing actions of ion channel, respectively. The constants p_n and $\bar{g}_K$ were obtained in such a way that the experimental curves fit the proposed model; it was found $p_n = 4$ and $\bar{g}_K = 36\text{mS/cm}^2$.

Unlike the potassium curve, the sodium conductance curve reaches a peak and decays back to rest during a constant voltage-clamp membrane polarization. The smooth rise and fall of conductance— as recorded by Hodgkin and Huxley — meant the channel transitioned from a closed-opened-closed state. Two specialized structures are involved during this process: activation and inactivation gates. Each gate can be opened or closed, as shown in Figure 2.5 (a). Sodium channel transitions are illustrated in Figure 2.5. The dynamic model involves two state variables: an activation variable m (for the fraction of opened activating gates) and an inactivation variable h (for the fraction of opened inactivation gates). Where $m, n \in [0, 1]$.

As depicted in Figure 2.5, if $m, h = 1$ means that all of the activation and inactivation gates are opened.

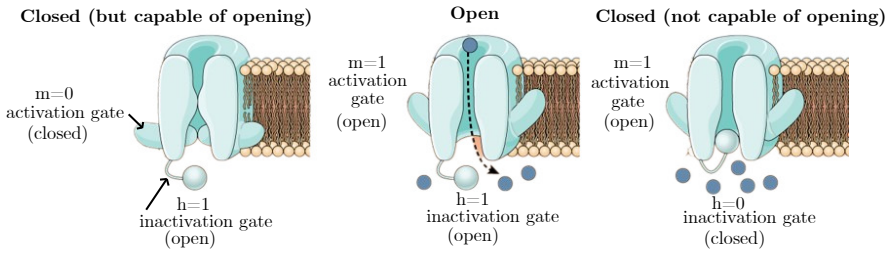

(a) (b) (c)

Figure 2.5: Gating states of a voltage-gated ion channel in the Hodgkin–Huxley model: (a) closed but activatable state ($m = 0$, $h = 1$), (b) open state ($m = 1$, $h = 1$), and (c) inactivated state ($m = 1$, $h = 0$).

The sodium conductance is modeled as:

$$g_{Na} = \bar{g}_K m^{p_m} h^{p_h} \tag{2.18}$$

where $\bar{g}_{Na}$ is the maximum conductance of sodium channels when opened, p_m and p_h are constants representing the probability of opening and closing of m and h gates. The dynamic model of m, n is described by:

$$\dot{m} = \frac{m_\infty(v) - m}{\tau_m(v)} \tag{2.19a}$$

$$\dot{h} = \frac{h_\infty(v) - h}{\tau_h(v)} \tag{2.19b}$$

$$\tag{2.19c}$$

Functions $m_\infty(v)$ and $h_\infty(v)$ represent the limiting fraction of activation and inactivation gates, respectively, when $v(t)$ reaches a steady state as $t \to \infty$.

$$m_\infty(v) = \alpha_m(v)\tau_m(v) \tag{2.20a}$$

$$h_\infty(v) = \alpha_h(v)\tau_h(v) \tag{2.20b}$$

the functions $\tau_m(v)$ and $\tau_h(v)$ are considered to be the time of approach to the steady state.

$$\tau_m(v) = \frac{1}{\alpha_m(v) + \beta_m(v)} \tag{2.21a}$$

$$\tau_h(v) = \frac{1}{\alpha_h(v) + \beta_h(v)} \tag{2.21b}$$

Where $\alpha_{m,h}(v)$ and $\beta_{m,h}(v)$ are functionals that determine the rate of opening and closing of the activation and inactivation gates, respectively. By means of numerical methods it was

found $g_{Na} = 120m\mathrm{S/cm}^2$, $p_m = 3$ and $p_h = 1$, where $\alpha_{m,h}(v)$, $\beta_{m,h}(v)$ are:

$$\alpha_m(v) = \frac{0.1(25-v)}{e^{\{\frac{25-v}{10}\}} - 1} \tag{2.22a}$$

$$\beta_m(v) = 4e^{-\{\frac{v}{18}\}} \tag{2.22b}$$

$$\alpha_h(v) = 0.07e^{-\{\frac{v}{20}\}} \tag{2.22c}$$

$$\beta_h(v) = \frac{1}{e^{\{\frac{30-v}{10}\}} + 1} \tag{2.22d}$$

Substituting (2.21a) in (2.19a) is obtained:

$$\dot{m} = \alpha_m(v)(1-m) - \beta_m(v)m \tag{2.23}$$

alternatively, substituting (2.21b) in (2.19b) is obtained:

$$\dot{h} = \alpha_h(v)(1-h) - \beta_h(v)h \tag{2.24}$$

From electrical circuit of figure 2.4 and conductances (2.12) and (2.18), the currents for sodium and potassium are:

$$i_K = \bar{g}_K n^4 (v - v_K) \tag{2.25}$$

$$i_{Na} = \bar{g}_{Na} m^3 h (v - v_{Na}) \tag{2.26}$$

To apply Kirchhoff's Current Law, the membrane current densities are scaled by the area A, then it is obtained:

$$\mathrm{A}(i_K + i_{Na} + i_{Cl} + i_C) = I_{ext} \tag{2.27}$$

Substituting (2.26), (2.10), (2.25) into (2.27) electrical behavior of neuron membrane proposed by the Hodgkin-Huxley is:

$$\dot{v} = \frac{1}{C}\left\{\frac{I_{ext}}{\mathrm{A}} - \bar{g}_K n^4 (v - v_K) - \bar{g}_{Na} m^3 h (v - v_{Na}) - \bar{g}_{Cl}(v - v_{Cl})\right\} \tag{2.28a}$$

$$\dot{n} = \alpha_n(v)(1-n) - \beta_n(v)n \tag{2.28b}$$

$$\dot{m} = \alpha_m(v)(1-m) - \beta_m(v)m \tag{2.28c}$$

$$\dot{h} = \alpha_h(v)(1-h) - \beta_h(v)h \tag{2.28d}$$

$$\alpha_n(v) = \frac{0.01(10-v)}{e^{\{\frac{10-v}{10}\}} - 1}, \quad \alpha_m(v) = \frac{0.1(25-v)}{e^{\{\frac{25-v}{10}\}} - 1}, \quad \alpha_h(v) = 0.07e^{-\{\frac{v}{20}\}}$$

$$\beta_n(v) = 0.125e^{\{\frac{-v}{80}\}}, \qquad \beta_m(v) = 4e^{-\{\frac{v}{18}\}}, \qquad \beta_h(v) = \frac{1}{e^{\{\frac{30-v}{10}\}} + 1}$$

In [22], the HH neuron model is usually written in terms of unshifted membrane voltage E and ion Nernst potentials E_K, E_{Na}, E_{Cl} [22], in contrast with the original representation

shown in (2.28). For which the coordinate translation is performed using (2.7), therefore equation (2.28a)-(2.28d) becomes:

$$\dot{E} = \frac{1}{C}\Big\{\frac{I_{ext}}{\mathrm{A}} - \bar{g}_K n^4(E - E_K) - \bar{g}_{Na} m^3 h(E - E_{Na}) - \bar{g}_{Cl}(E - E_{Cl})\Big\} \tag{2.29a}$$

$$\dot{n} = \alpha_n(E)(1 - n) - \beta_n(E)n \tag{2.29b}$$

$$\dot{m} = \alpha_m(E)(1 - m) - \beta_m(E)m \tag{2.29c}$$

$$\dot{h} = \alpha_h(E)(1 - h) - \beta_h(E)h \tag{2.29d}$$

$$\alpha_n(E) = \frac{0.01(E + 55)}{1 - e^{-\{\frac{E+55}{10}\}}} \quad (2.30) \qquad \alpha_m(E) = \frac{0.1(E + 40)}{1 - e^{\{\frac{E+40}{10}\}}} \quad (2.31) \qquad \alpha_h(E) = 0.07e^{-\{\frac{E+65}{20}\}} \quad (2.32)$$

$$\beta_n(E) = 0.125e^{-\{\frac{E+65}{80}\}} \quad (2.33) \qquad \beta_m(E) = 4e^{-\{\frac{E+65}{18}\}} \quad (2.34) \qquad \beta_h(E) = \frac{1}{e^{-\{\frac{E+65}{10}\}} + 1} \quad (2.35)$$

In summary, the constant parameters of the HH neuron model are:

Constant	C	$\bar{g}_K$	$\bar{g}_{Na}$	g_{Cl}	v_K	v_{Na}	v_{Cl}	E_{Cl}	E_K	E_{Na}
Value	1	36	120	0.3	12	-115	-10.6	-54.4	-77	50
Units	μF/cm^2	mS/cm^2	mS/cm^2	mS/cm^2	mV	mV	mV	mV	mV	mV

The dynamics of the HH neuron (2.29) can be rewritten as follows:

$$\dot{x} = f_{HH}(x) \tag{2.36}$$

where $x = (E, n, m, h)^\top \in \mathbb{R}^4$ and $f_{HH}(\cdot) = (f_1(\cdot), f_2(\cdot), f_3(\cdot), f_4(\cdot))^\top \in \mathbb{R}^4$, with $f_1(x), \cdots, f_4(x)$ functions described by the left side of equations (2.29a)-(2.29d) respectively.

2.1.3.1 Dynamical Analysis

Equilibrium Point Analysis

Let $x_e = (E_e, n_e, m_e, h_e)^\top$ an equilibrium point of (2.29a)-(2.29d) which satisfies:

$$0 = \frac{1}{C}\Big\{\frac{I_{ext}}{\mathrm{A}} - \bar{g}_K n_e^4(E_e - E_K) - \bar{g}_{Na} m_e^3 h_e(E_e - E_{Na}) - \bar{g}_{Cl}(E_e - E_{Cl})\Big\} \tag{2.37a}$$

$$0 = \alpha_{n_e}(E_e)(1 - n) - \beta_{n_e}(E_e)n_e \tag{2.37b}$$

$$0 = \alpha_{m_e}(E_e)(1 - m) - \beta_{m_e}(E_e)m_e \tag{2.37c}$$

$$0 = \alpha_{h_e}(E_e)(1 - h) - \beta_{h_e}(E_e)h_e \tag{2.37d}$$

$$E_e = \frac{\bar{g}_K n_e^4 E_K + \bar{g}_{Na} m_e^3 h_e E_{Na} + g_{Cl} E_{Cl} + \frac{I_{ext}}{A}}{\bar{g}_K n_e^4 + \bar{g}_{Na} m_e^3 h_e + g_{Cl}} \tag{2.38a}$$

$$n_e = \frac{\alpha_n(E_e)}{\alpha_n(E_e) + \beta_n(E_e)} \tag{2.38b}$$

$$m_e = \frac{\alpha_m(E_e)}{\alpha_m(E_e) + \beta_m(E_e)} \tag{2.38c}$$

$$h_e = \frac{\alpha_h(E_e)}{\alpha_h(E_e) + \beta_h(E_e)} \tag{2.38d}$$

Substituting (2.38b)-(2.38d) in (2.38a), it is obtained:

$$f_e(E) = \frac{\bar{g}_K \left(\frac{\alpha_n(E)}{\alpha_n(E)+\beta_n(E)}\right)^4 E_K + \bar{g}_{Na} \left(\frac{\alpha_m(E)}{\alpha_m(E)+\beta_m(E)}\right)^3 \left(\frac{\alpha_h(E)}{\alpha_h(E)+\beta_h(E)}\right) E_{Na} + g_{Cl} E_{Cl} + \frac{I_{ext}}{A}}{\bar{g}_K \left(\frac{\alpha_n(E)}{\alpha_n(E)+\beta_n(E)}\right)^4 + \bar{g}_{Na} \left(\frac{\alpha_m(E)}{\alpha_m(E)+\beta_m(E)}\right)^3 \left(\frac{\alpha_h(E)}{\alpha_h(E)+\beta_h(E)}\right) + g_{Cl}} - E \tag{2.39}$$

As can be seen, the roots of (2.39) depend on the input current I_{ext}. The roots of (2.39) can be obtained numerically, and the function $f_e(\cdot)$ is graphed for an adequate range of $E_e \in [-100, 0]$. Its intersection with the horizontal axis is obtained for several values of $I_{ext} = 0, 10, 40, 70$ μA/cm^2, and the cross-sectional area is $A = 1$cm^2. As can be seen in figure 2.6. In particular for $I_{ext} = 0$, $x_e = (-65, 0.3177, 0.0529, 0.5961)^\top$.

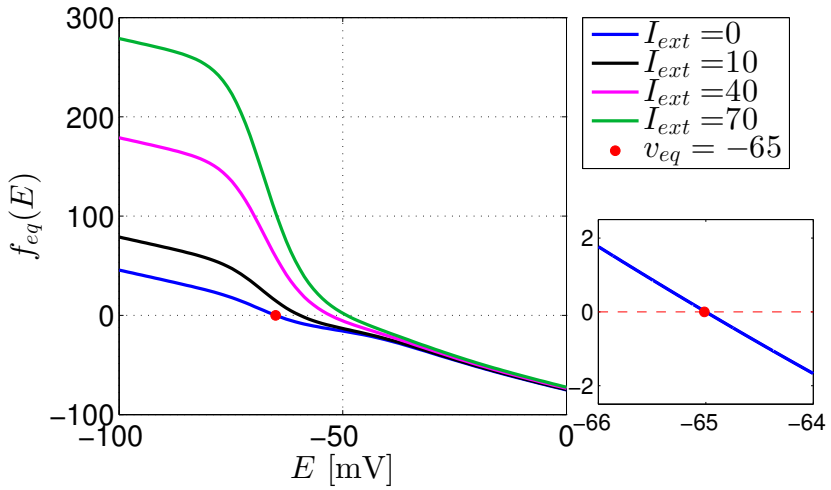

Figure 2.6: Graph of the roots (2.39) with respect to the external current I_{ext}

$$D_x f_{HH} = \begin{bmatrix} \frac{\partial f_1}{\partial E} & \frac{\partial f_1}{\partial n} & \frac{\partial f_1}{\partial m} & \frac{\partial f_1}{\partial h} \\ \frac{\partial f_2}{\partial E} & \frac{\partial f_2}{\partial n} & 0 & 0 \\ \frac{\partial f_3}{\partial E} & 0 & \frac{\partial f_3}{\partial m} & 0 \\ \frac{\partial f_4}{\partial E} & 0 & 0 & \frac{\partial f_4}{\partial h} \end{bmatrix} \tag{2.40}$$

$\frac{\partial f_1}{\partial E} = \frac{-g_K n^4 - g_{CL} - g_{Na} m^3 h}{C}$

$$\frac{\partial f_1}{\partial n} = \frac{-4g_K n^3(E-E_K)}{C}$$
$$\frac{\partial f_1}{\partial m} = \frac{-3g_{Na} m^2 h(E-E_{Na})}{C}$$
$$\frac{\partial f_1}{\partial h} = \frac{-g_{Na} m^3(E-E_{Na})}{C}$$
$$\frac{\partial f_2}{\partial E} = \left[\frac{0.01}{\left(1-e^{-\left\{\frac{E+55}{10}\right\}}\right)} - \frac{0.01(E+55)\frac{1}{10}e^{-\left\{\frac{E+55}{10}\right\}}}{\left(1-e^{-\left\{\frac{E+55}{10}\right\}}\right)^2} \right](1-n) + \frac{n}{640}e^{-\left\{\frac{E+65}{80}\right\}}$$
$$\frac{\partial f_2}{\partial n} = -\frac{0.01(E+55)}{\left(1-e^{-\left\{\frac{E+55}{10}\right\}}\right)} - 0.125e^{-\left\{\frac{E+55}{80}\right\}}$$
$$\frac{\partial f_3}{\partial E} = \left[\frac{0.01}{\left(1-e^{-\left\{\frac{E+40}{10}\right\}}\right)} - \frac{0.01(E+40)\frac{1}{10}e^{-\left\{\frac{E+40}{10}\right\}}}{\left(1-e^{-\left\{\frac{E+40}{10}\right\}}\right)^2} \right](1-m) + \frac{2m}{9}e^{-\left\{\frac{E+65}{18}\right\}}$$
$$\frac{\partial f_3}{\partial m} = -\frac{0.1(E+40)}{\left(1-e^{\left\{-\frac{E+40}{10}\right\}}\right)} - 4e^{-\left\{\frac{E+65}{18}\right\}}$$
$$\frac{\partial f_4}{\partial E} = -\frac{0.07e^{-\left\{\frac{E+65}{20}\right\}}}{20}(1-h) - \frac{he^{-\left\{\frac{E+35}{10}\right\}}}{10\left(e^{-\left\{\frac{E+35}{10}\right\}}+1\right)^2}$$
$$\frac{\partial f_4}{\partial h} = -0.07e^{-\left\{\frac{E+65}{20}\right\}} - \frac{1}{\left(e^{-\left\{\frac{E+35}{10}\right\}}+1\right)}$$

The Jacobian matrix of the HH neuron model is:

$$J(x)\Big|_{x=x_e} = \begin{bmatrix} -0.6773 & -55.4275 & 69.30821 & 2.0544 \\ 0.0028 & -0.1617 & 0 & 0 \\ 0.0263 & 0 & -4.2228 & 0 \\ -0.0041 & 0 & 0 & -0.1174 \end{bmatrix}$$

eigenvalues are $\lambda_1 = -4.6765, \lambda_2 = -0.1920 + 0.3826i, \lambda_3 = -0.1920 - 0.3826i, \lambda_4 = -0.1196 + 0.0000i$ which corresponds to a stable focus.

2.1.3.2 Bifurcation Diagram

The bifurcation theory investigates how solution behavior changes as system parameters change. The HH neuron model includes external current as a parameter. A bifurcation diagram of the HH neuron model (2.36) is obtained through Matlab by setting as an initial condition the resting potential x_e and varying the external current I_{ext}. Such numerical analysis shows two bifurcation points at $I_1 = 6.2135$ and $I_2 = 165\mu A/cm^2$. The first corresponds to the transition from an equilibrium point to a limit cycle. The second corresponds to transitioning from a limit cycle to a fixed point. For $I_{ext} \in (0, 6.2135)$, the trajectory returns to the resting potential, while for $I_{ext} \in (0, 165)$, the solution converges to a limit cycle called in neuroscience literature as the *action potential*.

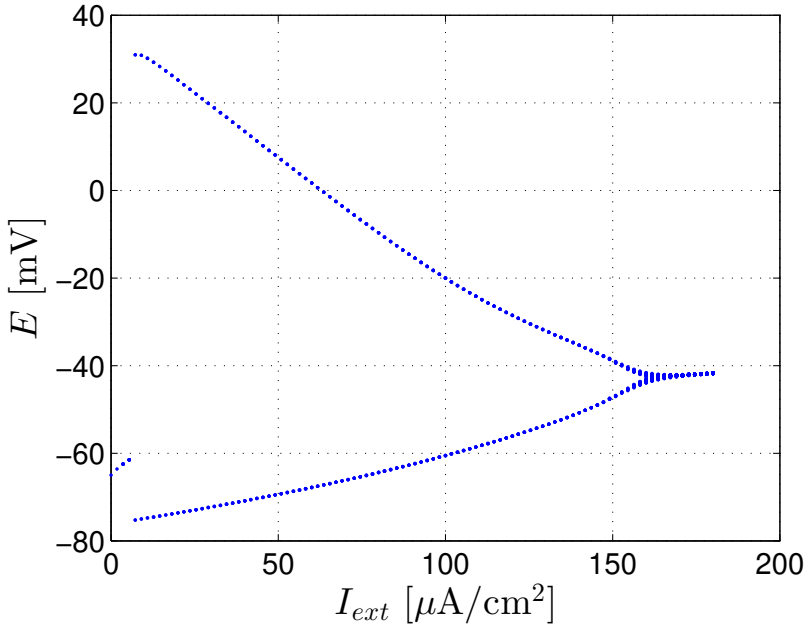

Figure 2.7: Bifurcation diagram of HH neuron model

2.1.3.3 Numerical solution

The course of an action potential is divided into four stages: resting, polarization, depolarization, and hyperpolarization. These stages are observed in Figure 2.8, which correspond to the following time intervals: $[0, 5), [5, 6.491), [6.491, 9.113), [9.113, 20)$.

At the resting stage — $t \in [0, 5)$ —, the potassium channels are open, and sodium channels are closed but capable of opening. As a result, K^+ ions leave the cell while Na^+ ions remain stationary, resulting in the membrane voltage at -65mV.

The application of an external current — $t = 5$ — yields the polarization stage during $t \in [5, 6.491)$, which begins when the sodium channel pores are unobstructed by the activation and inactivation gate respectively —*i.e.* the sodium channel is open as shown in Figure 2.5b —therefore Na^+ ions are free to enter the cell.— As more potassium channels open up, an increasing number of K^+ ions leave the cell, causing the membrane potential to increase until it reaches a maximum value (41.4 mV) at $t \approx 6.491$.

During the depolarization stage — $t \in [6.491, 9.113)$ —, the inactivation gates of the sodium channels block sodium channel pores — *i.e.* the sodium channels close as depicted in Figure 2.5c.— While more potassium channels close, less K^+ ions continue to leave the cell.

During the hyperpolarization phase $t \in [9.113, 20)$, the neuron voltage drops below its resting value because the sodium channels remain closed, while the potassium channels remain open; as a consequence, the K^+ ions continue to leave the cell.

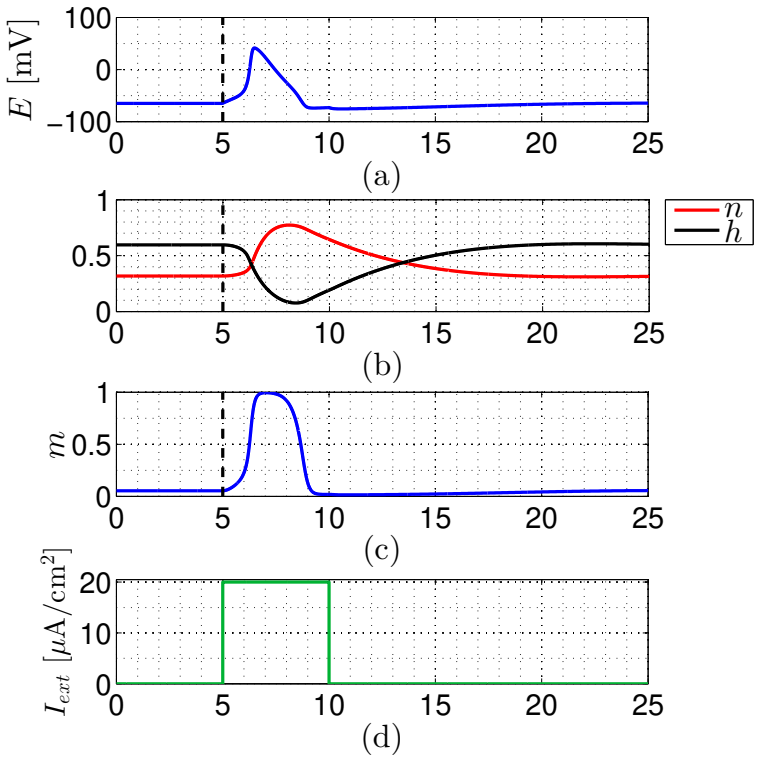

Figure 2.8: Temporal dynamics of the Hodgkin–Huxley neuron model under external stimulation: (a) membrane potential $E(t)$ showing an action potential triggered by the applied current (b) gating variables n (activation of potassium channel) and h (inactivation of sodium channels) (c) activation variable m (sodium channel activation), and (d) external current stimulus I_{ext} applied over a finite interval

For $t > 20$, the membrane potential returns to its resting state. The action potential can also be observed in the state space as a limit cycle. Figure 2.8 shows a projection of the state space in the $n - E$ plane.

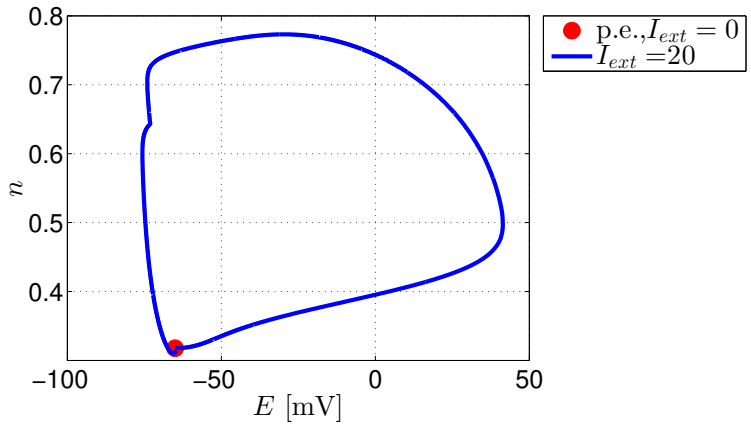

Figure 2.9: Phase-plane representation of the Hodgkin–Huxley model in the (E, n) space, showing the trajectory under a constant external current $I_{ext} = 20$. The red point denotes the equilibrium point corresponding to $I_{ext} = 0$.

As can be seen in Figure 2.8(b) and (c), the state variable m changes faster over time than n and h. This can also be illustrated by graphing the functions $\tau_n(E)$, $\tau_m(E)$, $\tau_h(E)$, which correspond to equations (2.21b)-(2.21b) respectively.

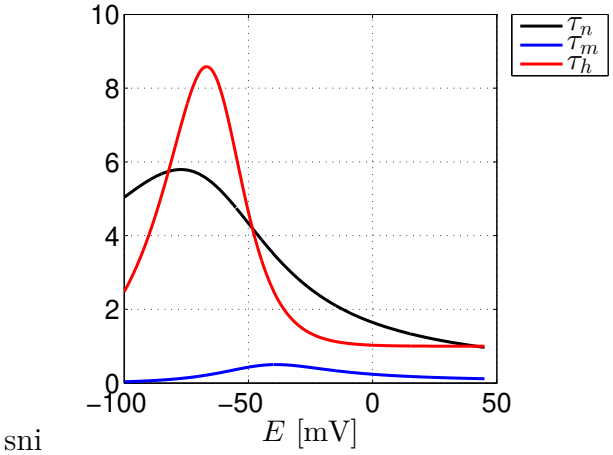

sni

Figure 2.10: Voltage dependence of the time constants τ_m, τ_n, and τ_h in the Hodgkin–Huxley model as functions of the membrane potential E.

Figure 2.10 shows $\tau_m(E) << \tau_{n,h}(E)$ for $E \in [-100, 50]$, which means that m evolves faster in time than n, h for $E \in [-100, 50]$. The above observation led Krinskii and Kokoz [24] to propose a reduced model for the HH neuron model (2.29), which consisted of a system of two differential equations, as described in the following.

2.1.4 Krinskii and Kokoz neuron model

The Krinskii and Kokoz model [24], known as the Krinskii-Kokoz (KK) neuron model, was obtained by reducing the order of the HH neuron model (2.29) to a second-order system. Such a reduced model significantly decreased the number of terms in the dynamic analysis in comparison to the HH model, for example, local stability analysis of equilibrium points. Furthermore, it allows us to use graphical analysis tools such as phase diagrams.

The state variable m, which is associated with the activation gate of the sodium channel, reaches its limiting value —given by the function $m_\infty(E)$— faster than the variable n, associated with the inactivation gate of the sodium channel. The first consideration, on HH neuron model reduction, was that the dynamics for m is infinitely fast, which can be replaced by its instantly reached value $m_\infty(E)$. The second consideration was that $n + h = 1$; for more reference on such reduction see reference [24].

$$\dot{E} = \frac{1}{C}\left\{\frac{I_{ext}}{\mathrm{A}} - \bar{g}_K n^4(E - E_K) - \bar{g}_{Na} m_\infty^3(E)(1-n)(E - E_{Na}) - \bar{g}_{Cl}(E - E_{Cl})\right\} \tag{2.41a}$$

$$\dot{n} = \alpha_n(E)(1-n) - \beta_n(E)n \tag{2.41b}$$

$$m_\infty(E) = \frac{\alpha_m(E)}{\alpha_m(E) + \beta_m(E)}$$

The neuron model (2.29) can be rewritten as follows:

$$\dot{x} = f_{KK}(x) \tag{2.42}$$

where $x = (E, n)^\top \in \mathbb{R}^2$ and $f(\cdot) = (f_1(\cdot), f_2(\cdot))^\top \in \mathbb{R}^2$, with $f_1(x), f_2(x)$ functions described by the left side of equations (2.41a)-(2.41b) respectively.

2.1.4.1 Dynamical Analysis

Equilibrium Point Analysis

Equilibrium points are obtained by solving the following polynomial:

$$\begin{aligned} &I_{ext} - g_{Cl}(E - E_{Cl}) - g_K\left[\frac{\alpha_n(E)}{\alpha_n(E) + \beta_n(E)}\right]^4 (E - E_K) \\ &- g_{Na} m_\infty^3(E)\left[1 - \left(\frac{\alpha_n(E)}{\alpha_n(E) + \beta_n(E)}\right)\right](E - E_{Na}) = 0 \end{aligned} \tag{2.43}$$

As a result we have three equilibrium points for $I_{ext} = 0$ which are $(-49.0529, 0.5643)^\top$, $(-21.5180, 0.8270)^\top$, $(-64.8322, 0.3203)^\top$

The Jacobian matrix of the Krinskii and Kokoz neuron model is:

$$D_x f_{KK} = \begin{bmatrix} \frac{\partial f_1}{\partial E} & \frac{\partial f_1}{\partial n} \\ \frac{\partial f_2}{\partial E} & \frac{\partial f_2}{\partial n} \end{bmatrix} \tag{2.44}$$

$$\frac{\partial f_1}{\partial E} = -g_k n^4 - g_{Na}(1-n)\left(3E\frac{dm_\infty}{dE}m_\infty^2(E) + m_\infty^3(E) - 3E_{Na}\frac{dm_\infty}{dE}m_\infty^2(E)\right) - g_{CL} \quad (2.45)$$

$$\frac{\partial f_1}{\partial n} = -4g_K n^3\left(E - E_K\right) + g_{Na}m_\infty^3(E)(E - E_{Na}) \quad (2.46)$$

$$\frac{\partial f_2}{\partial E} = \left[\frac{0.01}{\left(1 - e^{-\left\{\frac{E+55}{10}\right\}}\right)} - \frac{0.01(E+55)\frac{1}{10}e^{-\left\{\frac{E+55}{10}\right\}}}{\left(1 - e^{-\left\{\frac{E+55}{10}\right\}}\right)^2}\right](1-n) + \frac{n}{640}e^{-\left\{\frac{E+65}{80}\right\}} \quad (2.47)$$

$$\frac{\partial f_2}{\partial n} = -\frac{0.01(E+55)}{\left(1 - e^{-\left\{\frac{E+55}{10}\right\}}\right)} - 0.125e^{-\left\{\frac{E+55}{80}\right\}} \quad (2.48)$$

$$\frac{dm_\infty}{dE} = \frac{\left[\frac{0.1\left(\left(1-e^{-\left\{\frac{E+40}{10}\right\}}\right)-0.1(E+40)e^{-\left\{\frac{E+40}{10}\right\}}\right)}{\left(1-e^{-\left\{\frac{E+40}{10}\right\}}\right)^2}\right]4e^{-\left\{\frac{E+65}{18}\right\}} + 4\left[\frac{0.1(E+40)e^{-\left\{\frac{E+65}{18}\right\}}}{18\left(1-e^{-\left\{\frac{E+40}{10}\right\}}\right)}\right]}{\left[\frac{0.1(E+40)}{\left(1-e^{-\left\{\frac{E+40}{10}\right\}}\right)} + 4e^{\left\{\frac{-(E+65)}{18}\right\}}\right]^2} \quad (2.49)$$

The Jacobian matrix of the Krinskii and Kokoz neuron model is:

$$J(x)\Big|_{Q_1=(-64.8322,0.3203)^\top} = \begin{bmatrix} -0.1711 & -59.7189 \\ 0.0018 & -0.1835 \end{bmatrix} \quad (2.50)$$

eigenvalues are $\lambda_1 = -0.1773 + 0.3296i, \lambda_2 = -0.1773 - 0.3296i$, which corresponds to a stable focus.

$$J(x)\Big|_{Q_2=(-49.0529,0.5644)^\top} = \begin{bmatrix} 20.6000 & -961.3056 \\ 0.0019 & -0.2351 \end{bmatrix} \quad (2.51)$$

eigenvalues are $\lambda_1 = 120.5128, \lambda_2 = -0.1479$, which corresponds to a saddle node.

$$J(x)\Big|_{Q_3=(-21.5180,0.8270)^\top} = 1 \times 10^{-3}\begin{bmatrix} 0.0057 & -9.9771 \\ 0.0000 & -0.0004 \end{bmatrix} \quad (2.52)$$

eigenvalues are $\lambda_1 = 3.7851, \lambda_2 = 1.5353$, which corresponds to a unstable node.

The equilibrium points, nullclines, and vector field diagram of the KK neuron model, with $I_{ext} = 0$, are plotted in the phase plane illustrated in Figure 2.11.

The system (2.41a)-(2.41b) are:

$$f_1(E,n) = \frac{I_{ext}}{\mathrm{A}} - \bar{g}_K n^4(E - E_K) - \bar{g}_{Na}m_\infty^3(E)(1-n)(E - E_{Na}) - \bar{g}_{Cl}(E - E_{Cl}) \quad (2.53a)$$

$$f_2(E,n) = \alpha_n(E)(1-n) - \beta_n(E)n \quad (2.53b)$$

The vector field vectors are unitary and then scaled to fit properly in the phase plane. The vector field diagram shows that for any initial condition $(E(0), n(0))^\top \in [-80, 45] \times [0, 1]$, the variable E evolves faster than n; given that the second component of the vector $f_{KK}(E, n) = (f_1(E, n), f(E, n))^\top$ with $E, n \in [-80, 45] \times [0, 1]$, is considerably smaller compared to the first component. For this reason, (2.53a) and (2.53b) are called fast and slow nullclines, respectively.

If $E(0) \in (-64.8322, -21.5180)$, the trajectory moves horizontally away from the $E-$nullcline, in the appropriate direction. Until it reaches the $E-$nullcline, causing the trajectory to change its direction, moving very close to the $E-$nullcline, until it reaches Q_1 or Q_3. If the trajectory approaches to Q_2, through the $E-$nullcline, it moves away from Q_2, given that Q_2 is an unstable equilibrium point. On the other hand, if the trajectory is near Q_1, then it stays there, given that Q_1 is a locally stable equilibrium point.

Upon an external current $I_{ext} = 40$, the $E-$nullcline moves upwards as depicted in Figure 2.12. A closed trajectory is formed that passes through the points P_1, P_2, Q_3, P_3.

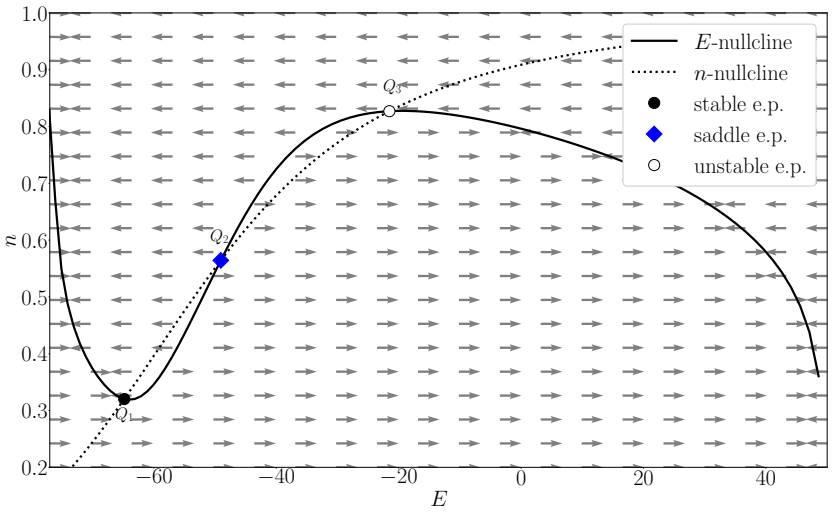

Figure 2.11: Nullcline analysis of the Krinskii–Kokoz neuron model in the (E, n) phase plane. The solid curve represents the E-nullcline, while the dotted curve corresponds to the n-nullcline. Their intersections define equilibrium points, classified as stable (black circle), saddle (blue diamond), and unstable (white circle). The vector field illustrates the system dynamics in the phase space.

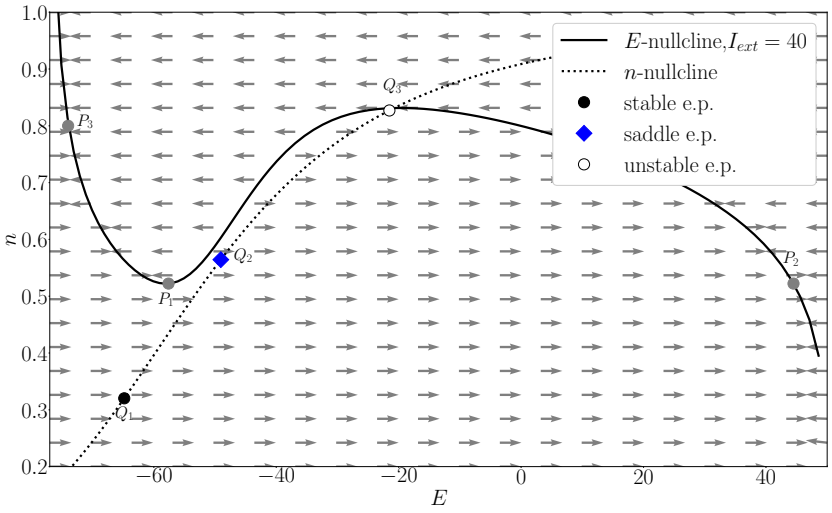

Figure 2.12: Nullcline analysis of the Krinskii–Kokoz neuron model in the (E, n) phase plane under $I_{ext} = 40$. The solid curve represents the E-nullcline, while the dotted curve corresponds to the n-nullcline. Their intersections define equilibrium points, classified as stable (black circle), saddle (blue diamond), and unstable (white circle). The vector field illustrates the system dynamics in the phase space.

2.1.4.2 Bifurcation Diagram

The Krinskii-Kokoz neuron model includes external current as a parameter. A bifurcation diagram of neuron model (2.41a)-(2.41b) is obtained through Matlab by setting as an initial condition the resting state $(-64.8322, 0.3203)^\top$ and varying the external current I_{ext}. Such numerical analysis shows a bifurcation point at $I_{ext} = 1.737$, corresponding to the transition from an equilibrium point to a limit cycle.

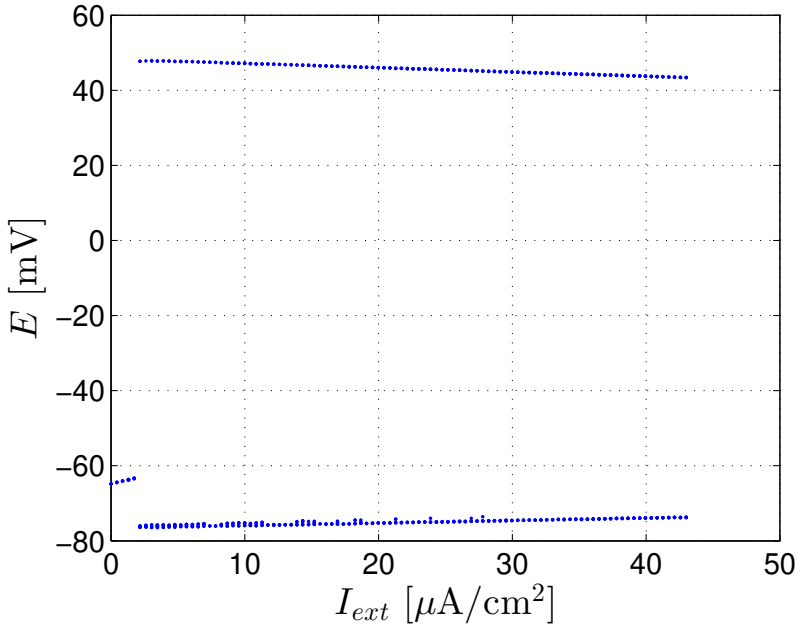

Figure 2.13: Dependence of the membrane potential E on the external current I_{ext} for the the Krinskii–Kokoz neuron model. The diagram shows the transition from a resting state to sustained oscillatory behavior as the external current increases.

2.1.4.3 Numerical solution

The numerical simulation of the KK model is obtained using Matlab. An external current is configured as a pulse that starts at $t = 10$ and ends at $t = 20$. In Figure 2.14, the graph of voltage versus time is observed, and it is observed that the voltage of the neuron changes from the resting state to a periodic behavior that corresponds to the *firing* state of the neuron. In figure 2.15, the periodic behavior is observed as a limit cycle in the phase plane.

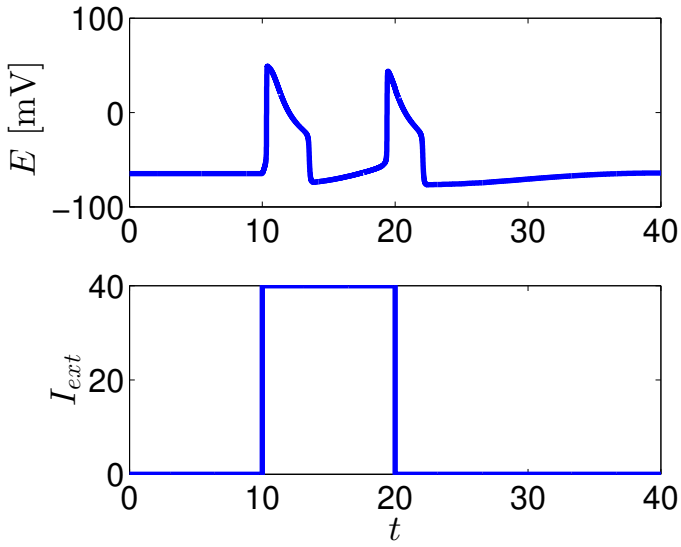

Figure 2.14: Temporal dynamics of the Krinskii–Kokoz neuron model under external stimulation: (a) membrane potential $E(t)$ showing an action potential triggered by the applied current (b) external current stimulus I_{ext} applied over a finite interval

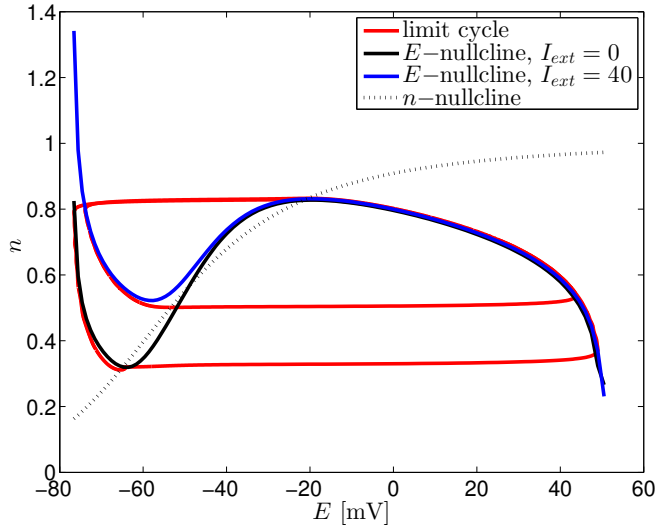

Figure 2.15: Phase-plane dynamics of the Krinskii–Kokoz neuron model in the (E, n) space. The E-nullclines for $I_{ext} = 0$ and $I_{ext} = 40$ are shown along with the n-nullcline. The red curve represents a stable limit cycle, indicating oscillatory (spiking) behavior arising from changes in the external current.

2.1.5 FitzHugh–Nagumo neuron model

One of the main features of the KK model is the cubic form of the $E-$nullcline, while the $n-$nullcline is a monotonically increasing function. FitzHugh [25] proposed a simplified model

—which is based on the van der Pol model— whose nullclines are similar to the KK model. Later, Nagumo [26] presented the equivalent circuit of the model [25]. The model's name is FitzHugh-Nagumo (FN), after both authors FitzHugh and Nagumo.

$$\dot{V} = g(V) - w + I \tag{2.54a}$$
$$\dot{w} = \epsilon(V - \gamma w) \tag{2.54b}$$

where V is the membrane potential (fast variable), and w (slow variable) represents the "recovery" actions of sodium channel deinactivation and potassium channel deactivation, with $0 < a < 1$, $\epsilon > 0$, $\gamma \geq 0$, $g(V) = V(V-a)(1-V)$ a third order polynomial. We can consider the fixed constants $a = 0.1, \epsilon = 0.005, \gamma = 0.5$. Notice if $I = 0$ and $\gamma = 0$ the system corresponds to the classic Van der Pol oscillator.

2.1.5.1 Dynamical Analysis

Equilibrium Point Analysis

Considering the above parameters and $I = 0$, the unique equilibrium point of (2.54a)-(2.54b) is the origin $(V_{eq}, w_{eq})^\top = (0, 0)^\top$. The eigenvalues of the system (2.54a)-(2.54b) Jacobian matrix evaluated at the origin are:

$$\lambda_{1,2} = \frac{-(\epsilon\gamma + a) \pm \sqrt{a^2 - 2\epsilon\gamma a + (\epsilon\gamma)^2 - 4\epsilon}}{2}$$

For $a = 0.1, \epsilon = 0.005, \gamma = 0.5$ the eigenvalues are $\lambda_{1,2} = -0.0512 \pm 0.0512i$, which corresponds to a stable focus.

The simplicity of this model presents the advantage of analytically analyzing the birth of other dynamic behaviors, such as periodic oscillations, due to the presence of the external current I. In the first instance, the following shows that the equilibrium point of the system depends on I, which can also be observed graphically through the system nullclines. The nullclines of the system (2.54a)-(2.54b) are obtained as follows.

V-nullcline:

$$w = g(V) + I \tag{2.55}$$

w-nullcline:

$$w = V/\gamma \tag{2.56}$$

where (2.55) and (2.56) correspond to the fast and slow nullcline respectively. The intersection of (2.55) and (2.56) give us the equilibrium point $(V_e, w_e)^\top \in \mathbb{R}^2$ of the system (2.54a)-(2.54b). It is observed equilibrium voltage V_e depends on I. Furthermore, V_e satisfies the following equation:

$$-V_e^3 + (a+1)V_e^2 - \left(a + \frac{1}{\gamma}\right) V_e + I = 0 \tag{2.57}$$

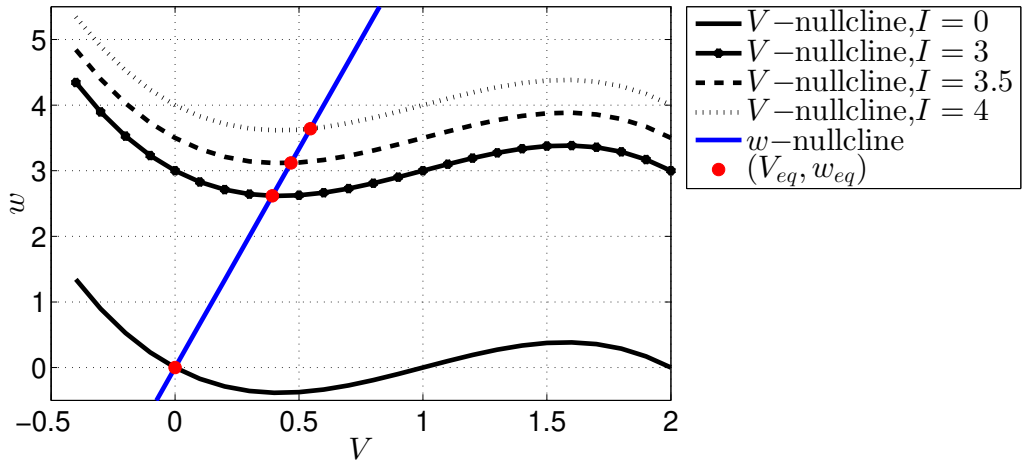

Figure 2.16: Nullcline analysis of the FitzHugh–Nagumo neuron model in the (V, w) phase plane. The V-nullclines are shown for different values of the input current I, while the w-nullcline is represented by the blue line. Their intersections define the equilibrium points (V_{eq}, w_{eq}), which vary with I.

From Figure (2.16) is observed that increasing the value of I causes the equilibrium point (V_e, w_e) to move from the left branch to the right branch of $V-$nullcline. A natural question that arises is the stability of the equilibrium point $(V_e, w_e)^\top$ for a given I. The system (2.54a)-(2.54b) can be rewritten in vector form as follows:

$$\dot{x} = f_{FN}(x) \tag{2.58}$$

where $x = (V, w)^\top \in \mathbb{R}^2$ and $f_{FN}(\cdot) = (f_1(\cdot), f_2(\cdot))^\top$, where $f_1(\cdot)$, $f_2(\cdot)$ are given by the left side of equations (2.54a),(2.54b) respectively.

The Jacobian matrix of (2.54a)-(2.54b) when $I \neq 0$ is:

$$D_x f_{FN} = \begin{pmatrix} \frac{dg}{dV} & -1 \\ \epsilon & -\gamma\epsilon \end{pmatrix} \tag{2.59}$$

where $\frac{dg}{dV} = 3V^2 + 2V(a+1) - a$. Let $J_{FN} = D_x f_{FN}\Big|_{V=V_{eq}}$, let $g'(V_e) = \frac{dg}{dV}\Big|_{V=V_e}$, the eigenvalues of matrix J_{FN} are given by:

$$\lambda_{1,2}(V_e) = \frac{1}{2}\left(g'(V_e) - \gamma\epsilon\right) \pm \frac{1}{2}\sqrt{(g'(V_e) - \gamma\epsilon)^2 - 4\epsilon(1 - \gamma g'(V_e))} \tag{2.60}$$

If $\Re\{\lambda_{1,2}(V_e)\} = 0$ where $\Re(\cdot)$ denotes the real part, the equilibrium point (V_e, w_e) is non-hyperbolic. Through bifurcation theory, it is determined the type of behavior that arises. Figure 2.17(a) shows the plot of the Fitz-Hugh Nagumo eigenvalues $\Re(\lambda_{1,2})$ vs $\Im(\lambda_{1,2})$ in the complex plane with respect to the parameter V_e. The characteristic loop pattern indicates that the eigenvalues start as complex conjugates, move toward the real axis, and then separate. The point where they cross the imaginary axis $\Re(\lambda_{1,2}) = 0$ marks the Hopf bifurcation point. Given that $\lambda_{1,2}(V_e)$ is a convex quadratic function of V_e, there are two

values of V_e, for which $\Re(\lambda_{1,2}(V_e)) = 0$. This Hopf bifurcation is expected to appear when $V_{e1} = 0.42918$ and $V_{e2} = 1.5708$ as shown in Figure 2.17(b) as a result, this zero-crossing is the Hopf bifurcation point where the system transitions from a stable fixed point to oscillatory behavior (limit cycle). In particular, when $V_e = 0.0568$, $\Re(\lambda_{1,2}(V_e)) = 0$, which correspond to $I = 0.0498$.

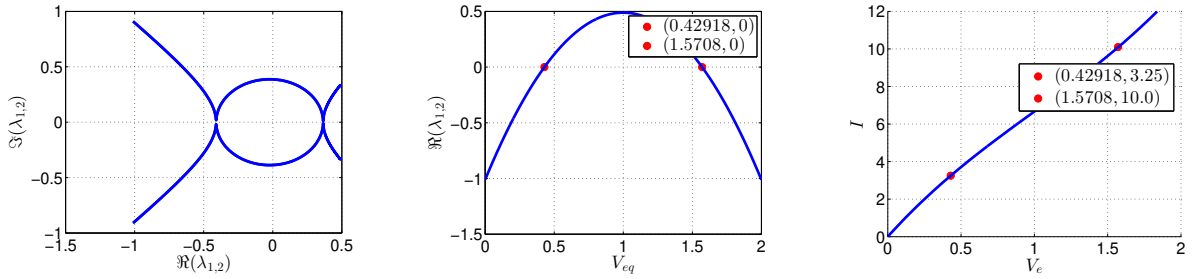

(a) (b) (c)

Figure 2.17: (a) Eigenvalue trajectory in the complex plane. The plot displays $\Re(\lambda_{1,2})$ vs $\Im(\lambda_{1,2})$, showing how the eigenvalues move as the neuron voltage V_e changes. (b) Bifurcation diagram showing $\Re(\lambda_{1,2})$ vs the parameter V_e. (c) The relationship between V_e and external current I

2.1.5.2 Bifurcation Diagram

Considering the external current I of the FN neuron model as a parameter. A bifurcation diagram of neuron model (2.41a)-(2.41b) is obtained through Matlab by setting as an initial condition the resting state $(-64.8322, 0.3203)^\top$ and varying the external current I_{ext}. Such numerical analysis shows one bifurcation point at $I_{ext} = 1.737$, which corresponds to the transition from an equilibrium point to a limit cycle.

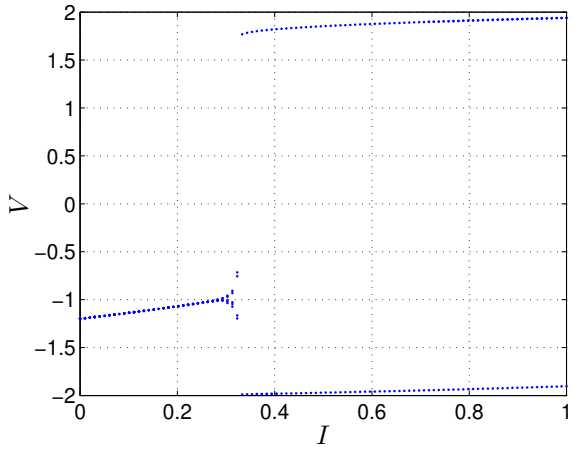

Figure 2.18: Bifurcation Diagram of FN neuron voltage vs External Current

2.1.6 Hindmarsh and Rose neuron model

After reaching a milestone in characterizing the electrical behavior of nerve cells in the giant squid [23], subsequent studies emerged focusing on the electrical activity of nerve cells in other invertebrates, like the Mollusca [4] and Aplysia [5].

In [5], it was reported that when the Aplysia neuron membrane, initially silent, was depolarized by a short current pulse, the neuron voltage showed periods of rapid and successive spikes for a time that greatly exceeded the stimulus, as shown in Figure 2.20. This behavior was also observed in the membrane potential of Lymnaea stagnalis when subjected to a short depolarizing current pulse [6]. One dynamic model that captures such behavior is proposed by [6] —in view of which it is known as the Hindmarsh-Rose (HR) neuron model—.

$$\begin{aligned} \dot{x}_1 &= x_2 - ax_1^3 + bx_1^2 + I_{ext} \\ \dot{x}_2 &= c - x_2 - dx_1^2 \end{aligned} \tag{2.61}$$

where x_1 is the neuron membrane potential, x_2 is called the recovery variable as in the FN model and $a = 1, b = 3, c = 1, d = 5$. The model (2.61) is commonly referred to as the two-dimensional HR neuron model due to the number of state variables it encompasses.

There exist three equilibrium points of the system (2.61) without external current $I_{ext} = 0$, which are $Q_1 = (-1.6180, -12.0901)^\top$,$Q_2 = (-1, -4)^\top$,$Q_3 = (0.6180, -0.9098)^\top$.

The nullclines of the system (2.61):

x_1-nullcline:

$$x_2 = -ax_1^3 + bx_1^2 + I_{ext} \tag{2.62}$$

x_2-nullcline:

$$x_2 = x - dx_1^2 \tag{2.63}$$

The e.p. Q_1,Q_2,Q_3 correspond to a stable node, saddle and unstable focus.

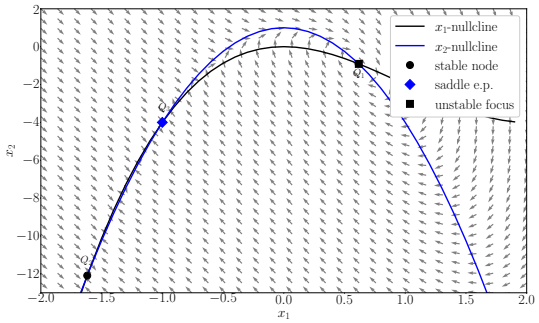

Figure 2.19: Nullcline analysis of the Hindmarsh-Rose neuron model in the x_1 and x_2 plane. The solid black curve represents the x_1 nullcline, the solid blue curve represents the x_2 nullcline. Gray arrows show the direction field indicating trajectory flow. The intersection of the x_1 and x_2 nullclines are the equilibrium points, with different symbols indicating their stability types as shown in the legend

Notice one of the main differences between the FN neuron model (2.54a)-(2.54b) and (2.61) is that the w-nullcline in the first model is linear while the x_2-nullcline is quadratic.

The simplicity of this model presents the advantage of analytically analyzing the birth of other dynamic behaviors, such as periodic oscillations, due to the presence of the external current I.

In the first instance, the following shows that the equilibrium point of the system depends on I, which can also be observed graphically through the system nullclines.

2.1.6.1 Dynamical Analysis

Equilibrium Point Analysis

$$\begin{aligned} 0 &= x_2 - ax_1^3 + bx_1^2 + I_{ext} \\ 0 &= c - x_2 - dx_1^2 \end{aligned} \tag{2.64}$$

Furthermore, the neuron did not fire indefinitely but slowed down and terminated with a slow after-hyperpolarizing wave [4].

This type of neural oscillation is called a burst. The period between bursts of activity is called an interburst interval, while the period between two adjacent spikes is named an interspike interval.

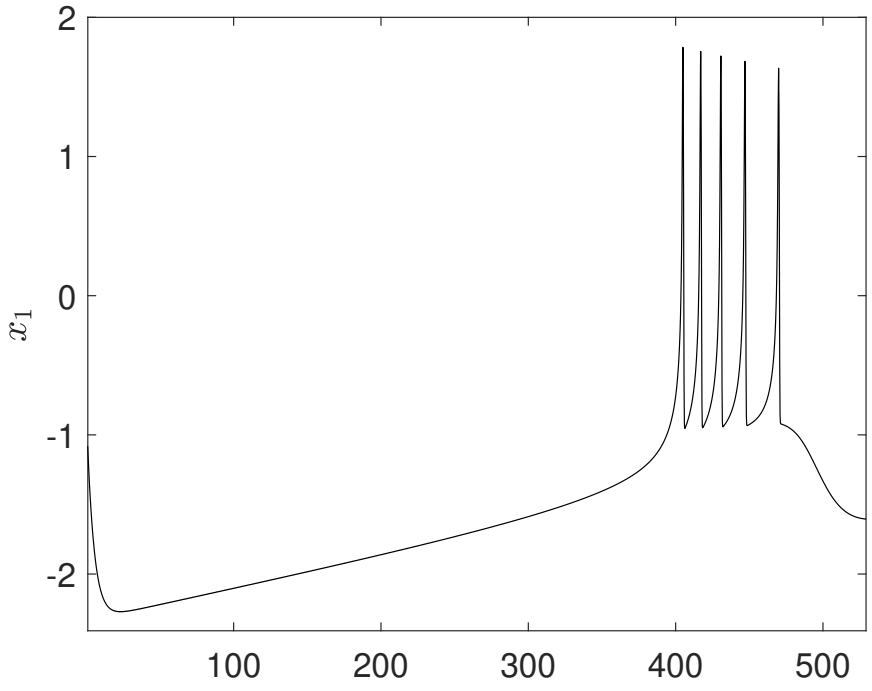

Figure 2.20: Bursting neural oscillation obtained from Hindmarsh-Rose neuron model

$$\begin{aligned}\dot{x}_1 &= x_2 - x_3 - ax_1^3 + bx_1^2 + I_{ext}\\ \dot{x}_2 &= c - x_2 - dx_1^2\\ \dot{x}_3 &= \varepsilon\left[\sigma\left(x_1 - x_0\right) - x_3\right]\end{aligned} \tag{2.65}$$

2.2 Synapse models

Although Ramon y Cajal findings was one of the major milestones in neuroscience, the transmission mechanisms among neurons were uncertain. It was until 1930 that Otto Loewi discovered the first chemical transmitted at the synapse, called *neurotransmitter*. From a neuroscience point of view, the synapse is a site where a neuron's dendrite is aligned with another neuron's axon terminal. The small space between both structures is called *synaptic cleft*, where electro-chemical signals are exchanged [27]. The mechanisms of chemical transmission were set up with Loewi experiments. Upon the arrival of an action potential to the neuron, which is called presynaptic neuron, the neurotransmitters are generated inside the neuron then released at the synaptic cleft and received by receptors in the receiving neuron, which is called postsynaptic neuron. The process is illustrated in figure 2.21.

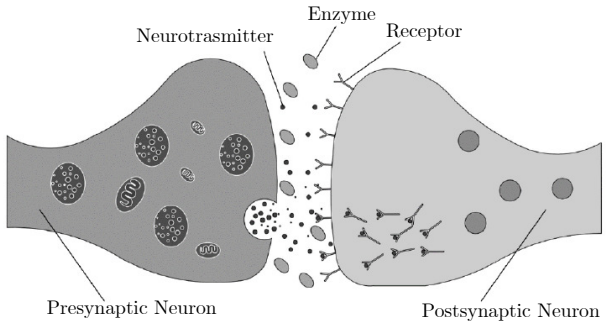

Figure 2.21: Schematic of a chemical synapse with a single active zone.

There is another specialized structure of connection called a gap junction, where the adjacent neurons are close together, forming a direct channel. This type of connection is also known as an electrical synapse. In an electrical synapse, ions flow through channels from one neuron to another. Ions' movement is triggered by the voltage difference between paired neurons, and they flow at a constant rate in either direction.

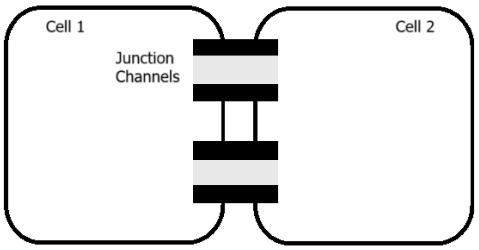

Figure 2.22: Schematic of a gap junction connection between two apposed neurites (dendrites or axons)

The electrical synapse can be characterized through an electrical circuit model, which in turn describes the postsynaptic response generated by the arrival of an action potential at the presynaptic terminal. In the case of the electrical synapse, as the ions flow directly from one neuron to another, it allows us to model the synapse as an electrical current that obeys Ohm's Law.

The purpose of these sections is to describe the chemical and electrical synapse models.

2.2.1 Chemical synapse

When a neurotransmitter is released into the synaptic cleft, it interacts with specialized receptors located on the postsynaptic membrane. This binding process triggers the opening of ion channels, allowing specific ions to flow in or out of the cell. These channels remain open for a limited duration, which determines both the length of time the ions can pass through and the volume of ions that enter or exit. In other words, conductance determines current.

The electrical current resulting from the release of a unit amount of neurotransmitter at time $t \geq t_s$ is:

$$i_{syn}(t) = g_{syn}(t)(v_{pos}(t) - v_{syn}) \tag{2.66}$$

where $g_{syn}(t)$ is the synaptic conductance which is function of time that represents the conductance change due to the opening of the postsynaptic receptors, v_{pos} is the voltage across the postsynaptic membrane, and v_{syn} represents the Nernst potential of the channels which are activated by the neurotransmitters. The two primary neurotransmitters in the mammalian nervous system are glutamate and α-aminobutyric acid.

The α-amino-3- *hydroxil-5-methyl-4-isoxazole-propinate* (AMPA) receptor mimics the effect of glutamate on the receptor. Channels activated by AMPA neurotransmitter are permeable to sodium Na^+ and potassium K_+ ions. The Nernst potential for channels permeable to sodium ions is v_{Na^+} =70mV, while for potassium ions, it is v_{K^+} = -110mV. Consequently, the Nernst potential associated with AMPA neurotransmitter is $v_{AMPA} \approx 0mV$. In contrast, channels activated by GABA are permeable to chloride ions Cl^- and their Nernst potential is v_{K^+} =68mV.

Additionally, the synaptic conductance $g_{syn}(t)$ has been characterized by Rall in his work [28] as a transient conductance exhibiting exponential decay.

$$g_{syn}(t) = \bar{g}_{syn} \exp\left(-\frac{t - t_s}{\tau}\right) \tag{2.67}$$

where $\bar{g}_{syn}$ is the average conductance ion channels activated by AMPA or GABA neurotransmitters as it correspond, t_s is the time of the presynaptic spike, τ is the time constant which determines how fast the conductance decays over time.

In [28], synaptic conductance was described as increasing gradually as channels open and then decaying exponentially after the channels close. This type of function is referred to as an *alpha* function and is expressed by:

$$g_{syn}(t) = \bar{g}_{syn} \frac{t - t_s}{\tau} \exp\left(-\frac{t - t_s}{\tau}\right) \tag{2.68}$$

2.2.2 Electrical synapse

The channels in a gap junction allow ions and other small molecules to flow rapidly and bidirectionally between cells. In [29], it is proposed that the gap junction has the property of permeability. Thus, this behavior allows us to model the synapse as an electrical current that obeys Ohm's Law, hence its *electrical* character [29]. The electrical circuit is depicted in Figure 2.23.

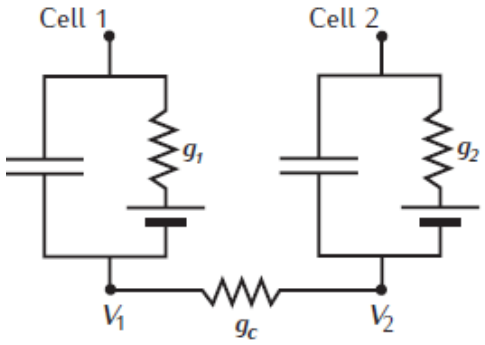

Figure 2.23: Equivalent circuit of gap junction

Where V_1, V_2 are the membrane potentials of cell one and cell two, respectively. Although this connection is simple, it gives rise to complex behavior, which is analyzed as follows. The current that flows from Cell 2 into Cell 1.

$$I_1 = g_c(V_2 - V_1) \tag{2.69}$$

while the current that flows from Cell 1 into Cell 2 is given by:

$$I_2 = g_c(V_1 - V_2) \tag{2.70}$$

Assume that voltage V_1 is held constant by injecting a current into Cell 1. Applying Kirchhoff's current law at node V_2 gives:

$$(V_1 - V_2)g_c = V_2 g_2 \tag{2.71}$$

rearranging 2.71 is obtained:

$$\frac{V_2}{V_1} = \frac{g_c}{g_2 + g_c} \tag{2.72}$$

assuming steady state of capacitor $\frac{dV_2}{dt} = 0$, from 2.72 it can be seen that $V_1 > V_2$ if $g_2 > 0$, which means that the V_2 is attenuated with respect to V_1. Similarly if V_2 is held constant the attenuation is:

$$\frac{V_1}{V_2} = \frac{g_c}{g_1 + g_c} \tag{2.73}$$

Synaptic strength is not fixed as in electrical synapse model and is determined not only by the opening of postsynaptic receptors as in the chemical synapse, but also by the temporal relationship between pre- and postsynaptic activity. When a sequence of action potentials arrives at the presynaptic terminal, the amplitude and time evolution of the postsynaptic response vary depending on the type of synapse and the activity history.

2.2.3 Synaptic Plasticity Mechanisms

Synaptic transmission can be modulated through several activity-dependent mechanisms. Among the most studied are facilitation, potentiation and depression, each involving distinct biophysical processes that regulate neurotransmitter release.

The first mechanism, facilitation, occurs when action potentials arrive in rapid succession. Each time an action potential reaches the presynaptic terminal, it causes the release of residual calcium. This accumulation of calcium from previous stimuli results in a greater release of neurotransmitter with each successive action potential. Consequently, the concentration of neurotransmitter in one instant is higher than in the previous instant. Recovery from facilitation is established in few hundreds of milliseconds following the termination fo the stimulation.

The second mechanism, potentiation, typically involves the activation of N-methyl-D-aspartate (NMDA) receptors during sufficient postsynaptic depolarization. This causes an influx of calcium ions (Ca^{2+}) in to the postsynaptic neuron, which results in an increase in AMPA receptors. After potentiation, the same presynaptic spike will produce a larger postsynaptic response. This strengths the synaptic connection between neurons. Under certain conditions potentiation can last for a very long amount of time, which can consolidate into long-term potentiation.

Finally depression, when high frequency stimulation occur, voltage-gated calcium channels open and Ca^{2+} ions flow. This sudden rise of calcium concentration causes vesicles fuse with the presynaptic membrane at specialized sites called active zones where their content is released into the synaptic cleft. The neurotransmitter diffusion occurs but the rate at which the vesicles release neurotransmitter is faster than the rate at which the vesicles are replenished. The number of active available vesicles at active zones decreases with each spike. This produces a weaker synaptic transmission strength.

2.3 Memristors

2.3.1 Mathematical Definition

The electrical response of the three fundamental two-terminal circuit elements is characterized by a relationship between the basic circuit variables: current i, voltage v, electric charge q, and magnetic flux φ. Out of the six possible combinations of these four variables, two are defined from the fundamental definition of voltage and current:

$$v = \frac{d\varphi}{dt} \tag{2.74}$$

$$i = \frac{dq}{dt} \tag{2.75}$$

alternatively (2.74) give us the definition of electric charge:

$$q(t) = \int_{-\infty}^{t} i(\tau)d\tau + q_0 \tag{2.76}$$

and (2.75) give us the definition of magnetic flux:

$$\varphi(t) = \int_{-\infty}^{t} v(\tau)d\tau + v_0 \tag{2.77}$$

The remaining four pairs can defined from the perspective of nonlinear circuit theory by a *constitutive relation*, an implicit relation of basic circuit variables [30]. The constitutive relation of a resistor is expressed by:

$$f(v, i) = 0 \tag{2.78}$$

The linear resistor is a special case in which:

$$f(v, i) = v - iR \tag{2.79}$$

where R is the resistance .This relation in equation (2.79) takes the explicit form, which is called Ohm's Law:

$$v = iR \tag{2.80}$$

The constitutive relation of a capacitor is defined in terms of charge and voltage.

$$f_C(q, v) = 0 \tag{2.81}$$

The linear capacitor is a special case in which:

$$f(q, v) = q - Cv \tag{2.82}$$

where C is the capacitance. This relation in equation (2.82) takes the explicit form:

$$q = Cv \tag{2.83}$$

The constitutive relation of an inductor is defined in terms of magnetic flux and the current flowing through it.

$$f_L(\varphi, i) = 0 \tag{2.84}$$

For a linear inductor, (2.84) simplifies to:

$$\varphi = Li \tag{2.85}$$

where L is the inductance (in Henrys). Critically, capacitance (C), inductance (L), and resistance (R) are not merely constants but emergent properties determined by both geometry and material properties.

In 1971, Chua proposed the existence of a fourth *theoretical* device, for which logical consistency and symmetry, the constitutive relation is defined as:

$$f_M(\varphi, q) = 0 \tag{2.86}$$

This device is named memristor (acronym for memory resistor), and it is charge-controlled if its constitutive relation can be expressed as:

$$\varphi = g_M(q) \tag{2.87}$$

or flux-controlled if its constitutive relation can be expressed as:

$$q = g_W(\varphi) \tag{2.88}$$

where f_M and g_W are continuous and piecewise-differentiable functions. Differentiating (2.87) and (2.88) with respect to time t, we obtain:

$$\frac{d\varphi}{dt} = \frac{d}{dq} g_M \frac{dq}{dt} \tag{2.89}$$

$$\frac{dq}{dt} = \frac{d}{d\varphi} g_W \frac{d\varphi}{dt} \tag{2.90}$$

rewriting (2.89) using (2.74) we obtain the charge-dependent Ohm's Law and electric charge dynamics for charge controlled memristor:

$$v = M(q)i \tag{2.91a}$$

$$\dot{q} = i \tag{2.91b}$$

where $M \triangleq \dfrac{d}{dq} g_M$ is called the memristance function and $M(q)$ is the memristance at electric charge q, which has units of Ohms (Ω).

Rewriting (2.90) using (2.75) we obtain the flux-dependent Ohm's Law and magnetic-flux dynamics for flux-controlled memristor:

$$i = W(\varphi)v \tag{2.92a}$$
$$\dot{\varphi} = v \tag{2.92b}$$

where $W \triangleq \dfrac{d}{d\varphi} g_W$ is the memductance function. Furthermore, $W(\varphi)$ is the memductance at φ, which has units of Siemens (S).

An important feature of this device is the non-volatility property; that is, once the input signal across its terminals becomes zero, its magnetic flux (electric charge *resp.*) remains fixed until the input signal changes again. This property is the reason for the device name, an acronym for "memory" and "resistor".

Among the different definitions of the memductance function $W(\cdot)$, in [31], it is proposed that the memductance function is constant by parts.

$$w(\varphi) = \begin{cases} b & , \quad \varphi < -l \\ a & , \quad -l \leq \varphi \leq l \\ b & , \quad l < \varphi \end{cases} \tag{2.93}$$

where a, b, l are positive constants and $a < b$. Other memductance functions can be found to be quadratic.

Other memductance functions can also be defined using smooth nonlinear functions, such as quadratic or hyperbolic tangent functions, which allow modeling saturation effects and bounded responses. For instance, a quadratic memductance function can be expressed as:

$$W(\varphi) = a\varphi^2 + b \tag{2.94}$$

where a and b are real constants chosen to ensure physical consistency of the model.

More generally, the choice of the memductance function $W(\cdot)$ plays a crucial role in determining the dynamical behavior of memristive systems, which are defined as follows.

In [7], a generalization of the original memristor proposed in [32] is introduced, known as memristive systems. These systems are characterized by a state and input-output equations expressed as follows:

$$\dot{x} = f(x, u) \tag{2.95a}$$
$$y = g(x, u)u \tag{2.95b}$$

where $u \in \mathbb{R}$ and $y \in \mathbb{R}$ denote the input and output of the system, $x \in \mathbb{R}^n$ denotes the state of the memristive system. Here $f : \mathbb{R}^n \times \mathbb{R} \to \mathbb{R}^n$ is a continuous vector function, $g : \mathbb{R}^n \times \mathbb{R} \to \mathbb{R}$ is a continuous scalar function. Moreover, it is assumed that the state equation (2.95a) has a unique solution $x(t : x_0)$ for any initial condition $x_0 \in \mathbb{R}^n$. Also, the output y is zero whenever the input is zero.

Memristive systems are *one-ports* or two-terminal *devices* when they interact with the external circuit through a single pair of electrical terminals, voltage, and current. One-port

Memristive Systems can be classified as either current-controlled or voltage-controlled. Both consists of two equations, a state-dependent Ohm's Law and state dynamics.

An n-th-order current-controlled memristive time-invariant one-port is represented by:

$$\dot{x} = f(x, i) \tag{2.96a}$$
$$v = g(x, i)i \tag{2.96b}$$

An n-th-order voltage-controlled memristive time-invariant one-port is represented by:

$$\dot{x} = f(x, v) \tag{2.97a}$$
$$i = h(x, v)v \tag{2.97b}$$

$x \in \mathbb{R}^n$ and f is similarly defined as in (2.96a); $h, g : \mathbb{R}^n \to \mathbb{R}$ are a continuous scalar functions and $g(x, 0) \neq \infty$, $h(x, 0) \neq \infty$. Memristive systems exhibit several distinguishing properties that set them apart from other nonlinear devices. In this section, the most relevant properties are presented for the theoretical framework.

A current-controlled memristive one-port time-invariant (2.96a),(2.96b) is *passive* if and only if the following hold:

$$g(x, i) \geq 0, \quad \forall x, i \tag{2.98}$$

proof of the previous property can be found in [7].

The memristive system (2.96a)-(2.96b) exhibits *non-volatile memory* if, for $u = 0$, the state dynamics satisfy:

$$f(x, u) = 0, \quad \forall x \in \mathbb{R}^n \tag{2.99}$$

therefore a continuum of equilibrium points $\pi_e = \{(x_e, 0)^\top \in \mathbb{R}^n \times \mathbb{R} : x_e \in \mathbb{R}^n\}$ is obtained. Furthermore, in [7], it is pointed out that the continuum of equilibrium points is stable [7]. Although this claim of stability is based on the physical behavior of the ideal memristor, rather than a mathematical proof of stability.

From (2.96a)-(2.96b), two particular subclasses of memristive systems are derived. *Generic* memristor is a particular case of a memristive system, when its output function only depends on the state variable x, that is, a current-controlled generic memristor is described by:

$$\dot{x} = f(x, i) \tag{2.100a}$$
$$v = g(x)i \tag{2.100b}$$

or equivalently, for a voltage-controlled generic memristor:

$$\dot{x} = f(x, v) \tag{2.101a}$$
$$i = h(x)v \tag{2.101b}$$

A subclass of a memristive system is classified as *ideal* when the time evolution of the state depends linearly on the input signal, for example:

$$\dot{x} = u \tag{2.102a}$$
$$y = g(x)u \tag{2.102b}$$

in this definition the state variable x corresponds to magnetic flux in the case of a charge-controlled ideal memristor and electric charge for a flux-controlled ideal memristor and $g : \mathbb{R}^n \to \mathbb{R}$ is a continuous scalar function. Memristor (2.91) and memductor (2.92) belong to the *Ideal* category.

2.3.2 Locally active memristors

Since the mathematical generalization of the concept of memristor in 1976 [7], a more flexible interpretation allows us to consider memristive devices that are not strictly passive; i.e., for some intervals of the memristor's internal variable, its memristance is negative, and it is therefore said to be locally active.

2.3.3 Experimental Definition

A memristor can be experimentally characterized; this method is called the axiomatic definition or black box definition of the device, and the internal composition of the device is irrelevant. The axiomatic definition includes device fingerprints that serve to identify the memristive nature of the system based on experimental data.

The first fingerprint of the memristor (2.91) and memductor (2.92) is characterized by Lissajous figures of the voltage-current relationship $((v(t), i(t)))$ in response to any periodic input signal, which are pinched at the origin. The pinched hysteresis loop is odd symmetric when the input source is driven by a half-wave odd symmetric.

A current-controlled memristive (voltage controlled *resp.*) one-port time-invariant system (2.96a)-(2.96b) (or (2.97a)-(2.97b)) exhibits a *pinched hysteresis*, at the origin in the sense $(i, v) = (0, 0)$, in the v-i plane when subjected to a periodic input *i.e.* $i(t) = I\cos(\omega t)$ ($v(t) = I\cos\omega t$ *resp.*). This pinched hysteresis is called in the literature *pinched hysteresis loop* (PHL). Furthermore, when the input signal of memristor (2.96a)-(2.96b) is a periodical signal described by an odd function of time, then the $(v - i)$ PHL will be odd symmetric, the proof of the property can be found [7].

The second property is referred to as *no energy discharge*, which says that memristors can not release stored energy to the external circuit *i.e.*, $\int_{-\infty}^{t} p(\tau)d\tau \geq 0$, where $p(\tau) = v(\tau)i(\tau)$ is the instantaneous power. As a result, the PHL loop is confined to the first quadrant when $v, i > 0$ and in the third quadrant when $v, i < 0$ of the $v - i$ plane.

The third property is called *limiting linear characteristics* if the time-invariant current controlled memristive one-port bounded input bounded-state stable, then under periodic input as the frequency $\omega \to \infty$, then the system (2.96a)-(2.96b) behaves as a linear time-invariant resistor. The same property holds for a time-invariant voltage-controlled memristive one-port (2.97a)-(2.97b).

2.3.3.1 Example charge-controlled ideal memristor

In [31] an example of an ideal charge-controlled memristor is given, and the PHL is visualized in the $v - i$ plane. The charge controlled memristor is defined by (2.91) and the constitutive relation written in explicit form as $\varphi = g_M(q)$:

$$g_M(q) = q + \frac{1}{3}q^3 \tag{2.103}$$

Also the memristance can be obtained through (2.91a)

$$M \triangleq \frac{d}{dq}g_M = 1 + q^2 \tag{2.104}$$

notice $R(q) > 0 \quad \forall q$, therefore the memristor is passive.

Given (2.103), and the input current defined as:

$$i(t) = \begin{cases} 0 & t < 0 \\ A\sin(\omega t) & t \geq 0 \end{cases} \tag{2.105}$$

where $\omega = 1$ is the angular frequency and the amplitude is $A = 1$. The electric charge can be calculated as follows:

$$q(t) = \frac{A}{\omega}(1 - \cos(\omega t)) \quad t \geq 0 \tag{2.106}$$

substituting (2.106) in (2.103) it is obtained the magnetic flux for $t \geq 0$:

$$\varphi(t) = \frac{A}{\omega}(1 - \cos(\omega t)) \left[1 + \left(\frac{A^2}{3\omega^2}\right)(1 - \cos(\omega t))^2\right] \tag{2.107}$$

differentiating (2.107) it is obtained the voltage across memristor terminals:

$$v(t) = A\sin(\omega t)\left(1 + \frac{A^2}{\omega^2}(1 - \cos(\omega t))^2\right) \tag{2.108}$$

the Lissajous figure of $(v(t), i(t))$ can be obtained through (2.105) and (2.108) is shown in figure (2.24)

From figure 2.24 we can observe the hysteresis is pinched at the origin, which occurs because both $i(t)$ and $v(t)$ become zero at the same time as can be seen in figure 2.24 and from equation (2.91a). The PHL can be divided into six segments. The line segment a, which is colored in green, corresponds to the segment in time where both $i(t)$ and $v(t)$ increase until the current reaches maximum at $t = \pi/2$. After this, the segment b, which is colored in blue, is characterized by a decrease in current and an increase in voltage; this segment ends when the voltage reaches its maximum value at $t \approx 2.21$. Notice, the curve segment b seems to have a negative slope, but this is not possible considering the memristor is passive; the reason of this because the voltage lags behind the input current, or in other words, the maxima of the input current occurs before the maxima of the voltage. The segment c, occurs when both $i(t)$ and $v(t)$ decrease at the same time until $t = \pi$. Therefore, the right lobe of the PHL

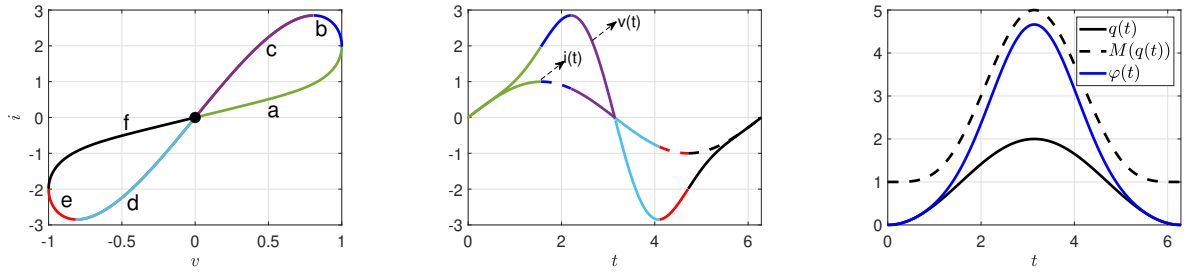

(a) (b) (c)

Figure 2.24: For memristor 2.103 (a) Lissajous figure of $(v(t), i(t))$ (b) input current $i(t)$ and output voltage $v(t)$ (c) electric charge $q(t)$, magnetic flux $\varphi(t)$, $M(q)$ meristance

corresponds to $v(t), i(t)$ for $0 \leq t \leq \pi$. This behavior is repeated symmetrically; furthermore, PHL is odd-symmetric with respect to the origin.

In the following subsection, numerous examples of real two-terminal devices that exhibit a pinched hysteresis loop in response to any periodic input with zero DC component will be presented.

2.3.3.2 Example of Generic Memristor

In 2008, HP Labs launched the first fabricated memristor constructed from a thin film of titanium dioxide of constant length D. This structure is divided into two regions: one region is doped with oxygen, referred to as TiO_2, while the other region is undoped, designated as TiO_{2-x}. Upon the application of an external current $i(t)$ to this device, the width of the region TiO_{2-x} is modified, which is expressed by the variable $w(t) \in [0, D]$. The electrical behavior of such a device is described by:

$$v(t) = M(w(t))i(t) \tag{2.109a}$$

$$\frac{dw(t)}{dt} = \hat{w}(w(t))i(t) \tag{2.109b}$$

where $M : [0, D] \to [R_{on}, R_{off}]$ is de the memristance function defined as:

$$M(w(t)) = R_{on}\frac{w(t)}{D} + R_{off}\left(1 - \frac{w(t)}{D}\right) \tag{2.110}$$

where R_{off}, R_{on} are constants that represent off and on resistance respectively, $\hat{w}(w) \triangleq K = \mu\frac{R_{on}}{D}$. It worth noticing that $M : [0, D] \to [R_{off}, R_{on}]$.

From equation (2.109b), the equation relating the electric charge $q(t)$ and the width of the TiO_{2-x} region $w(t)$ can be obtained. First, equation (2.109b) is rewritten as:

$$dw = Ki(t)dt \tag{2.111}$$

integrating both side of equation (2.111) it is obtained:

$$w(t) = Kq(t) \tag{2.112}$$

Memristance in (2.110) can be rewritten in terms of electric charge, by substituting (2.112) in (2.110) is obtained:

$$M(Kq(t)) = \left[KR_{on}\frac{q(t)}{D} + R_{off}\left(1 - \frac{Kq(t)}{D}\right)\right] \tag{2.113}$$

2.3.4 Two terminal devices exhibiting PHL

Before the memristor was discovered, several electrical devices exhibited behaviors of electrical properties that could not be categorized as those of a resistor, capacitor, or inductor. After 1971, it was experimentally found that some of these materials exhibited memristive properties, with the most revealing a pinched hysteresis loop (PHL) in the $v - i$ plane.

The gas discharge lamp produces light when a voltage is applied across two aligned carbon electrodes, separated by a specific distance. This causes gas to become ionized, leading to the emission of light [33]. In 2014, a model was proposed to characterize the electrical behavior of a discharge lamp as a memristor. The validation of this model demonstrated a significant correlation between the experimental measurements and the theoretical predictions.

From 1948 to 1970, the formation of oxide films on various metals, including aluminum and copper, was studied. This process is an important aspect of semiconductor technologies. The earliest study was reported by Hickmott [34]. In [35], it is later pointed out that the Lissajous figures presented in Hickmott's publication [34] reveal the presence of a pinched hysteresis loop in the voltage-current $v - i$ plane. Following 1971, a number of works focused on devices exhibiting memristive properties, among others [36–39].

Biological systems exhibit memristive properties [40–43]. For instance, the electrical properties of human skin can be modeled through a memristor, particularly the electro-osmotic transport in human sweat ducts. A unicellular organism exhibiting memristive behavior is the Amoeba. When a periodic voltage is applied to an amoeba, the resulting Lissajous figure is a PHL in the $v - i$ plane [42]. Within the *Plantae* kingdom, the *venus flytrap* plant shows a PHL when a periodic voltage is applied through $Ag/AgCl^{+}$ electrodes [43].

2.4 Dynamical Modeling of Memristive Neurons and Synapses

Memristive systems have been proposed to model properties of neuron [7, 10, 44–46] and synapse models [3, 9, 47]. Hodgkin and Huxley introduced an electrical model of the squid axon membrane, in which potassium and sodium channel conductances—initially represented by time-varying conductances driven by time-varying gating variables—are modeled as memristors. In this characterization [44], an ion channel is modeled as a memristor governed by an internal-state equation and an input-output equation. The conductance is explicitly described by voltage and state variables, which capture the opening and closing mechanisms of ion channels based on past membrane activity. In addition to the sodium and potassium ion currents that shape the neuronal membrane potential, the magnetic flux induced across the

neuronal membrane also contributes to its dynamics. Authors in [45] [10] proposed a memristive Hindmarsh–Rose neuron model, which captures the magnetic flux across the membrane, and a memristor is used to model the coupling between the magnetic flux and the neuron's membrane potential. Authors from [46] presented a slight variation of the model from [45], using a different formulation of the memristance function to describe the coupling between magnetic flux and membrane potential in a neuron.

Beyond the neuronal membrane itself, memristive devices have also been extended to describe synaptic dynamics. Regarding electrical synapses, the term memductive synapse has been used in [47–49] to refer to a model used as a coupling device between neuron models and that adopts the behavior of a memductor. Different from the models mentioned above, in references [9] [50], it was proposed a synapse model based on the idea that neuron voltage fluctuation and signal propagation induced a magnetic flux in the media of the nervous system and an additional current in the neuron, which was called electromagnetic induction effect in the electrical activity of neurons [45]. Such an induced current was characterized by the one generated by a memductor; therefore, it is called a memductive synapse.

In this section, we are going to describe the memristive HH [44] and HR [45] models, along with their memductive synapse counterparts [9, 50], which serve as coupling mechanisms between neurons. These formulations form the basis for analyzing the synchronization and collective dynamics in memristive neural networks presented in the following subsections.

2.5 Memristive Neurons

2.5.1 Hodgkin-Huxley Ionic Channels as Memristive Elements

Hodgkin and Huxley proposed a model to describe the electrical properties of the squid axon membrane. In their model, the conductances of potassium and sodium channels are time-dependent and are influenced by gating variables that evolve according to ordinary differential equations describing gating kinetics. In this characterization, the gating dynamics are governed by empirical rate laws, where the transition rates $\alpha(v)$ and $\beta(v)$– as shown in equations (2.22)– are externally prescribed functions of the membrane voltage.

In contrast, the memristive description presented in [7] reframes the ion channel as a dynamical system whose internal state and membrane potential co-evolve bidirectionally. This introduces a crucial property that the internal state variable carries a memory of the input voltage history. Consequently, the channel's opening and closing dynamics is not solely determined by the instantaneous voltage but are also shaped by its past activity, providing a more physical basis for the model's behavior. In this section, we present the memristive description of potassium and sodium channels, as shown in [7]- consisting of an internal-state equation and an input-output equation.

(a) Time-varying resistor (b) Memristor element

Figure 2.25: Equivalent representation between a time-varying resistor (a) and a memristor (b).

The electrical representation of the potassium channel in the Hodgkin-Huxley (HH) model [23] is used to define the voltage across the time-varying resistor R_K, denoted u_K. This voltage can be expressed in terms of the shifted membrane potential v, which is derived from (2.7), and the shifted equilibrium potassium potential v_K. This relationship can be expressed as follows:

$$u_K = v - v_K \tag{2.114}$$

The gating variable n, representing the fraction of opened potassium channels, is defined generically through the state variable $n \equiv x_1$. Therefore, we can define the current, denoted as y_K, on the resistor R_K as:

$$y_K = G_K(x_1)u_K \tag{2.115}$$

where G_K is the conductance of of potassium channel defined as:

$$G_K(x_1) \triangleq \bar{g}_K x_1^4 \tag{2.116}$$

the dynamics of the state variable x_1 (2.17) can be rewritten using the change of variable (2.114) as follows:

$$\dot{x}_1 = \alpha_n(u_K)(1 - x_1) - \beta_n(u_K)x_1 \triangleq f_n(x_1, u_K) \tag{2.117}$$

where $\alpha_n(u_K)$ and $\beta_n(u_K)$ are defined as:

$$\alpha_n(u_K) = \frac{0.01\,(10 - (u_K + v_K))}{e^{\left(\frac{10-(u_K+v_K)}{10}\right)} - 1}, \tag{2.118a}$$

$$\beta_n(v) = 0.125\, e^{-\frac{(u_K+v_K)}{80}}. \tag{2.118b}$$

therefore, we obtain the input-output equation and the dynamics of the potassium channel that define the memristor

$$y_K = G_K(x_1)u_K \tag{2.119a}$$
$$\dot{x}_1 = f_n(x_1, u_K) \tag{2.119b}$$

it is observed that memristor (2.119a)-(2.119b) is a particular case of a generic memristor (2.101a), where there a single state variable. By treating potassium channels as memristors, we structure the model to emphasize their true nature. It reveals the fundamental physical property of the channel; its conductance depends on the history of the voltage across it, making it a device with inherent memory. This shift in perspective is what enables deeper analysis using nonlinear dynamics.

On the other hand, we have the sodium channel, represented by a time-varying conductance controlled by two gating variables, m and h. Following the same memristive formulation, we define the voltage across the sodium conductance as:

(a) Time-varying resistor (b) Memristor element

Figure 2.26: Equivalent representation between a time-varying resistor (a) and a memristor (b).

$$u_{Na} = v - v_{Na} \tag{2.120}$$

where v_{Na} is the shifted equilibrium potential for sodium. The sodium current y_{Na} is then given by:

$$y_{Na} = G_{Na}(x_2, x_3)u_{Na} \tag{2.121}$$

where G_{Na} is the conductance of the sodium channel, defined in terms of two independent state variables $x_2 \equiv m$, $x_3 \equiv h$:

$$G_{Na}(x_2, x_3) \triangleq \bar{g}_{Na}x_2^3x_3 \tag{2.122}$$

the dynamics sodium state variables are dfined by:

$$\dot{x}_2 = \alpha_m(u_{Na})(1 - x_2) - \beta_m(u_{Na})x_2 \triangleq f_m(x_2, u_{Na}) \tag{2.123a}$$
$$\dot{x}_3 = \alpha_h(u_{Na})(1 - x_3) - \beta_h(u_{Na})x_3 \triangleq f_h(x_3, u_{Na}) \tag{2.123b}$$

the rate functions α_m, β_m, α_h,β_h are similarly expressed as functions of u_{Na}

$$\alpha_m(u_{Na}) = \frac{0.1(25 - (u_{Na} + v_{Na}))}{e^{\left(\frac{25-(u_{Na}+v_{Na})}{10}\right)} - 1} \tag{2.124a}$$

$$\beta_m(u_{Na}) = 4e^{-\frac{(u_{Na}+v_{Na})}{18}} \tag{2.124b}$$

$$\alpha_h(u_{Na}) = 0.07e^{-\frac{(u_{Na}+v_{Na})}{20}} \tag{2.124c}$$

$$\beta_h(u_{Na}) = \frac{1}{e^{\left(\frac{30-(u_{Na}+v_{Na})}{10}\right)} + 1}. \tag{2.124d}$$

therefore, we obtain the memristive system for the sodium channel:

$$y_{Na} = G_{Na}(x_2, x_3)u_{Na} \tag{2.125a}$$

$$\begin{bmatrix} \dot{x}_2 \\ \dot{x}_3 \end{bmatrix} = \begin{bmatrix} f_m(x_2, u_{Na}) \\ f_h(x_3, u_{Na}) \end{bmatrix} \tag{2.125b}$$

it is observed that the memristor (2.125) is a particular case of a generic memristor (2.101a) that involves two state variables. This higher dimensionality is what enables the channel's complex temporal behavior, such as rapid activation followed by slower inactivation. The co-evolution of its internal activation and inactivation states, both of which retain their own distinct memory of past voltages. Describing the potassium and sodium channels as first and second-order memristors reveals that global behavior for membrane potential, that is, the action potential, is an emergent property of memory-driven conductance changes in ion channels. Furthermore, the membrane adapts to its recent input, given the neuron's past history of voltage across its ion channels.

2.5.2 Memristive Hindmarsh-Rose neuron model

A different line of work introduced by [45], proposes a memductive synapse from a distinct physical analogy. Building on the electromagnetic-induction argument, models from [10, 11] assume that fluctuations in neuronal membrane voltage generate a time-varying magnetic flux in the surrounding medium. This flux is then used to define an additional current term—interpreted as an induction-like contribution to the membrane dynamics. Under this formulation, the synapse is termed memductive because the self-induced current is governed by a flux-dependent memductance function. As this is a self-induced current, this synapse is called an autapse, given that it is a chemical connection of a neuron onto itself [51].

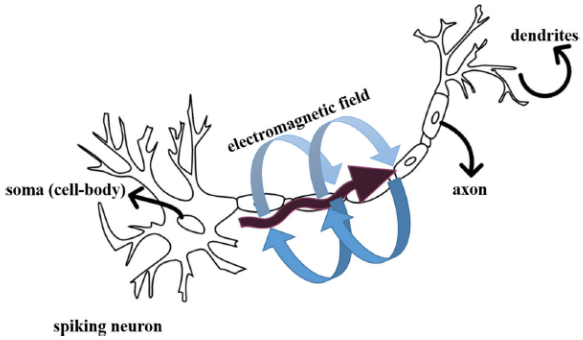

Figure 2.27: Memristive Hindmarsh-Rose Neuron model

To represent this flux-dependent contribution to the membrane current, a memristive element is introduced. In this formulation, the magnetic flux serves as the memristor's internal state variable, its rate of change being driven by the membrane voltage. The resulting memristive current is then expressed as the product of the voltage and a flux-dependent memductance function.

The dynamical equations for the improved four-dimensional HR neuron model are described by:

$$\begin{aligned} \dot{x}_1 &= x_2 - x_3 - ax_1^3 + bx_1^2 + I_{ext} - k_1 W(\varphi) x_1 \\ \dot{x}_2 &= c - x_2 - dx_1^2 \\ \dot{x}_3 &= \varepsilon \left[\sigma \left(x_1 - \gamma\right) - x_3\right] \\ \dot{\varphi} &= x_1 - k_2 \varphi \end{aligned} \tag{2.126}$$

where a, b, c, d, γ are constants, where the variables x_1, x_2, x_3 represent the membrane potential, slow current for recovery variable, and adaptation current, respectively. I_{ext} denotes the external forcing current, and the fourth variable φ describes the magnetic flux across the membrane. $W : \mathbb{R} \to \mathbb{R}$ is the memductance function, which is described

$$W(\varphi) = \alpha + 3\beta\varphi^2 \tag{2.127}$$

where α and β are fixed constants. The term $k_1 W(\varphi) x_1$ could be regarded as an induction current on the membrane, which the author [45] describes as the suppression modulation on membrane potential.

Electromagnetic induction effect is relevant given that time-varying electric field and magnetic fields can introduce non-negligible feedback coupling effects that are not capture by purely resistive elements. Generally, the electromagnetic induction effect is bounded above and below, reflecting physical saturation constraints. For this reason, authors from [3, 52] emulate electromagnetic induction using a memristor whose memductance function is modeled by a hyperbolic tangent function. This function is monotonic, continuous, and differentiable, and it is commonly used as a neuron activation function in the Hopfield neural network. The resulting device is referred to as a threshold flux-controlled, which is described as:

$$W(\varphi) = -\tanh(\varphi) \tag{2.128}$$

Considering the above effect the resulting memristive two-dimensional Hindmarsh-Rose neuron model is described as:

$$\begin{aligned}\dot{x}_1 &= x_1 - x_1 - ax_1^3 + bx_1^2 + k\tanh(\varphi)x_1 \\ \dot{x}_2 &= c - x_1 - dx_1^2 \\ \dot{\varphi} &= x_1\end{aligned} \tag{2.129}$$

where φ is the flux variable representing the time integral of the membrane potential x_1. The term $k\tanh(\varphi)x_1$ stands for the electromagnetic induction current on the membrane and k indicates the electromagnetic induction strength.

2.5.3 Memristive Integrate and Fire neuron model

The Leaky-Integrate-Fire (LIF) neuron model, as described by equation (2.4), can be viewed as a simplified representation of the Hodgkin-Huxley model. In which the nerve membrane polarization is modeled as a leaky capacitive element. While the LIF model describes the passive electrical properties of the neuron membrane, it does not account for ionic channel dynamics. To address this limitation, [1] introduced a memristive element to replace the resistive component, thereby capturing the opening and closing behavior of ion channels.

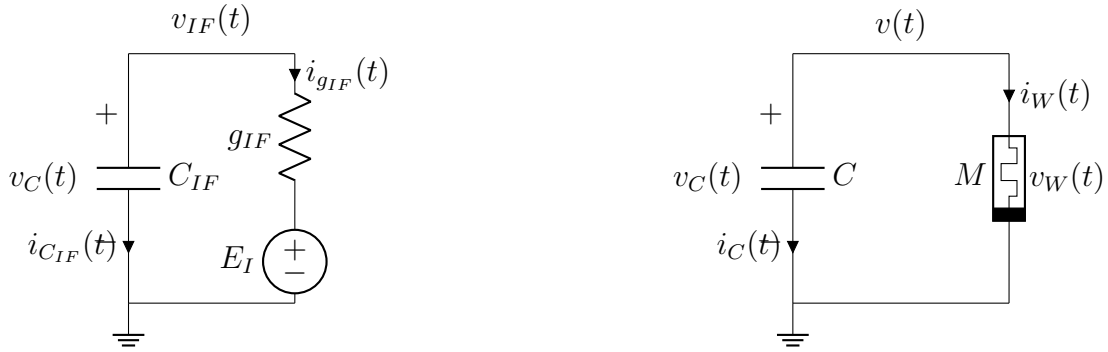

(a) IF neuron circuit

(b) Memristive equivalent circuit

Figure 2.28: Equivalent representation between an integrate-and-fire neuron model (a) and its memristive realization (b).

A memristor whose constitutive relation is obtained from equation (2.88) is used in the circuit (2.28b). The current $i_W(t)$ and voltage $v_W(t)$ of the memristor are the time derivatives of its charge and flux, then from equation (2.88) is obtained:

$$i_W = W(\varphi)v_W \tag{2.130}$$

where $W(\varphi) = \frac{dg_W(\varphi)}{d\varphi}$ is the memductance of the memristor in Ω^{-1}.

From Figure 2.28b, using Kirchhoff's currents law

$$i_C + i_M = 0 \tag{2.131}$$

where the capacitor current $i_C \in \mathbb{R}$ is:

$$i_C = C\dot{v}_C \tag{2.132}$$

with $v_C \in \mathbb{R}$ the voltage across the capacitor and C its capacitance. Using the Kirchhoff's voltage law $v_C - v_W = 0$, therefore $v_C = v_W = v$.

From the above, the MIF neuron model is given by:

$$C\dot{v} = -W(\varphi)v_C \tag{2.133a}$$

$$\dot{\varphi}_W = v \tag{2.133b}$$

with initial conditions $\varphi(t_0) = \varphi_0$ and $v(t_0) = v_0$.

The equilibrium points of (2.133a)-(2.133b) are a continuum given by:

$$\pi_e = \{[0, \varphi]^\top \in \mathbb{R}^2 : \varphi \in \mathbb{R}\}. \tag{2.134}$$

It is important to note that for a given fixed initial condition, there exists a unique equilibrium point $[0, \varphi_e]^\top \in \mathbb{R}^2$ for (2.133). Furthermore, this equilibrium point, if stable, is the *memory state* of the MIF neuron model.

2.6 Modeling of Multi-Modal Coupling in Memristive Hindmarsh–Rose Neurons

The concept of the self-induced current phenomenon, proposed by [45], is further developed by [10], [11], and [53]. They suggest fluctuations in a neuron's action potential generate a magnetic flux in its surrounding medium. The rate of change of this magnetic flux is proportional to the difference between neighboring magnetic fluxes.

Specifically in [11], it is proposed two memristive Hindmarsh-Rose neurons are coupled through a magnetic-flux mediated memductive coupling, that is, the magnetic flux interacts in a diffusive manner among neighboring neurons, leading to an indirect coupling. This diffusive interaction allows variations in the magnetic flux of one neuron to influence the membrane dynamics of nearby neurons. Such a mechanism provides a physical interpretation of field-induced coupling and establishes a link between neuronal activity and memductive synaptic dynamics.

$$\begin{aligned}
\dot{x}_{11} &= x_{12} - x_{13} - ax_{11}^3 + bx_{11}^2 + k(\alpha + 3\beta\varphi_1^2)x_{11} + I_{ext} \\
\dot{x}_{12} &= c - x_{12} - dx_{11}^2 \\
\dot{x}_{13} &= \varepsilon[\sigma(x_{11} + 1.6) - x_{13}] \\
\dot{\varphi}_1 &= k_1 x_{11} - k_2\varphi_1 + D(\varphi_2 - \varphi_1) \\
\dot{x}_{21} &= x_{22} - x_{23} - ax_{21}^3 + bx_{21}^2 + k(\alpha + 3\beta\varphi_2^2)x_{21} + I_{ext} \\
\dot{x}_{22} &= c - x_{22} - dx_{21}^2 \\
\dot{x}_{23} &= \varepsilon[\sigma(x_{21} + 1.6) - x_{23}] \\
\dot{\varphi}_2 &= k_1 x_{21} - k_2\varphi_2 + D(\varphi_1 - \varphi_2)
\end{aligned} \tag{2.135}$$

where x_{i1}, x_{i2}, x_{i3}, φ describe the membrane potential, recovery variable for slow current, and adaptation current, respectively. I_{ext} is the external forcing current, and $a, b, c, d, \varepsilon, \sigma$ are parameters, k, k_1, k_2 are positive feedback gains, φ is the magnetic flux across the membrane. The term $k(\alpha + 3\beta\varphi_i^2)x_{i1}$ characterizes the self-induced current arising from electromagnetic induction effects. The rate of change of magnetic flux φ_i is proportional to the membrane potential x_{i1} and to the difference between neighboring magnetic fluxes $D(\varphi_i - \varphi_j)$ with $i \neq j$. Moreover, this term accounts for flux diffusion between neurons. The term $k_2\varphi_i$ models the gradual decay of induced magnetic flux caused by resistive losses in the neural environment.

In contrast to the views presented by [10], [11], and [53], the study by [54] proposes that each neuron generates its own electromagnetic field. However, these fields do not interact directly; rather, interaction occurs through chemical and electrical synapses.

$$\begin{aligned}
\dot{x}_{11} &= x_{12} - ax_{11}^3 + bx_{11}^2 - x_{13} + I_{\text{ext}} - k_1 W(\varphi_1)x_{11} \\
&\quad - I_{c1} - \varepsilon_e(x_{11} - x_{21}), \\
\dot{x}_{12} &= c - dx_{11}^2 - x_{12}, \\
\dot{x}_{13} &= \varepsilon[\sigma(x_{11} - r) - x_{13}], \\
\dot{\varphi}_1 &= kx_{11} - k_2\varphi_1, \\
\dot{x}_{21} &= x_{22} - ax_{21}^3 + bx_{21}^2 - x_{23} + I_{\text{ext}} - k_1 W(\varphi_2)x_{21} \\
&\quad - I_{c2} - \varepsilon_e(x_{21} - x_{11}), \\
\dot{x}_{22} &= c - dx_{21}^2 - x_{22}, \\
\dot{x}_{23} &= \varepsilon[\sigma(x_{21} - r) - x_{23}], \\
\dot{\varphi}_2 &= kx_{21} - k_2\varphi_2.
\end{aligned} \tag{2.136}$$

where I_{ci} is the current due to chemical synapse, with V_c the reversal potential which tunes excitatory or inhibitory behavior, ε_i is the strength of chemical synaptic coupling.

$$I_{ci} = \varepsilon_i \left(\frac{x_{i1} + V_c}{1 + \exp\left(\frac{x_{j1} - x_{i1}}{\sigma}\right)} \right) \tag{2.137}$$

with $i \neq j$ and $\varepsilon_e(x_{21} - x_{11})$ is the current due to the electrical synapse, $W(\varphi)$ is the memductance function depending on the magnetic flux, characterizing the memory effect of the memristive synapse.

2.7 Memristive Synapses

In the context of electrical synapses, the term memductive synapse has been used in [47] [48] to describe coupling elements that behave as memductors, providing a conductance that depends on an internal state rather than being fixed.

Memductive devices have been proposed to model synaptic properties [9]– [2]. In [9], two FitzHugh–Nagumo neurons are coupled through a memristive synapse, and their synchronous behavior is numerically investigated by fixing the initial condition of the memristor

and the external input current, while varying the coupling strength associated with electromagnetic interaction between adjacent neurons. Subsequently, [55] extended this framework by incorporating a gradual decay term for the induced magnetic flux, thereby accounting for dissipative effects in the electromagnetic coupling.

A different line of work in [2, 3, 12, 13, 50, 55] indicates that differences in membrane potential between nearby neurons can induce changes in the electromagnetic field, thereby generating a current, similar to the behavior of a memristor. The following is the model presented by [3]:

$$\begin{aligned}
\dot{x}_{11} &= x_{12} - x_{13} - ax_{11}^3 + bx_{11}^2 + \tanh(\varphi_1)x_{11} + k\tanh(\varphi)(x_{11} - x_{21}) \\
\dot{x}_{12} &= c - x_{12} - dx_{11}^2 \\
\dot{\varphi}_1 &= x_{11} \\
\dot{x}_{21} &= x_{22} - x_{23} - ax_{21}^3 + bx_{21}^2 + \tanh(\varphi_2)x_{21} + k\tanh(\varphi)(x_{21} - x_{11}) \\
\dot{x}_{22} &= c - x_{22} - dx_{21}^2 \\
\dot{\varphi}_2 &= x_{21} \\
\dot{\varphi} &= x_{11} - x_{21}
\end{aligned} \tag{2.138}$$

where φ_i represents the magnetic flux of the $i-$th neuron, the term $\tanh\varphi_i x_{i1}$ characterizes the self-induced current arising from bounded electromagnetic induction effect, which motivates the use of $\tanh(\cdot)$ to ensure saturation. Here, φ denotes the magnetic flux generated by the difference in membrane potential of neighboring neurons. The term $k\tanh\varphi(x_{i1} - x_{j1})$ represents the coupling current induced by electromagnetic interaction between adjacent neurons.

2.8 Memristive neural networks

Dynamical models of memristive neurons and memristive synapses have been presented [45]– [2]. By introducing a memristive element into the neuronal model, a memristive neuron is constructed. The resulting system dynamics have been investigated using Lyapunov exponent spectra and bifurcation analysis to characterize the emergence of diverse firing patterns [10,45, 46]. On the other hand, by embedding a memristor into the synaptic coupling structure, the synchronization behavior of the coupled neuronal system has been analyzed using analytical techniques [3] and numerical simulations [54] [2] [55] [13] [56].

Collectively, the works in [45]– [10] and [54]– [56] establish the fundamental framework of memristive neural networks (MNN), in which memristors are used to characterize the behavior of synapses and neurons.

Building upon these studies, an example of MNN is presented in [8]. It is presented a network consisting of N identical Hindmarsh-Rose neurons $\mathcal{N} = \{n_1, \cdots, n_N\}$ called the nodes of the network, the set of the edges $\mathcal{S} \subset \mathcal{N} \times \mathcal{N}$, with $s_{ij} \in \mathcal{S}$ which mean that n_i and n_j are connected. The connections of in the network are presented by the adjacency matrix $A = \{a_{ij}\} \in \mathcal{R}^{N\times N}$, where $a = 1$ if $s_{ij} \in \mathbb{S}$ and $a_{ij} = 0$ otherwise.

$$
\begin{aligned}
\dot{x}_{i1} &= x_{i2} - a x_{i1}^3 + b x_{i1}^2 + I_{\text{ext}} + k_0 M(\varphi_i) \sum_{k=1}^{N} A_{ik}(x_{k1} - x_{i1}), \\
\dot{x}_{i2} &= c - d x_{i1}^2 + b x_{i2}, \\
\dot{\varphi}_i &= -\varphi_i^3 + \varphi_i - \sum_{k=1}^{N} A_{ik}(x_{i1} - x_{k1}).
\end{aligned}
\tag{2.139}
$$

In this network, each neuron generates an intrinsic magnetic flux φ_i, induced by electromagnetic flux effects. The flux variables are coupled diffusively across the network topology, enabling neighboring neurons to exchange electromagnetic information. The resulting induced current is incorporated into the membrane potential dynamics via a memductive diffusive coupling term with an identical memductive function for all couplings. In this work [8], the network firing patterns are investigated through spatial-temporal plots under different adjacency matrix configurations, including regular network, random network, and small-world interaction.

2.9 Stability Theory

Stability of dynamical systems is one of the most fundamental problems in nonlinear dynamics and control theory, as it provides a rigorous framework for assessing the stability of equilibrium points without requiring explicit solutions of the system trajectories. One of the important scientists of 18th century, Leonhard Euler, posed the question of whether a mechanical system – described by state variables such as position or velocity– would maintain its motion or return to a reference state after being subjected to small perturbations. Euler´s main contribution to stability was to establishing an analytical and mechanical foundations upon which modern stability theory was later formalized [57].

Subsequently Joseph-Louis Lagrange, another prominent scientist of the late eighteenth century and early nineteenth centuries, addressed the problem of whether the stability of a system could be determined directly from the structure of its equations, without relying on the specific mechanical interpretation of the system. in this context, Lagrange sought a general analytical stability criterion which was based on energy methods [58].

Later, in late nineteenth century and early twentieth centuries Henri Poincaré made a fundamental contribution by transforming the study of differential equations into a qualitative theory. By introducing geometric and topological methods, Poincare enabled the analysis of global system behavior, extending beyond local neighborhoods to the investigation of trajectories and invariant sets over large regions of phase space.

However, an abstract and rigorous definition of stability for dynamical systems, together with a systematic characterization of stability, was not established until the late nineteenth century by Aleksandr M. Lyapunov. In his seminal work (1892) Lyapunov introduced two fundamental methods for stability analysis. The first, known as Lyapunov's first method or Lyapunov's indirect method, investigates the stability of an equilibrium point through the linearization of the nonlinear system. The second approach, known as Lyapunov's direct method, establishes stability by constructing an appropriate Lyapunov function without requiring linearization or explicit solutions of the system trajectories.

In this chapter it is considered systems of the form

$$\dot{x} = f(x) \tag{2.140}$$

where $f : D \to \mathbb{R}^n$ is a locally Lipchitz map from a domain $D \subset \mathbb{R}^n$ into $\mathbb{R}^n$. $\bar{x} = 0 \in \mathbb{R}^n$ is an equilibrium point of equation (2.140); which means $f(\bar{x}) = 0$. The study of the stability of $\bar{x}$ is characterized as follows.

Definition 2.1. The equilibrium point $\bar{x} = 0$ of (2.140) is stable if, for each ε, there is $\delta = \delta(\epsilon)$ such that:

$$\|x(0)\| < \delta \Rightarrow \|x(t)\| < \varepsilon, \forall t \geq 0 \tag{2.141}$$

Definition 2.2. The equilibrium point $\bar{x} = 0$ of (2.140) is asymptotically stable if it is stable and δ can be chosen such that:

$$\|x(0)\| < \delta \Rightarrow \lim_{t \to \infty} x(t) = 0 \tag{2.142}$$

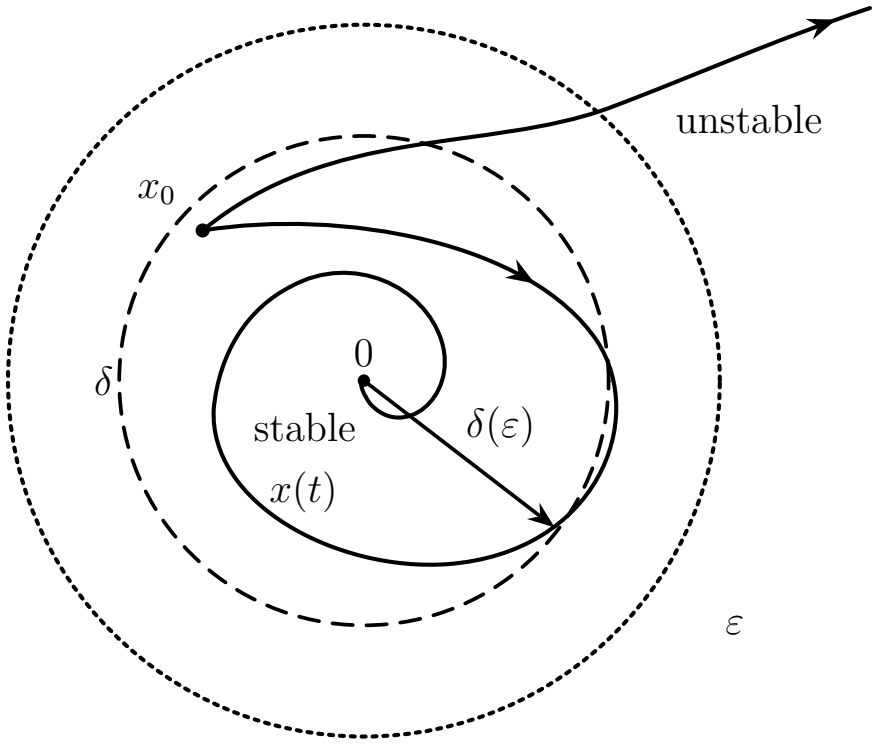

Figure 2.29: Lyapunov stability illustration: trajectories starting within the $\delta(\varepsilon)$ ball (dashed), remain within the ε ball (dotted) and converge to the stable equilibrium point at the origin

In mechanical systems, stability is often analyzed using energy-like scalar functions that decrease along system trajectories due to dissipation. Lyapunov's direct method generalized this idea by relying on scalar functions with suitable mathematical properties, known as Lyapunov functions, which are positive definite. This allows it to be applied without requiring a physical energy interpretation to general nonlinear systems. As a first step, it is introduced the notion of positive definite functions, which play a fundamental role in the construction of Lyapunov functions. The following definitions are obtained from [59].

Definition 2.3. A continuous differentiable function $V : \mathbb{R}^n \to \mathbb{R}$ is said to be *positive definite* in a neighborhood of the origin if

$$V(0) = 0 \quad \text{and} \quad V(x) > 0 \quad \text{for all } x \neq 0. \tag{2.143}$$

Definition 2.4. Let $V : \mathbb{R}^n \to \mathbb{R}$ be continuously differentiable. The derivative of V along the trajectories of system (2.140) is defined as

$$\dot{V}(x) = \nabla V(x)^\top f(x). \tag{2.144}$$

using this notion we now define a Lyapunov function

Definition 2.5. A continuously differentiable function $V : \mathbb{R}^n \to \mathbb{R}$ is called a *Lyapunov function* for a system 2.140 if $V(x)$ is positive definite and its derivative along system trajectories satisfies.

$$\dot{V}(x) \leq 0 \tag{2.145}$$

in a neighborhood of the equilibrium point $x = 0$

2.9.1 Direct method

Based on the concept of a Lyapunov function, Lyapunov's direct method provides sufficient conditions for determining the stability properties of an equilibrium point without requiring explicit solutions of the systems trajectories.

Theorem 2.1. *Let $\bar{x} = 0$ be an equilibrium point for (2.140) and $D \subset \mathbb{R}^n$ be a domain containing $\bar{x} = 0$. Let $V : D \to \mathbb{R}$ be a continuous differentiable function such that*

$$V(0) = 0 \quad \textit{and} \quad V(x) > 0 \quad \forall x \in D \setminus \{0\}. \tag{2.146}$$

then, $\bar{x} = 0$ is stable if $\dot{V} \leq 0$. Moreover if

$$\dot{V}(x) < 0 \quad \forall x \in D \setminus \{0\}. \tag{2.147}$$

then, $\bar{x} = 0$ is asymptotically stable

While Lyapunov's direct method provides sufficient conditions for stability through the construction of a Lyapunov function, such functions are not always easy to find in practice. An alternative approach, known as Lyapunov's indirect method, analyzes stability by examining the linearized system around an equilibrium point.

2.9.2 Indirect Method

Through this method, conclusions about the local stability of the equilibrium point for the nonlinear system can be drawn by investigating its stability as an equilibrium point of the linearized system.

Theorem 2.2. *Let $\bar{x} = 0$ be an equilibrium point for the nonlinear system where $f : D \to \mathbb{R}^n$ is continuously differentiable and D is a neighborhood of the origin. Let*

$$A = \frac{\partial f}{\partial x}(x)\bigg|_{x=0} \tag{2.148}$$

be the Jacobian matrix of the system evaluated at the equilibrium point. Then

- *The origin is* asymptotically stable *if all the eigenvalues of A satisfy $Re[\lambda_i] < 0$*
- *The origin is* unstable *if for one or more the eigenvalues of A $Re[\lambda_i] > 0$*

It should be noted that the Lyapunov's indirect method provides only local stability results and does not yield conclusions when the eigenvalues of the Jacobian matrix have zero real parts.

Lyapunov theory is fundamental to state the problem of synchronization. Before establishing the problem of synchronization it is necessary to define mathematically what is synchronization and all of the types of Lyapunov stability theory provides the mathematical foundation for analyzing the stability of invariant sets in dynamical systems, including synchronization manifolds. Before addressing stability properties of synchronized motion, it is necessary to introduce a precise mathematical definition of synchronization and to distinguish between its different forms.

2.10 Synchronization

The term *synchronous* originates from the Greek words *sync* (meaning together or common) and *chronos* ($\chi\rho o\nu o\varsigma$), meaning time. Literally, synchronization refers to the phenomenon of sharing a common temporal evolution. Furthermore, it means correlation in time of different processes [60]. Synchronization is ubiquitous phenomenon observed in nature, science, social systems, and engineering, and it plays a fundamental role in the collective behavior of coupled dynamical systems.

One of the earliest documented observations of synchronization is attributed to Christiaan Huygens. In a letter written in 1665, Huygens reported that two pendulum clocks mounted in a common support eventually oscillated with a coherent rhythm, with their pendula swinging in opposite directions. In modern terminology, this behavior is described as anti-phase synchronization, which results from weak mechanical coupling mediated by a common supporting beam.

In [61], synchronization is defined as a form of collective dynamics arising in coupled nonlinear systems, including chaotic systems. A nonlinear dynamical system is said to exhibit chaotic behavior when its long-term evolution depends sensitively on initial conditions. As a

consequence, two identical chaotic systems that start from arbitrarily close initial conditions will generally evolve along trajectories that diverge exponentially in time.

Several synchronization regimes have been identified in coupled dynamical systems [62]. Complete (or identical) synchronization occurs when the states of the coupled systems evolve along trajectories that become identical asymptotically in time. Phase synchronization arises when the phases of the oscillations are locked, while the amplitudes remain uncorrelated. Lag synchronization (LS) is characterized by the alignment of both phases and amplitudes, with one system following the other with a constant delay.

Generalized synchronization (GS) typically occurs between nonidentical systems and is said to emerge when there exists a function relationship that maps the state of one system to that of the other. Complete synchronization can be viewed as a special case of generalized synchronization, in which the functional relationship reduces to the identity map. This function need to be invertible, implying that the state of one system may be predicted from the other [63].

2.10.1 Complete Synchronization

Continuous chaotic systems are said to achieve complete synchronization when the states of the coupled systems asymptotically become identical. Geometrically, this corresponds to the collapse of the system trajectories onto an invariant subspace, known as the synchronization manifold, defined by the equality of the state variables of the coupled systems. Consequently, the dimensionality of the synchronized dynamics is reduced. For instance, if the full coupled system evolves in a six-dimensional phase space, the synchronized motion is confined to a three-dimensional manifold, identical for each node.

Coupled dynamical systems may be arranged in two fundamental configurations. In a unidirectional (driver–response) configuration, the dynamics of the driver system influence the response system, while no feedback from the response to the driver is present. In contrast, a bidirectional (mutual) coupling configuration allows the states of the dynamical units to influence each other symmetrically.

2.10.1.1 Bidirectional coupling

Bidirectionally coupled chaotic systems can be modeled through the introduction of a symmetric dissipative coupling term in the system dynamics, given by

$$\dot{x} = f(x) + A(y - x), \tag{2.149}$$

$$\dot{y} = f(y) + A(x - y). \tag{2.150}$$

The bidirectional coupling model uses symmetric diffusive terms $A(y - x)$ and $A(x - y)$, which drive the states x and y toward each other. Where $x, y \in \mathbb{R}^n$ are the state vector of the chaotic systems, while f is the vector field $f : \mathbb{R}^n \to \mathbb{R}^N$, $A \in \mathbb{R}^{n\times n}$ is a matrix whose coefficients rule the dissipative coupling, and $^\top$ stands for matrix transposition. On the synchronization manifold where $x = y$, these terms vanish, allowing the coupled system to follow the isolated system's chaotic dynamics exactly.

The full phase space for the coupled system is $2n$-dimensional, but synchronization confines motion to the n-dimensional diagonal subspace (manifold) $x = y$. The coupling terms vanish on the synchronization manifold defined by $x = y$, ensuring that the synchronized motion coincides with the dynamics of the isolated system.

The synchronization manifold is defined as:

$$\mathcal{M} = \left\{(x^\top, y^\top)^\top \in \mathbb{R}^{2n} : x = y\right\} \tag{2.151}$$

2.10.2 Phase synchronization

Phase synchronization can arise in both unidirectionally and bidirectionally coupled oscillators systems, depending on the nature and strength of the interaction between them. In unidirectionally coupled systems, phase synchronization typically manifests as phase locking of the response system to the driving system. In contrast, in bidirectionally coupled systems the oscillators mutually adjust their phases through the coupling interaction.

When two oscillators are coupled, each system can be associated with an instantaneous phase, denoted by $\phi_1(t)$ and $\phi_2(t)$. Phase synchronization is said to occur when the phases satisfy a rational locking condition. Specifically, two oscillators exhibit $n\!:\!m$ phase synchronization if there exist integers n and m and a constant C such that:

$$|n\phi_1 - m\phi_2| < C \tag{2.152}$$

for all t. In this regime, the phase difference remains bounded in time, even though the amplitudes of the oscillations may remain uncorrelated.

In chaotic systems, there is no unique method for determining phase synchronization, since the instantaneous phase of a chaotic signal is not uniquely defined. In [61], three different strategies are proposed to estimate the instantaneous phase of chaotic signals. For a detailed discussion of these approaches, see [61].

2.10.3 Lag synchronization

Lag synchronization occurs when the trajectories of two coupled systems coincide after a constant time shift $x_2(t) \approx x_1(t - \tau)$. This synchronization regime can arise in both unidirectional coupled drive-response systems, where the response follows the drive with a delay, and in bidirectionally coupled systems, where one system spontaneously leads while the other lags.

In a unidirectional coupling, the dynamical system is described as:

$$\dot{x}_1 = f(x_1) \tag{2.153}$$
$$\dot{x}_2 = f(x_2) + H(x_1, x_2) \tag{2.154}$$

where x_1,$x_2 \in \mathbb{R}^n$ and the coupling function $H : \mathbb{R}^n \times \mathbb{R}^n \to \mathbb{R}$.

In this case, lag synchronization is defined as:

$$x_2(t) \approx x_1(t-\tau) \tag{2.155}$$

which means that the response system reproduces the drive system's trajectory with a delay.

In a bidirectional coupling, the dynamical system is described as:

$$\dot{x}_1 = f(x_1) + H(x_1, x_2) \tag{2.156}$$
$$\dot{x}_2 = f(x_2) + H(x_1, x_2) \tag{2.157}$$

lag synchronization can still occur, but now:

$$x_1(t) \approx x_2(t+\tau) \tag{2.158}$$

or

$$x_2(t) \approx x_1(t-\tau) \tag{2.159}$$

Lag synchronization is usually detected using the similarity function:

$$S(\tau) = \frac{\left\langle [x_2(t+\tau) - x_1(t)]^2 \right\rangle^{1/2}}{\langle x_1^2(t) \rangle^{1/2} \langle x_2^2(t) \rangle^{1/2}} \tag{2.160}$$

where $\langle \cdot \rangle$ denotes time averaging $\langle f(t) \rangle = \lim_{T\to\infty} \frac{1}{T} \int_0^T f(t)\, dt$. In numerical simulations, the time average $\langle \cdot \rangle$ is usually computed in a discrete form using sampled data $\langle f(t) \rangle = \frac{1}{N} \sum_{k=1}^{N} f(t_k)$, where N denotes the number of sampled time points.

If lag synchronization exists, there is a value $\tau = \tau_0$ such that $S(\tau_0) \approx 0$.

2.10.4 Generalized synchronization

So far, the synchronization phenomena between identical coupled systems have been discussed. When non-identical systems are coupled, the manifold in the state space that attracts the trajectories may have a more complicated structure. A more general way to describe the temporal relationship between coupled systems is through a functional relationship between their states that holds asymptotically.

In this context, generalized synchronization is introduced for a unidirectional (driver-response) coupling scheme:

$$\dot{x}_1 = F(x_1) \tag{2.161}$$
$$\dot{x_2} = G(x_2, h_\mu(x_1)) \tag{2.162}$$

where $x_1 \in \mathbb{R}^n$ is the n-dimensional state vector of the driver and $x_2 \in \mathbb{R}^m$ is the m-dimensional state vector of the response.The functions $F : \mathbb{R}^n \to \mathbb{R}^n$ and $G : \mathbb{R}^m \times \mathbb{R}^m \to \mathbb{R}^m$ are vector fields describing the dynamics of the driver and response systems, respectively. The coupling between the response and the driver is described by the function $h_\mu(x) : \mathbb{R}^n \to \mathbb{R}^m$,

where μ denotes a (parameter or a set of parameters) controlling the coupling strength or structure. In the literature, μ is the parameter that controls the transition to synchronization.

Generalized synchronization in unidirectionally coupled systems occurs if, after a transient time $t > t_T$, there exists a transformation $\Upsilon : \mathbb{R}^n \to \mathbb{R}^m$ such that [63]:

$$x_2(t) = \Upsilon(x_1(t)) \quad \forall t > t_T \tag{2.163}$$

the synchronization manifold is defined as:

$$\mathcal{M} = \left\{(x_1, x_2)^\top \in \mathbb{R}^{n+m} : x_2 = \Upsilon(x_1)\right\} \tag{2.164}$$

For bidirectionally coupled systems:

$$\dot{x_1} = F(x_1) + H_1(x_1, x_2) \tag{2.165}$$
$$\dot{x_2} = G(x_2) + H_2(x_2, x_1) \tag{2.166}$$

where $x_1 \in \mathbb{R}^n$ is the n-dimensional state vector of the first system and $x_2 \in \mathbb{R}^m$ is the m-dimensional state of the second system. The functions $F : \mathbb{R}^n \to \mathbb{R}^n$ and $G : \mathbb{R}^m \to \mathbb{R}^m$ are vector fields describing the dynamics of the first and second systems, respectively. $H_1 : \mathbb{R}^{n\times m} \to \mathbb{R}^n$ and $H_2 : \mathbb{R}^{n\times m} \to \mathbb{R}^m$ are coupling functions

The bidirectionally coupled system is said to achieve the generalized synchronization regime if, after a transient time $t > t_T$, its states are related through a static function $\Phi(\cdot)$ that holds uniformly in time, such that [64]:

$$x_1(t) = \Phi(x_2(t)) \quad t > t_T \tag{2.167}$$

which in implicit form can be written as:

$$\Psi(x_1(t), x_2(t)) = x_1(t) - \Phi(x_2(t)) = 0 \quad \forall t > t_T \tag{2.168}$$

where the functional relation $\Psi(\cdot)$ must be independent of time and state variables, the synchronization manifold becomes:

$$\mathcal{M} = \left\{(x_1, x_2)^\top \in \mathbb{R}^{n+m} : \Psi(x_1, x_2) = 0\right\} \tag{2.169}$$

The synchronization regimes described above illustrate the diverse ways in which coupled nonlinear dynamical systems can exhibit coordinated behavior. Depending on the nature of the interaction and the properties of the systems, synchronization may appear as complete synchronization, phase locking, lagged correspondence between trajectories, or more general functional relationships between system states. These concepts provide the theoretical foundation for analyzing collective dynamics in coupled systems. In the following section, the stability of synchronized motion is analyzed.

2.10.5 The stability of the synchronized motion

The emergence of synchronization in coupled dynamical systems can be understood by studying the stability of the synchronization manifold. The synchronization manifold represents

the subset of the state space in which the states of the coupled systems satisfy the synchronization condition. If the synchronization is stable with respect to perturbations transverse to it, then the coupled systems converge toward a synchronized motion.

Different analytical tools can be employed to prove stability. The Lyapunov method can be used to establish sufficient conditions for global asymptotic synchronization by constructing an appropriate Lyapunov function for the error system. Global asymptotic synchronization is achieved if for any initial condition $(x_1^\top(0), x_2^\top(0))^\top \in \mathbb{R}^{n+m}$ it is fulfilled:

$$\|x_1(t) - x_2(t)\| \to 0 \quad \text{as} \quad t \to \infty \tag{2.170}$$

The synchronization problem can be analyzed in terms of the error between the system states:

$$e = x_1 - x_2 \tag{2.171}$$

taking the time derivative of change (2.171) is obtained:

$$\dot{e} = \dot{x}_1 - \dot{x}_2 \tag{2.172}$$

The stability of the synchronization manifold can therefore be analyzed through the stability of the equilibrium point $e = 0$ of the error system. If the equilibrium point is asymptotically stable, then the trajectories of the coupled system converge to the synchronization manifold and synchronization motion is achieved.

Alternatively, the Lyapunov indirect method, based on linearizing the error dynamics about the equilibrium point $e = 0$, establishes conditions for local asymptotic synchronization.

For bidirectionally coupled systems (2.149)

$$\begin{aligned} \dot{x} &= f(x) + A(y - x), \\ \dot{y} &= f(y) + A(x - y). \end{aligned}$$

the synchronization problem is addressed in terms of the error:

$$e = x - y \tag{2.173}$$

the error dynamics is obtained by differentiating:

$$\dot{e} = \dot{x} - \dot{y} \tag{2.174}$$

by substituting the system's equations (2.149) in equation (2.174) is obtained:

$$\dot{e} = (f(x) + A(y - x)) - (f(y) + A(x - y)) \tag{2.175}$$

now simplifying the coupling terms:

$$A(y - x) - A(x - y) = A[(y - x) - (x - y)] \tag{2.176}$$

since $y - x = -(x - y)$ this becomes

$$A[(y - x) - (x - y)] = -2Ae \tag{2.177}$$

the error system is given by:

$$\dot{e} = f(x) - f(y) - 2Ae \tag{2.178}$$

on the synchronization manifold $x = y = s(t)$, where $s(t)$ satisfies:

$$\dot{s} = f(s) \tag{2.179}$$

so synchronization means:

$$x(t) \to s(t), \quad y(t) \to s(t) \tag{2.180}$$

and equivalently:

$$e(t) \to 0 \tag{2.181}$$

thus, the problem becomes the stability of the equilibrium $e = 0$ of the error system. The linearization of the error dynamics about $e = 0$ is obtained. First-order Taylor expansion around the synchronized trajectory is obtained:

$$f(x) \approx f(s(t)) + Df(s(t))(x - s(t)) \tag{2.182}$$

$$f(y) \approx f(s(t)) + Df(s(t))(y - s(t)) \tag{2.183}$$

where the Jacobian matrix is defined as:

$$Df(s(t)) = \begin{bmatrix} \left.\frac{\partial f_1}{\partial x_1}\right|_{x=s(t)} & \cdots & \left.\frac{\partial f_1}{\partial x_n}\right|_{x=s(t)} \\ \vdots & \ddots & \vdots \\ \left.\frac{\partial f_n}{\partial x_1}\right|_{x=s(t)} & \cdots & \left.\frac{\partial f_n}{\partial x_n}\right|_{x=s(t)} \end{bmatrix} \tag{2.184}$$

subtracting the vector fields:

$$f(x) - f(y) \approx Df(s(t))[(x - s(t))]e \tag{2.185}$$

the linearized error system is obtaining by substituting (2.185) into (2.174) therefore it is obtained:

$$\dot{e} = (Df(s(t)) - 2A)e \tag{2.186}$$

If the zero solution of this linear time-varying system is asymptotically stable, then the synchronization manifold is locally asymptotically stable, and hence the coupled systems achieve local asymptotic synchronization.

To introduce the stability of the synchronized motion in complex networks, it is necessary to introduce complex networks theory. In the following, the mathematical description of a complex network is presented, followed by a description of the type of coupling between nodes, such as undirected, directed, and weighted.

To study the stability of synchronized motion in complex networks, it is first necessary to introduce the basic concepts of complex network theory. In the following section, the mathematical representation of a complex network is presented. Subsequently, the types of coupling between nodes are described, including undirected, directed, and weighted connections. In addition it is described adjacency and Laplacian matrices which provide mathematical representations of the connectivity structure of a network, describing how nodes are interconnected. However, the organization of connections between nodes can follow different structural patterns. These patterns define the topology of the network and play an important role in determining the collective behavior of dynamical systems evolving on the network. For this reason, several network models have been proposed to describe different types of connectivity structures.

2.11 Complex Networks

A network, which is a visual representation of a physical structure. Networks can represent social interactions, power grids, and communication systems. A network can be mathematically described as a graph composed of a set of nodes and edges, which represent the interactions or relationships between the elements.

2.11.1 Graphs

Let G be a nonempty graph with at least one node (or vertex). The nodes are described by the set $\mathcal{N} = \{n_1, ..., n_N\}$, the number of nodes is $N = |\mathcal{N}|$. The set of edges of the network $E \subset \mathbb{N} \times \mathbb{N}$, where $e_{ij} \in E$ indicates that there exists a connection between nodes n_i and n_j are coupled, the number of edges is $M = |E|$.

Definition 2.6. A graph $G = (\mathcal{N}, E)$ is said to be *undirected* if the edges have no orientation. In this case, the edge (n_i, n_j) is identical to the edge (n_j, n_i). Therefore, if $(n_i, n_j) \in E$, then $(n_j, n_i) \in E$ also holds.

Definition 2.7. A graph $G = (\mathcal{N}, E)$ is said to be *directed* if the edges have orientation. In this case, connections are not symmetric; this means that an edge is represented as an ordered pair $(n_i, n_j) \in E$, indicating a connection from node n_i to n_j. Unlike the undirected case, the existence of $n_i, n_j \in E$ does not necessarily imply that $n_j, n_i \in E$.

Definition 2.8. A graph $G = (\mathcal{N}, E)$ is said to be *weighted* if each edge (n_i, n_j) is associated with a real number w_{ij} called the weight of the edge. The weight represents the strength or intensity of the connection between the nodes n_i and n_j.

2.11.1.1 Adjacency and Laplacian Matrices

For a graph G with N nodes, labeled as $N(G) = 1, 2, ..., N$ its adjacency matrix $A = (a_{ij})$ is defined the $N \times N$ constant matrix whose (i, j)th entry is equal to 1, if nodes i,j are connected, and is 0 otherwise, with $a_{ii} = 0$ for all $i = 1, ..., N$.

$$a_{ij} = \begin{cases} 1, & \text{if nodes } i \text{ and } j \text{ are connected,} \\ 0, & \text{otherwise.} \end{cases}$$

In addition, $a_{ii} = 0$ for all $i = 1, \ldots, N$.
The properties of the adjacency matrix are the following:

- An adjacency matrix is symmetrical, that is, $a_{ij} = a_{ji}$.
- All main diagonal elements of the adjacency matrix are 0, i.e., $a_{ii} = 0$.
- The concept of degree is the most fundamental characteristic for describing the structure of a network. In an undirected network, the degree of node i, denoted by k_i, is defined as the number of edges connected to that node.

$$k_i = \sum_{j=1}^{N} a_{ij}.$$

- For directed networks, two types of degree are defined: the in-degree and the out-degree. The in-degree of node i is the number of incoming edges,

$$k_i^{in} = \sum_{j=1}^{N} a_{ji},$$

while the out-degree is the number of outgoing edges,

$$k_i^{out} = \sum_{j=1}^{N} a_{ij}.$$

The degree matrix D is defined as the diagonal matrix

$$D = \text{diag}(k_1, k_2, \ldots, k_N).$$

The Laplacian matrix of the graph is defined as:

$$L = D - A \tag{2.187}$$

one of the properties of the adjacency matrix is:

$$\sum_{j=1}^{N} L_{ij} = 0 \tag{2.188}$$

2.11.2 Structural Properties

Structural properties are quantitative measures that characterize the topology of a network and describe how nodes are connected and organized. One of the most fundamental measures is the *distance* (d_{ij}) between two nodes, labeled i and j, respectively, which measures the number of links along the shortest path between them. On the other hand, the maximum distance between any pair of nodes is called *diameter* (D).

A related measure that characterizes the network's global connectivity is the *average path length*. This quantity represents the average of the shortest path distances between all pairs of nodes in the network and is defined as:

$$L = \frac{1}{N(N-1)} \sum_{i \neq j} d_{ij},$$

where N is the number of nodes in the network and d_{ij} denotes the shortest path distance between node i and j.

2.11.3 Network Models

Mathematical network models are important for understanding the relationships between the topology and dynamics of complex networks. This section introduces several basic network models, such as regular networks, random-graph networks, small-world networks, navigable networks, scale-free networks.

Definition 2.9. A regular network is a network in which each node has the same number of connections (degree). In other words, the connectivity pattern is uniform across the entire network. Such networks exhibit a high degree of structural regularity and symmetry.

$$k_i = k \quad \forall i \tag{2.189}$$

Formally, a graph is k-regular if every node has degree k.

2.11.3.1 Fully-connected network

A fully connected network has the average path length

$$L_{full} = 1 \tag{2.190}$$

and the average clustering coefficient

$$C_{full} = 1 \tag{2.191}$$

The number of edges is $N(N-1)/2$ edges

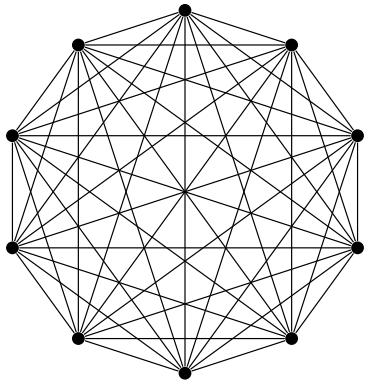

Figure 2.30: Complete graph with 10 nodes $N = 10$

2.11.3.2 Ring-shaped network

A ring network is a regular network in which nodes are arranged in a circular topology and each node is connected to its nearest neighbors. In a k-regular ring network, every node is connected to $k/2$ neighbors on each side.

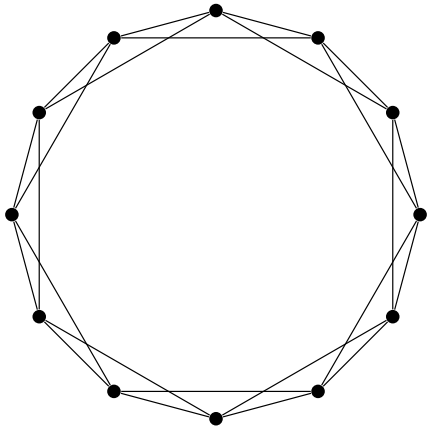

(b)

Figure 2.31: Network topology of a ring graph with 12 nodes ($N = 12$) and 4 neighbors per node

Chapter 3

Synchronization of Memristive Neural Networks

In this chapter, the main contributions of this thesis are presented. These contributions focus on the dynamical analysis of Memristive Neural Networks, which are dynamical models in which memristors are used to characterize the behavior of synapses and neurons.

The first contribution considers a memristive integrate-and-fire (MIFN) neuron model as the node of the network, where time-varying resistances are used to couple the nodes. This leads to the formulation of a time-varying MIFNN model, for which simple conditions are derived to establish the existence of a unique stable equilibrium point for each initial condition.

The second contribution studies a pair of Hindmarsh–Rose neurons coupled through an ideal memristor. It is shown that, for sufficiently large positive memductance, the Hindmarsh–Rose neurons achieve synchronization.

The third contribution analyzes two Hindmarsh–Rose neurons coupled through identical active memristive synapses. It is shown that Generalized Synchronization occurs when the memristor parameter exceeds a certain threshold value. It is also investigated the influence of the memristor strength coefficient on the temporal characteristics of their firing patterns.

3.1 Stability of the memory state of a time-varying memristive neural network model

The brain is capable of information integration and processing incoming from several different organs resulting in capabilities like memory and reasoning. The neuron is the basic processing unit of the brain, has been studied in many different ways. The neuron's electrical behavior is captured by the Hodgkin and Huxley model (HH) [65]. In particular, the action potential phenomenon is the result of the physiological excitability of the ionic currents in the neuron's membrane. The so-called *Integrate and Fire* (IF) neural model is a simplified model that captures this phenomenon as a charge and discharge of a capacitor [66].

The electrical representation of neural models required the use of time-varying conductance to model the opening and closing of ion channels in the membrane. No basic discrete electronic component had these features until in 1971 L. O. Chua theorized the existence of a fourth electric basic element called Memristor [32]. That name is a contraction of words: resistance and memory.

The memristor is an electronic device characterized by a relation between its electric charge and its magnetic flux. Since these variables are related to the current and voltage across the device via its derivative, the resistance value of the memristor depends on the *history* of the voltage that passed through it, furthermore as the derivative goes to zero the resistance value is maintained in the device without new current been needed. As a result, *non-volatility* is a property of this resistive memory [31].

As presented in [67], the memristor is a candidate to represent the time-varying conductances of the neural model [65]. The possibility of implementing memristive circuits as a representation of biological neurons gives interest in them as neuromorphic circuits [68]. In particular, [1] proposes a memristive version of the IF neural model.

As biological neurons communicate with each other through synapses, several memristive neurons can be coupled together into networks where dynamical phenomena can emerge. Yet, the dynamical behavior of memristive neurons, in particular Memristive Integrate and Fire neurons, needs to be studied further.

An important feature of the MIFN model is that it has a continuum of equilibrium points. However, for a given fixed initial condition there exists only an equilibrium point and further this unique equilibrium point is stable, as such, in the sense of a memristor resistance, this unique stable equilibrium point is the memory state of the MIFN model [1].

This contribution aims to establish under what conditions a network on identical MIFN models with a time-varying coupling structure has a memory state. In other words, under what conditions, both in terms of the memristor description and the coupling structure of time-varying connections, of a memristor IF neural network (MIFNN) has a unique stable fixed point for a given fixed initial condition.

In the next section, the memory state problem for the time-varying MIFNN model is described in detail.

3.1.1 Problem statement

Consider the Memristive Integrate and Fire neuron model as proposed in [1] consisting of a memristor M connected in parallel to a capacitor C as represented in Fig. 3.1.

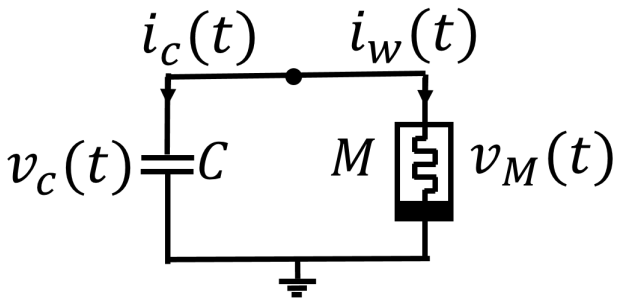

Figure 3.1: Electrical circuit of the MIFN model

From Fig. 3.1, the current $i_c(t) \in \mathbb{R}$ of the capacitor is defined by:

$$i_c(t) = C\dot{v_C}(t) \tag{3.1}$$

where $v_C(t) \in \mathbb{R}$ is the capacitor voltage and C is its capacitance. The memristor current $i_w(t)$ is defined by:

$$i_w(t) = w(\varphi(t))v_M(t) \tag{3.2}$$

as before $w(\varphi)$ is the memductance of the memristor. According to Kirchhoff's Voltage Law $v_C(t) - v_M(t) = 0$, therefore $v_C(t) = v_M(t) = v(t)$. The dynamical model of the circuit in Fig. 3.1 is obtained by the Kirchhoff's Current Law.

$$i_c(t) + i_w(t) = 0 \tag{3.3}$$

Substituting equations (3.1) and (3.2) in (3.3) and recalling (3.61a), the following MIFN model equations are obtained:

$$C\dot{v}(t) = -w(\varphi(t))v(t) \tag{3.4a}$$
$$\dot{\varphi}(t) = v(t) \tag{3.4b}$$

with initial conditions $\varphi(t_0) = \varphi_0$ and $v(t_0) = v_0$.

The equilibrium points of (3.4a)-(3.4b) are a continuum given by

$$\pi_e = \{[0, \varphi]^\top \in \mathbb{R}^2 : \varphi \in \mathbb{R}\}. \tag{3.5}$$

It is important to note that for a given fixed initial condition, there exists a unique equilibrium point $(0, \varphi_e) \in \mathbb{R}^2$ for (3.4). Furthermore, if stable, this equilibrium point is the *memory state* of the MIFN model.

In the following section, the MIFNN model is presented and investigated under time-varying couplings.

3.1.2 Model description

Consider a set of N identical MIFN (3.4) called *nodes* $\mathcal{M} = \{m_1, ..., m_N\}$. Where each node has unitary capacitances $C_1 = .. = C_N = 1$ and identical characteristic memristive

functions $f_{w_1}(\cdot) = ... = f_{w_N}(\cdot) = f_w(\cdot)$. Therefore, all nodes have identical memductance $w(\cdot) = w_1(\cdot) = ... = w_N(\cdot)$.

If node m_i is connected to node m_j by a *fixed* edge $s_{ij} \in \mathcal{S} \subset \mathcal{M} \times \mathcal{M}$ where $i \neq j$, then $a_{ij} = 1$. Alternatively, if these nodes are not connected $a_{ij} = 0$. Since the edges are undirected, $a_{ij} = a_{ji}$ $\forall i, j$ and there are no isolated nodes in the network. The coupling structure is given by the adjacency matrix $A = \{a_{ij}\} \in \mathbb{R}^{N\times N}$.

Let every edge has an associated *time-dependent* connection weight given by a function $c_{ij} : \mathbb{R}_+ \to \mathbb{R}_{>0}$ locally Lipschitz in $\mathbb{R}_+$. The time-varying Laplacian matrix $\mathcal{L}(t) = (\ell_{ij}(t))_{N\times N}$ associated to this connection topology is given by:

$$\ell_{ij}(t) = \begin{cases} \sum\limits_{k=1,k\neq i}^{N} a_{ik}c_{ik}(t), & i = j \\ -a_{ij}c_{ij}(t), & i \neq j \end{cases} \tag{3.6}$$

The dynamics of the $i-$th node is given by:

$$\dot{v_i}(t) = -w(\varphi_i(t))v_i(t) - \sum_{j=1}^{N} \ell_{ij}(t)v_j(t) \tag{3.7a}$$

$$\dot{\varphi}_i(t) = v_i(t) \tag{3.7b}$$

for $i = 1, 2, \cdots, N$.

A vectorial form of (3.7) is:

$$\dot{V}(t) = -W(\phi(t))V(t) - \mathcal{L}(t)V(t) \tag{3.8a}$$

$$\dot{\phi}(t) = V(t) \tag{3.8b}$$

where $V(t) = [v_1(t), ..., v_N(t)]^\top \in \mathbb{R}^N$ and $\phi(t) = [\varphi_1(t), ..., \varphi_N(t)]^\top \in \mathbb{R}^N$ are the voltage and magnetic flux vectors, respectively. With the memductance matrix $W(\phi(t)) = \text{diag}(w(\varphi_1(t)), .., w(\varphi_N(t))) \in \mathbb{R}^{N\times N}$.

From (3.6) we have that the time-varying Laplacian matrix of the MIFNN is uniformly diffusive, that is, the sum by row and by columns is zero at all times. As a consequence the eigenvalues of $\mathcal{L}(t)$, denoted as $\lambda_i(t)$ $(i = 1, \cdots, N)$ can be arrange as [69]:

$$\lambda_N(t) \geq \cdots \lambda_2(t) \geq \lambda_1 = 0 \tag{3.9}$$

In other words, the coupling of the MIFNN is captured by a Laplacian matrix that is semi-possitive at each time instant.

As before, for (3.7a)-(3.7b) there is a continuum of the equilibrium points defined by the set

$$\beta_e = \{[0, \phi]^\top \in \mathbb{R}^{2N} : \phi \in \mathbb{R}^N\}. \tag{3.10}$$

The equilibrium point $[0, \phi_e]^\top \in \beta_e$ is a memory state of the MIFNN model, if for a given fixed initial condition $[V_0, \phi_0]^\top \in \mathbb{R}^{2N}$, $[0, \phi_e]^\top$ is unique and stable equilibrium point to which the network model converges, as shown in the following section, where we determine the conditions for the existence and stability of a unique equilibrium point of (3.7a-b) for a given fixed initial condition.

$$\mathcal{L}(t) = \begin{pmatrix} \ell_{11}(t) & -1.5 & -6 & -0.5+\exp(2-0.1t) & -0.5-t\exp(-0.1t) & -0.1t^2 \\ -1.5 & \ell_{22}(t) & -\exp(0.1t-6) & -6\cos^2(t)\sin(0.1\pi t)-7 & -\exp(-0.5t) & -\exp(0.1t) \\ -6 & -\exp(0.1t-6) & \ell_{33}(t) & -0.1t & -\cos(t)-1.1 & -\arctan(t) \\ -0.5-\exp(2-0.1t) & -6\cos^2(t)\sin(0.1\pi t)-7 & -0.1t & \ell_{44}(t) & -10 & -3 \\ -0.5-t\exp(-0.1t) & -\exp(-0.5t) & -\cos(t)-1.1 & -10 & \ell_{55}(t) & -\sin(\pi t)-1.1 \\ -0.1t^2 & -\exp(0.1t) & -\arctan(t) & -3 & -\sin(\pi t)-1.1 & \ell_{66}(t) \end{pmatrix} \tag{3.11}$$

$$\begin{aligned} \ell_{11}(t) &= 1.5+6+0.5+\exp(2-0.1t)+0.5+t\exp(-0.1t)+0.1t^2 \\ \ell_{22}(t) &= 1.5+6\cos^2(t)\sin(0.1\pi t)+\exp(0.1t-6)+7+\exp(-0.5t)+\exp(0.1t) \\ \ell_{33}(t) &= 6+\exp(0.1t-6)+0.1t+\cos(t)+1.1+\arctan(t) \\ \ell_{44}(t) &= 0.5+\exp(2-0.1t)+6\cos^2(t)\sin(0.1\pi t)+7+0.1t+10+3 \\ \ell_{55}(t) &= 0.5+t\exp(-0.1t)+\exp(-0.5t)+\cos(t)+1.1+10+\sin(\pi t)+1.1 \\ \ell_{66}(t) &= 0.1t^2+\exp(0.1t)+\arctan(t)+3+\sin(\pi t)-1.1 \end{aligned} \tag{3.12}$$

In following section the results are illustrated with numerical simulations, then the contribution is finished with closing remarks.

To establish the existence and stability of a unique equilibrium point for the MIFNN model given fixed initial condition $[V_0, \phi_0]^\top$, we start considering the voltage equation (3.7a).

Assuming:

1. There exists a solution to the magnetic flux equation (3.7b) which is unique and continuous on $\mathbb{R}$ for each node i.

2. The memristive characteristic $f_w(\cdot)$ of the neurons is a monotonic and strictly increasing function.

The voltage equation of the MIFNN model (3.8a) can be written as

$$\dot{V}(t) = -B(t)V(t) \tag{3.13}$$

where $B(t) = W(\phi(t)) + \mathcal{L}(t)$,

We have the following results:

Theorem 3.1. *The voltage equation (3.13) has a unique equilibrium point given by*

$$V_e = 0 \in \mathbb{R}^N \tag{3.14}$$

Proof. Given that the $\mathcal{L}(t)$ is a positive semidefinite matrix for all time instants, and $W(\phi(t))$ is positive definite due to assumption (2). Their sum is positive definite $\forall t$, and as a consequence $B(t)$ is a non-singular matrix $\forall t$, therefore get that $V_e = 0$ is the only solution to its equilibrium point algebraic equation. □

From the above result we can derive the following:

Theorem 3.2. *Under assumptions (1) and (2) the unique equilibrium point $V_e = 0 \in \mathbb{R}^N$ is uniformly asymptotically stable.*

Proof. To establish the stability of $V_e = 0$ consider the Lyapunov candidate function, $E(V(t)) = \frac{1}{2}V^\top(t)PV(t)$ with P a constant symmetric and positive definite matrix of appropriate dimensions. Its derivative on the trajectories of (3.13) is given by

$$\dot{E}(V(t)) = -V^\top(t)\left[PB(t)\right]V(t) \tag{3.15}$$

If $\exists Q \in \mathbb{R}^{N\times N}$ definite positive for all time, such that $PB(t) > -Q$, would imply that $\dot{E}(V(t)) < 0$, $\forall t$, that is, $V_e = 0$ is uniformly asymptotically stable equilibrium point of (3.8a). □

As a consequence of Theorem 3.2 we know that the right side of (3.8b) will converge to zero. Then, we have the following result:

Corollary 3.3. *Under assumptions of Theorem 3.2. If $B(t)$ is positive definite $\forall t$, then the solution of the magnetic flux equation of the MIFNN model (3.8b) will converge asymptotically to a fixed value $\phi \in \mathbb{R}^N$. Furthermore,*

$$\phi_e = \lim_{t\to\infty} \int_{t_0}^{t} V(\tau)d\tau + \phi_0 \tag{3.16}$$

Proof. Integrating both sides of (3.8b) we have

$$\phi(t) = \int_{t_0}^{t} V(\tau)d\tau + \phi_0$$

From the result in Theorem 3.2 we have that for a sufficiently large T, $V(T) = 0$, regardless of the initial condition $[V_0, \phi_0]^\top \in \mathbb{R}^{2N}$, and given that $V(t)$ is a unique and continuous function, the limit in (3.16) exists and is a unique fixed value that depends on the history of the voltage across the memristive neurons and the initial conditions. □

Finally, combining the above results we have

Theorem 3.4. *Under assumptions of Theorem 3.2, for a given fixed initial condition the time-varying MIFNN model (3.8a-b) has a unique equilibrium point $[0, \phi_e]^\top \in \mathbb{R}^{2N}$ and it is uniformly asymptotically stable.*

Proof. It follows from the previous results. □

3.1.3 Simulation Example

In this numerical analysis, we illustrate Theorems 3.2 and 3.4, by constructing six node network as described in (3.8a)-(3.8b), where every node is connected to its five neighbor nodes, the network topology consists of a six-node fully connected network, where its time-varying Laplacian is described in equation (3.11). Let the initial conditions be:

$$V_0 = [-5.5, 4.5, -3.1, 6.3, -2.2, 5.2]^\top \tag{3.17}$$

$$\phi_0 = [1, -1, -2, -1.4, -1.6, 3]^\top \tag{3.18}$$

Let the memductance matrix be:
$W(\phi) = \text{diag}(w(\varphi_1), \cdots, w(\varphi_6)) \in \mathbb{R}^{6\times 6}$, where $w(\varphi_i) = \frac{df_w(\varphi_i)}{d\varphi_i}$ is the memductance function and $f_w(\varphi_i)$ the memristive characteristic function described by:

$$f_w(\varphi_i) = \begin{cases} 0.1\varphi_i - 4, & \varphi_i \leq -2 \\ 2.1\varphi_i, & -2 < \varphi_i < 2 \\ 0.1\varphi_i + 4, & \varphi_i \leq 2 \end{cases} \tag{3.19}$$

Therefore, assumption (2) is satisfied, and we proceed to solve system of the six node network, described above via numerical integration using Matlab$^{\text{©}}$ software, through *Runge-Kutta* method. First is verified Theorem 2, that is, asymptotic convergence of nodes voltages towards zero solution as shown in Fig. 3.2.

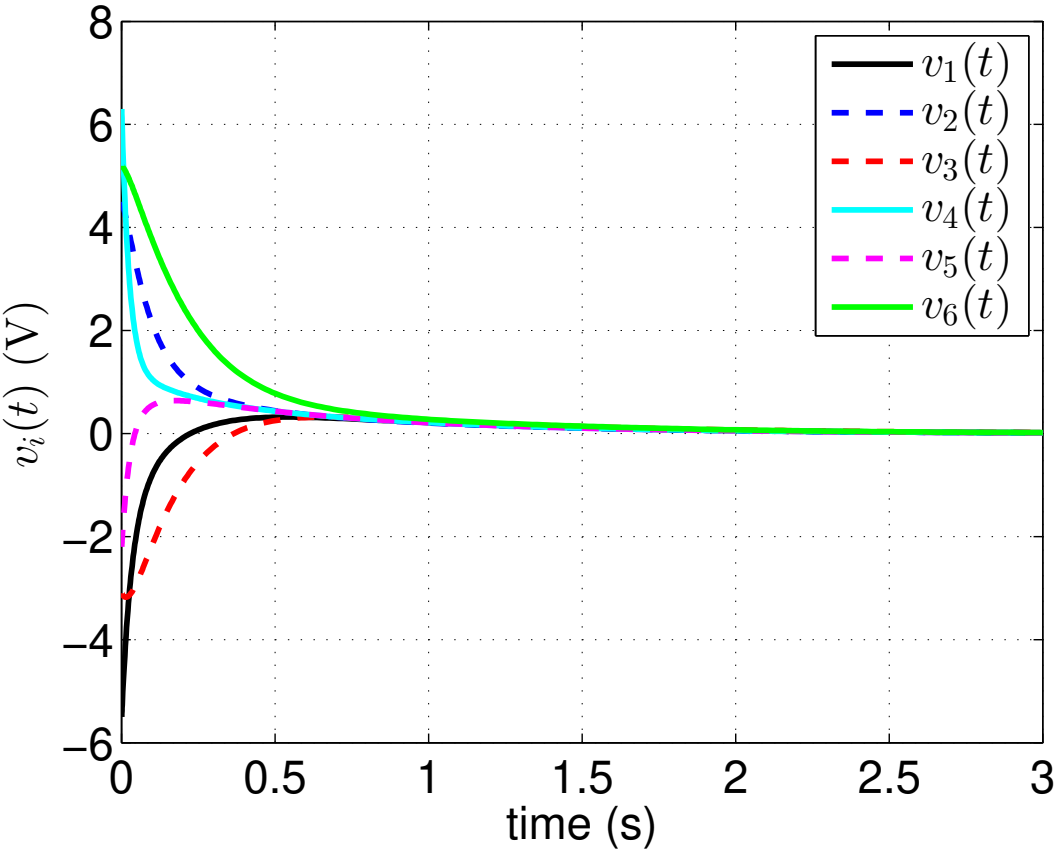

Figure 3.2: Numerical integration of the MIFNN network described by (3.8a-b). Plot of node voltages $V(t) = [v_1(t), v_2(t), v_3(t), v_4(t), v_5(t), v_6(t)]$

Subsequently, to verify the results of Corollary 2.1, that is, the asymptotic convergence of nodes magnetic fluxes towards different constant values, dependent on the initial conditions $[V_0, \phi_0]^\top \in \mathbb{R}^{12}$, as shown in Fig. 3.3.

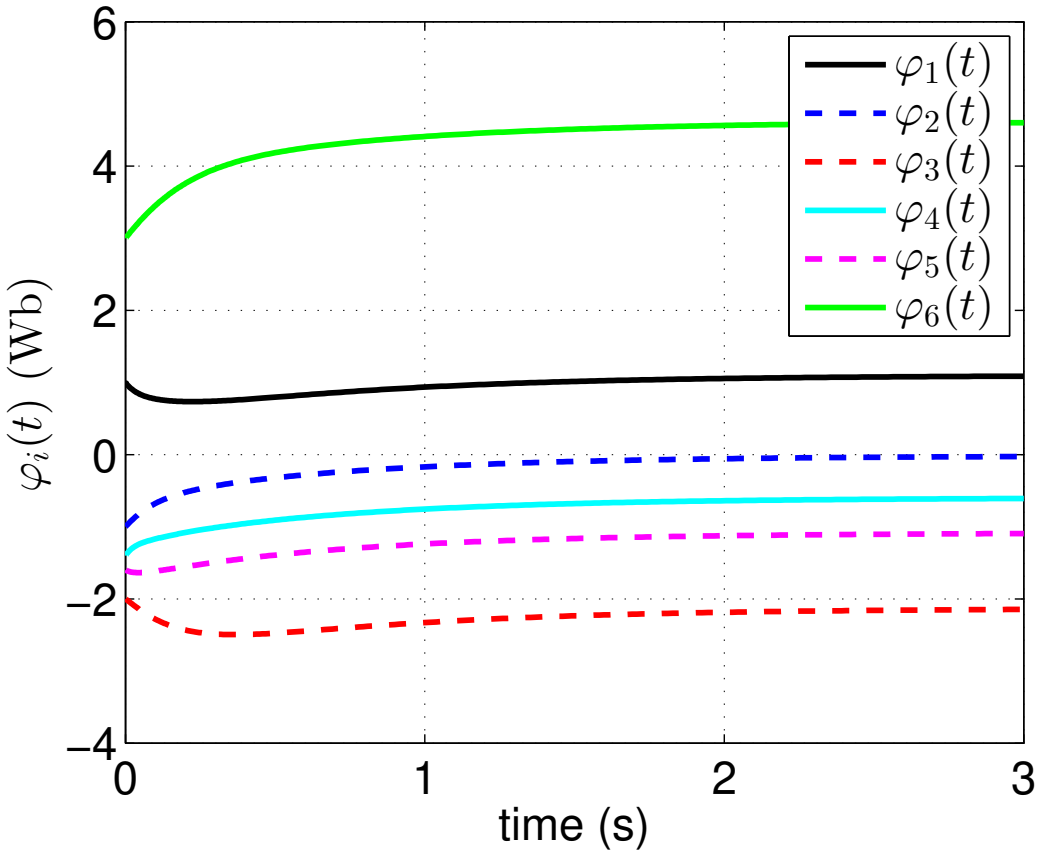

Figure 3.3: Numerical integration of the six nodes network described by (3.8a-b). Plot of nodes magnetic fluxes $\phi(t) = [\varphi_1(t), \varphi_2(t), \varphi_3(t), \varphi_4(t), \varphi_5(t), \varphi_6(t)]$

As shown in Fig. 3.3 the corresponding equilibrium point ϕ_e as described in equation (25) in Corollary 2.1 is:

$$\phi_e = [1.1002, -0.0152, -2.1316, -0.5967, -1.0827, 4.6169]^\top \tag{3.20}$$

As a result of the numerical analysis preformed in Fig. 4 and Fig.5 is verified Theorem 3, in which is shown that for the initial condition (3.17), the equilibrium point $[0, \phi_e]^\top$, where ϕ_e is given in (3.20), is an asymptotic stable equilibrium point of (17a-b).

We proposed a time-varying MIFNN model and derived simple conditions to establish the existence of a memory state, e.g. a unique stable equilibrium point for each initial condition. The conditions for the existence of a memory state are the increasing monotonicity of the memristive characteristic function and uniform dissipation of the time-varying Laplacian matrix to describe the neuron connections. Further, we show using the Lyapunov approach that the voltage equation of the MIFNN model converges to the zero solution as its only equilibrium point and that is uniformly asymptotically stable. As a consequence of this, for a given initial condition the entire time-varying network has a unique stable equilibrium point, which represents the network's memory of its initial conditions.

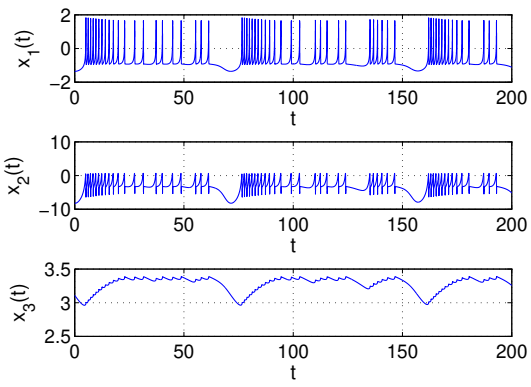

(a) states vs time

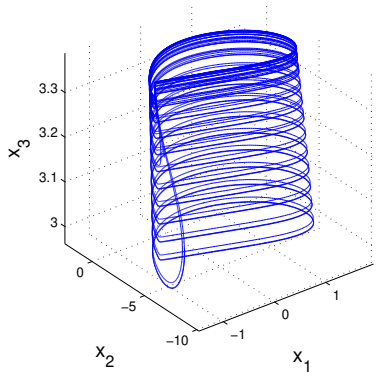

(b) Chaotic spiking attractor

Figure 3.4: HR model with chaotic bursting behavior where (a) states vs time (b) Chaotic spiking attractor

3.2 Synchronization of memristor-based bidirectionally coupled Hindmarsh-Rose neurons

In this contribution, it is investigated the emergence of identical synchronization in an array of two identical Hindmarsh-Rose neurons bidirectionally coupled by memristors through their voltage variable. It is shown that, for a sufficiently large positive memductance, the states of the neurons synchronize and the memristors converge to constant values. The results are illustrated with numerical simulations.

The HR neuron model is described by:

$$\begin{aligned} \dot{x}_1(t) &= -ax_1^3(t) + bx_1^2(t) + x_2(t) - x_3(t) + I(t) \\ \dot{x}_2(t) &= c - dx_1^2(t) - x_2(t) \\ \dot{x}_3(t) &= \varepsilon \left[\sigma \left(x_1(t) - r\right) - x_3(t)\right] \end{aligned} \tag{3.21}$$

where $x_1(t)$ is related to the neuron voltage, $x_2(t)$ to the recuperation variable, $x_3(t)$ to the adaptation variable, and $I(t)$ is the excitation current. With the following parameters $a = 1, b = 3, c = 1, d = 5, \sigma = 4, r = -1.6$,$I(t) = 5$, $\varepsilon = 0.0021$ a chaotic bursting behavior as observed as shown in Figures 3.4(a)-3.4(b).

Rewriting (3.21) is in vector form one gets:

$$\dot{\mathbf{x}}(t) = f(\mathbf{x}(t)) \tag{3.22}$$

where $\mathbf{x}(t) = [x_1(t), x_2(t), x_3(t)]^\top$ and $f(\cdot)$ is the vector field described by equation (3.21), $f : \mathbb{R}^3 \to \mathbb{R}^3$, where $f(\cdot)$ is locally Lipschitz in $\mathbb{R}^3$.

Biological neural systems can be characterized through memristors. An ideal memristor is defined in [32] as theoretically being a basic electronic passive two terminal device that relates electric charge to magnetic flux, such that the following relationship is found:

$$q_w(t) = g(\varphi_w(t)) \tag{3.23}$$

where $q_w(t) \in \mathbb{R}$ is the electric charge, and $\varphi_w(t) \in \mathbb{R}$ is the magnetic flux, $g : \mathbb{R} \to \mathbb{R}$ is its characteristic function, that satisfies the conditions: (i) $g(0) = 0$, $g(\cdot) \in C^1$; and (ii) $g(\cdot)$ is strictly monotonic increasing. The electrical representation of such device is shown in Figure 3.5.

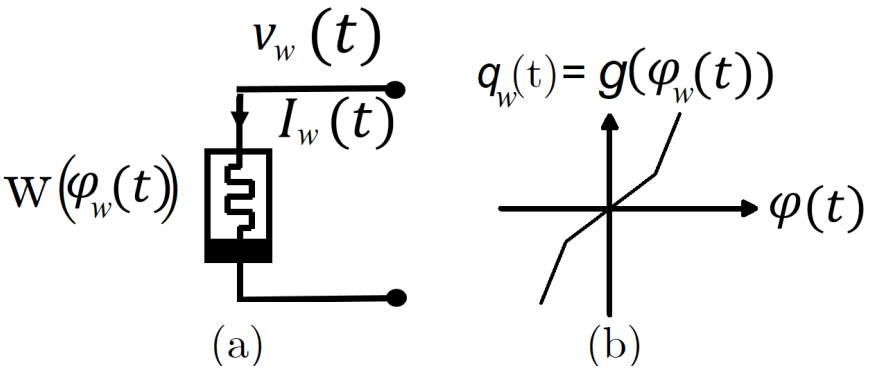

Figure 3.5: (a) electric representation (b) memristive characteristic function [70]

For the ideal memristor a current-voltage relation is given by:

$$i_w(t) = w(\varphi_w)v_w(t) \tag{3.24}$$

where $v_w(t) = \dot{\varphi}_w(t)$ and $i_w(t) = \dot{q}_w(t)$ are the voltage and current of the memristor, respectively; with its memductance given by:

$$w(\varphi_w) = \frac{dg(\varphi_w)}{d\varphi_w} \tag{3.25}$$

where $w(\varphi_w) > 0, \forall \varphi_w$, $w(\cdot)$ is a bounded function.

By integrating the voltage variable with respect to time, the magnetic flux $\varphi_w(t)$ is found to be:

$$\varphi_w(t) = \int_0^t v_w(\tau)d\tau + \varphi_w(0) \tag{3.26}$$

where $\varphi_w(t_0)$ is the initial magnetic flux. Therefore, the magnetic flux described by (3.26) depends on the *history* of the memristor voltage $v_w(t)$.

3.2.1 Synchronization problem

Consider a MNN consisting of two identical HR neurons bidirectionally coupled by two ideal memristors, let $\mathbf{x}_1(t)$ the state of neuron 1 and $\mathbf{x}_2(t)$ the state of neuron 2. One says that the MNN achieves identical synchronization when the states of each nodes move at unison, *i.e.*,

$$\mathbf{x}_1(t) = \mathbf{x}_2(t) = s(t).$$

Where $s(t)$ is called synchronization solution of the network.

The dynamics of MNN are described by:

$$\dot{\mathbf{x}}_1(t) = f(\mathbf{x}_1(t)) + w_{21}(\varphi_{21}(t))\Gamma(\mathbf{x}_2(t) - \mathbf{x}_1(t)) \tag{3.27a}$$
$$\dot{\mathbf{x}}_2(t) = f(\mathbf{x}_2(t)) + w_{12}(\varphi_{12}(t))\Gamma(\mathbf{x}_1(t) - \mathbf{x}_2(t)) \tag{3.27b}$$
$$\dot{\varphi}_{21}(t) = v_2(t) - v_1(t) \tag{3.27c}$$
$$\dot{\varphi}_{12}(t) = v_1(t) - v_2(t) \tag{3.27d}$$

where $\mathbf{x}_1(t) = [x_{11}(t), x_{21}(t), x_{31}(t)]^\top$ is the state of neuron one, and $\mathbf{x}_2(t) = [x_{12}(t), x_{22}(t), x_{32}(t)]^\top$ is that of neuron two, $\Gamma = \text{diag}(1, 0, 0) \in \mathbb{R}^{3\times3}$ is the internal coupling matrix, and the voltage of neurons are $v_1(t) = \gamma\mathbf{x}_1(t), v_2(t) = \gamma\mathbf{x}_2(t)$, where $\gamma = [1, 0, 0]$. In this example is considered a perturbation signal in the first neuron. The memristor that connects neuron 1 with neuron 2 is M_{12} with $\varphi_{12}(t)$ its magnetic flux (3.28a). While M_{21} is the memristor that connects neuron 2 with neuron 1, with its magnetic flux $\varphi_{21}(t)$ given by (3.28b).

$$\varphi_{12}(t) = \int_0^t (v_1(\tau) - v_2(\tau))d\tau + \varphi_{12}(0) \tag{3.28a}$$
$$\varphi_{21}(t) = \int_0^t (v_2(\tau) - v_1(\tau))d\tau + \varphi_{21}(0) \tag{3.28b}$$

the memristive characteristic function of M_{12} is:

$$\begin{array}{rl} g_{12}(\varphi_{12}) & = a_{12}\varphi_{12} + \frac{1}{2}(b_{12} - a_{12})(|\varphi_{12} + l_{12}|) \\ & -\frac{1}{2}(b_{12} - a_{12})(|\varphi_{12} - l_{12}|) \end{array} \tag{3.29}$$

where a_{12},$b_{12}, l_{12} > 0$ are constants, $b_{12} < a_{12}$, taking the derivative of (3.29) is obtained its memristance function:

$$w_{12}(\varphi_{12}) = \frac{dg_{12}(\varphi_{12})}{d\varphi_{12}} = \begin{cases} a_{12} & , \quad \varphi_{12} < -l_{12} \\ b_{12} & , \quad -l_{12} \leq \varphi_{12} \leq l_{12} \\ a_{12} & , \quad l_{12} < \varphi_{12} \end{cases} \tag{3.30}$$

On the other hand, the memristive characteristic function of M_{21} is:

$$\begin{array}{rl} g_{21}(\varphi_{21}) & = a_{21}\varphi_{21} + \frac{1}{2}(b_{21} - a_{21})(|\varphi_{21} + l_{21}|) \\ & -\frac{1}{2}(b_{21} - a_{21})(|\varphi_{21} - l_{21}|) \end{array} \tag{3.31}$$

where a_{21},$b_{21}, l_{21} > 0$ are constants, $b_{21} < a_{21}$, taking the derivative of (3.31) is obtained its memristance function:

$$w_{21}(\varphi_{21}) = \frac{dg_{21}(\varphi_{21})}{d\varphi_{21}} = \begin{cases} a_{21} & , \quad \varphi_{21} < -l_{21} \\ b_{21} & , \quad -l_{21} \leq \varphi_{21} \leq l_{21} \\ a_{21} & , \quad l_{21} < \varphi_{21} \end{cases} \tag{3.32}$$

as consequence of identical synchronization, $\varphi_{12}(t) = \bar{\varphi}_{12}$ and $\varphi_{21}(t) = \bar{\varphi}_{21}$, where:

$$\begin{array}{rl} \bar{\varphi}_{12} & = \lim_{t\to\infty} \int_0^t (v_1(\tau) - v_2(\tau))d\tau + \varphi_{12}(0) \\ \bar{\varphi}_{21} & = \lim_{t\to\infty} \int_0^t (v_2(\tau) - v_1(\tau))d\tau + \varphi_{21}(0) \end{array}$$

At the synchronized state $s(t)$ the coupling term in the MNN goes to zero, therefore one has that its behavior is that of an isolated node:

$$\dot{s}(t) = f(s(t)) \tag{3.33}$$

Lets define the synchronization error as

$$\mathbf{e}_1(t) = \mathbf{x}_1(t) - s(t) \tag{3.34a}$$
$$\mathbf{e}_2(t) = \mathbf{x}_2(t) - s(t) \tag{3.34b}$$

where $\mathbf{e}_1(t) = [e_{11}(t), e_{21}(t), e_{31}(t)] \in \mathbb{R}^3$, and $\mathbf{e}_2(t) = [e_{12}(t), e_{22}(t), e_{32}(t)] \in \mathbb{R}^3$. Therefore, identical synchronization in the MNN is equivalent to the stability of the zero solution of the synchronization error dynamics.

Notice that when identical synchronization occurs $\mathbf{e}_1(t) = \mathbf{e}_2(t) = 0$, therefore $s(t) = \mathbf{x}_1(t) = \mathbf{x}_2(t)$. The error dynamics is obtained by taking the derivative of (3.34a)-(3.34b)

$$\dot{\mathbf{e}}_1(t) = \dot{\mathbf{x}}_1(t) - \dot{s}(t) \tag{3.35a}$$
$$\dot{\mathbf{e}}_2(t) = \dot{\mathbf{x}}_2(t) - \dot{s}(t) \tag{3.35b}$$

substituting $\mathbf{x}_1(t) = \mathbf{e}_1(t) + s(t)$ in (3.35a), and $\mathbf{x}_2(t) = \mathbf{e}_2(t) + s(t)$ (3.35b) one obtains:

$$\begin{aligned}\dot{\mathbf{e}}_1(t) &= f(\mathbf{x}_1(t)) - \dot{s}(t) \\ &\quad + w_{21}(\varphi_{21}(t))\Gamma(\mathbf{e}_2(t) + s(t) - \mathbf{e}_1(t) - s(t))\end{aligned} \tag{3.36a}$$
$$\begin{aligned}\dot{\mathbf{e}}_2(t) &= f(\mathbf{x}_2(t)) - \dot{s}(t) \\ &\quad + w_{12}(\varphi_{12}(t))\Gamma(\mathbf{e}_1(t) + s(t) - \mathbf{e}_2(t) - s(t))\end{aligned} \tag{3.36b}$$

substituting (3.33) in (3.36a),(3.36b) and rearranging:

$$\begin{aligned}\dot{\mathbf{e}}_1(t) &= f(\mathbf{x}_1(t)) - f(s(t)) \\ &\quad + w_{21}(\varphi_{21}(t))\Gamma(\mathbf{e}_2(t) - \mathbf{e}_1(t))\end{aligned} \tag{3.37a}$$
$$\begin{aligned}\dot{\mathbf{e}}_2(t) &= f(\mathbf{x}_2(t)) - f(s(t)) \\ &\quad + w_{12}(\varphi_{12}(t))\Gamma(\mathbf{e}_1(t) - \mathbf{e}_2(t))\end{aligned} \tag{3.37b}$$

where $f(\cdot)$ is described by (3.22), expressing (3.37a) in vector form becomes:

$$\dot{\mathbf{e}}(t) = F(\mathbf{X}(t)) - F(\mathbf{S}(t)) + W(\varphi(t)) \otimes \Gamma\mathbf{e}(t) \tag{3.38a}$$
$$\dot{\varphi}(t) = G \otimes \gamma\mathbf{e}(t) \tag{3.38b}$$

where $\mathbf{e}(t) = [\mathbf{e}_1^\top(t), \mathbf{e}_2^\top(t)]^\top \in \mathbb{R}^6$, $F(\cdot) = [f^\top(\cdot),\ f^\top(\cdot)]^\top \in \mathbb{R}^6$, $\mathbf{X}(t) = [\mathbf{x}_1^\top(t), \mathbf{x}_2^\top(t)]^\top \in \mathbb{R}^6$, $\mathbf{S}(t) = [s^\top(t), s^\top(t)]^\top \in \mathbb{R}^6$ is the synchronous solution, $\varphi(t) = [\varphi_{12}(t), \varphi_{21}(t)]^\top \in \mathbb{R}^2$, $\Gamma = \text{diag}(\gamma) \in \mathbb{R}^{3\times3}$, $\gamma = [1, 0, 0]$, and $\otimes$ is the Kronecker product.

Under the assumption of exists of solution to magnetic flux equation (3.38b), which is bounded on $\mathbb{R}^2$, therefore the time dependent connection matrix is:

$$W(\varphi(t)) = \begin{bmatrix} -w_{21}(\varphi_{21}(t)) & w_{21}(\varphi_{21}(t)) \\ w_{12}(\varphi_{12}(t)) & -w_{12}(\varphi_{12}(t)) \end{bmatrix} \tag{3.39}$$

where $W(\varphi(t))$ is a continuous piecewise linear matrix

$$W(\varphi(t)) = \begin{cases} W_1(\varphi(t)), & & \varphi_{12}(t) < & l_{12} & , & & \varphi_{21}(t) & < -l_{21} \\ W_2(\varphi(t)), & & \varphi_{12}(t) < & -l_{12} & , & -l_{21} \leq & \varphi_{21}(t) & < l_{21} \\ W_3(\varphi(t)), & & \varphi_{12}(t) < & -l_{12} & , & _{21} \leq & \varphi_{21}(t) & \\ W_4(\varphi(t)), & -l_{12} \leq & \varphi_{12}(t) < & l_{12} & , & & \varphi_{21}(t) & < -l_{21} \\ W_5(\varphi(t)), & -l_{12} \leq & \varphi_{12}(t) < & l_{12} & , & -l_{21} \leq & \varphi_{21}(t) & < -l_{21} \\ W_6(\varphi(t)), & -l_{12} \leq & \varphi_{12}(t) < & l_{12} & , & l_{21} \leq & \varphi_{21}(t) & \\ W_7(\varphi(t)), & l_{12} \leq & \varphi_{12}(t) & & , & & \varphi_{21}(t) & < -l_{21} \\ W_8(\varphi(t)), & l_{12} \leq & \varphi_{12}(t) & & , & -l_{21} \leq & \varphi_{21}(t) & < l_{21} \\ W_9(\varphi(t)), & l_{12} \leq & \varphi_{12}(t) & & , & l_{21} \leq & \varphi_{21}(t) & \end{cases}$$

where:

$$W_1(\varphi(t)) = \begin{bmatrix} -a_{12} & , & a_{12} \\ a_{21} & , & -a_{21} \end{bmatrix}$$

$$W_2(\varphi(t)) = \begin{bmatrix} -b_{12} & , & b_{12} \\ a_{21} & , & -a_{21} \end{bmatrix}$$

$$W_3(\varphi(t)) = \begin{bmatrix} -a_{12} & , & a_{12} \\ a_{21} & , & -a_{21} \end{bmatrix}$$

$$W_4(\varphi(t)) = \begin{bmatrix} -a_{12} & , & a_{12} \\ b_{21} & , & -b_{21} \end{bmatrix}$$

$$W_5(\varphi(t)) = \begin{bmatrix} -a_{12} & , & a_{12} \\ b_{21} & , & -b_{21} \end{bmatrix}$$

$$W_6(\varphi(t)) = \begin{bmatrix} -a_{12} & , & a_{12} \\ b_{21} & , & -b_{21} \end{bmatrix}$$

$$W_7(\varphi(t)) = \begin{bmatrix} -a_{12} & , & a_{12} \\ a_{21} & , & -a_{21} \end{bmatrix}$$

$$W_8(\varphi(t)) = \begin{bmatrix} -b_{12} & , & b_{12} \\ a_{21} & , & -a_{21} \end{bmatrix}$$

$$W_9(\varphi(t)) = \begin{bmatrix} -a_{12} & , & a_{12} \\ a_{21} & , & -a_{21} \end{bmatrix}$$

$$G = \begin{bmatrix} -1 & 1 \\ 1 & -1 \end{bmatrix} \tag{3.40}$$

where $W(\varphi(t))$ is non-symmetric and the sum of its rows is zero uniformly in time, therefore it is negative semidefinite uniformly in time, furthermore its eigenvalues are $\lambda_{1,2}(W(\varphi(t)))$, where $\lambda_1(W(\varphi(t))) = 0, \forall \varphi \in \mathbb{R}^2$ and $\lambda_2(W(\varphi))$ is given by (3.41).

$$\lambda_2(W(\varphi(t))) = \begin{cases} -(a_{12}+a_{21}), & & \varphi_{12}(t) < & -l_{12} & , & & \varphi_{21}(t) & < -l_{21} \\ -(a_{12}+b_{21}), & & \varphi_{12}(t) < & -l_{12} & , & -l_{21} \leq & \varphi_{21}(t) & < \ l_{21} \\ -(a_{12}+a_{21}), & & \varphi_{12}(t) < & -l_{12} & , & \ l_{21} \leq & \varphi_{21}(t) & \\ -(b_{12}+a_{21}), & -l_{12} \leq & \varphi_{12}(t) < & \ l_{12} & , & & \varphi_{21}(t) & < -l_{21} \\ -(b_{12}+b_{21}), & -l_{12} \leq & \varphi_{12}(t) < & \ l_{12} & , & -l_{21} \leq & \varphi_{21}(t) & < -l_{21} \\ -(b_{12}+a_{21}), & -l_{12} \leq & \varphi_{12}(t) < & \ l_{12} & , & \ l_{21} \leq & \varphi_{21}(t) & \\ -(a_{12}+a_{21}), & \ l_{12} \leq & \varphi_{12}(t) & & , & & \varphi_{21}(t) & < -l_{21} \\ -(a_{12}+b_{21}), & \ l_{12} \leq & \varphi_{12}(t) & & , & -l_{21} \leq & \varphi_{21}(t) & < \ l_{21} \\ -(a_{12}+a_{21}), & \ l_{12} \leq & \varphi_{12}(t) & & , & \ l_{21} \leq & \varphi_{21}(t) & \end{cases} \tag{3.41}$$

Equation (3.38a) is rewritten:

$$\dot{\mathbf{e}}(t) = \hat{F}(t, \mathbf{e}(t)) \tag{3.42}$$

where $\hat{F}(t, \mathbf{e}(t)) = F(\mathbf{X}(t)) - F(\mathbf{S}(t)) - W(\varphi(t)) \otimes \Gamma \mathbf{e}(t)$.

We aim to determine if $\mathbf{e}(t) \to 0$ exponentially in time at lest locally, which means that $\mathbf{S}(t)$ is a solution exponentially stable of (3.38a) and consequently $\varphi(t) \to \bar{\varphi}$ in (3.38b), where $\bar{\varphi} = [\bar{\varphi}_{12}, \bar{\varphi}_{21}]^\top$ is a constant value denominated the memory states of the memristive synapses.

Let $\|\cdot\|$ be the euclidean norm, with $B_r = \{\mathbf{e} \in \mathbb{R}^6 : \|\mathbf{e}\| < r\}$ the following properties of $\hat{F}(\cdot)$ are satisfied: (I) $\hat{F}(t, \mathbf{e})$ is Locally Lipschitz on B_r and piecewise continuous with respect to t. (II) Linearizing (3.42) around the origin we obtain:

$$\dot{\mathbf{e}}(t) = A(\mathbf{S}(t))\mathbf{e}(t) + W(\varphi(t)) \otimes \Gamma \mathbf{e}(t) \tag{3.43}$$

where $A(\mathbf{S}(t))$ is black diagonal matrix:

$$A(\mathbf{S}(t)) = \begin{bmatrix} Df(s(t)) & 0 \\ 0 & Df(s(t)) \end{bmatrix} \in \mathbb{R}^{6\times 6}$$

which is locally Lipschitz in B_r uniformly in t and $Df(s(t)) \in \mathbb{R}^{3\times 3}$ is the Jacobian of $f(\cdot)$.

Theorem 3.5. *Assume:*
*(**A1**) $s(t)$ is an exponentially stable solution of single node dynamics (3.22), and*
*(**A2**) $||D(f(s(t)))|| < \alpha$, where $||\cdot||$ is a matrix induced norm and $\alpha > 0$ a positive constant. If the memductance matrix $W(\cdot)$ is negative semidefinite uniformly in time, then the linearized error dynamics (3.43) are exponentially in time ($\mathbf{e}(t) \to 0$). Furthermore, since the origin is a locally exponentially stable solution of the nonlinear system (3.42) identical synchronization between the neurons is achieved.*

Proof. The system (3.43) is rewritten:

$$\dot{\nu}(t) = Df(s(t))\nu(t) + \Gamma\nu(t)(W\varphi(t))^\top \tag{3.44}$$

where $\nu(t) = [\mathbf{e}_1(t), \mathbf{e}_2(t)] \in \mathbb{R}^{3\times 2}$ for the given $W(\varphi(t))$ there exists a non singular matrix $Z(t) \in \mathbb{R}^{2\times 2}$ such that:

$$\Lambda(t) = Z^{-1}(\varphi(t))W(\varphi(t))Z(\varphi(t))$$

where $\Lambda(t) = \text{diag}(\lambda_1(t), \lambda_2(t)) \in \mathbb{R}^{2\times 2}$ and

$$Z(\varphi(t)) = \begin{bmatrix} -\frac{w_{12}(\varphi_{12}(t))}{w_{21}(\varphi_{21}(t))} & 1 \\ 1 & 1 \end{bmatrix}$$

a change of base is considered:

$$\eta(t) = \nu(t)Z^{-1}(\varphi(t)) \tag{3.45}$$

taking the derivative of (3.45) is obtained:

$$\dot{\eta}(t) = \dot{\nu}(t)Z(\varphi(t)) + \nu(t)\dot{Z}(\varphi(t)) \tag{3.46}$$

substituting (3.43) in (3.46):

$$\dot{\eta}(t) = Df(s(t))\eta(t) + \Gamma\eta(t)\Lambda(t) - \eta(t)\dot{Z}^{-1}(\varphi(t))Z(\varphi(t)) \tag{3.47}$$

given that $Z(\varphi(t))$ is a piece-wise constant matrix $\dot{Z}(\varphi(t)) = \text{diag}(0, 0) \in \mathbb{R}^{2\times 2}$, then equation (3.47) becomes:

$$\dot{\eta}(t) = Df(s(t))\eta(t) + \Gamma\eta(t)\Lambda(t) \tag{3.48}$$

expanding (3.48) by columns and considering $\lambda_1(t) = 0\ \forall t$ is obtained:

$$\dot{\eta}_1(t) = Df(s(t))\eta_1(t) \tag{3.49a}$$

$$\dot{\eta}_2(t) = Df(s(t))\eta_2(t) + \lambda_2(t)\Gamma\eta_2(t) \tag{3.49b}$$

given that $s(t)$ is a exponentially stable solution of (3.22) by converse Lyapunov theorem $\eta_1(t) \to 0$ exponentially in (3.49a), to determine if $\eta_2(t)$ converges exponentially to the origin, we propose a Lyapunov candidate function:

$$V(\eta_2(t)) = \frac{1}{2}\eta_2^\top(t)\eta_2(t) \tag{3.50}$$

taking the derivative of (3.50) is obtained:

$$\dot{V}(\eta_2(t)) = \eta_2^\top(t)\dot{\eta}_2(t) \tag{3.51}$$

substituting (3.49b) in (3.51) is obtained:

$$\dot{V}(\eta_2(t)) = \eta_2^\top(t)D(f(s(t)))\eta_2(t) + \lambda_2(t)\eta_2^\top(t)\Gamma\eta_2(t) \tag{3.52}$$

given that $Df(s(t))$ is bounded and $\Gamma = \text{diag}(1, 0, 0) \in \mathbb{R}^{3\times 3}$, equation (3.52) becomes

$$\dot{V}(\eta_2(t)) = c\|\eta_2(t)\|^2 + \lambda_2(t)\eta_{12}^2(t) \tag{3.53}$$

we know $\eta_{12}^2(t) < \|\eta_2(t)\|^2, \forall\eta_2(t) \neq 0$, therefore (3.53) becomes:

$$\begin{array}{ll} \dot{V}(\eta_2(t)) & < c\|\eta_2(t)\|^2 + \lambda_2(t)\|\eta_2(t)\|^2 \\ \dot{V}(\eta_2(t)) & < (c + \lambda_2(t))\|\eta_2(t)\|^2 \end{array} \tag{3.54}$$

considering $-(b_{12} + b_{21}) \leq \lambda_2(t) \leq -(a_{12} + a_{21})$, if $a_{12} + a_{21} > c$, then $\dot{V}(\eta_2(t)) < 0\ \forall\eta_2 \neq 0$. We conclude that $\eta_2(t) = 0$ is an exponential solution (3.49b), therefore $\mathbf{e}(t)$ converge exponentially in time to zero solution in the linearized error dynamics (3.43); by converse Lyapunov theorem $\mathbf{e} = 0$ is an exponentially stable equilibrium point of nonlinear dynamics (3.42). □

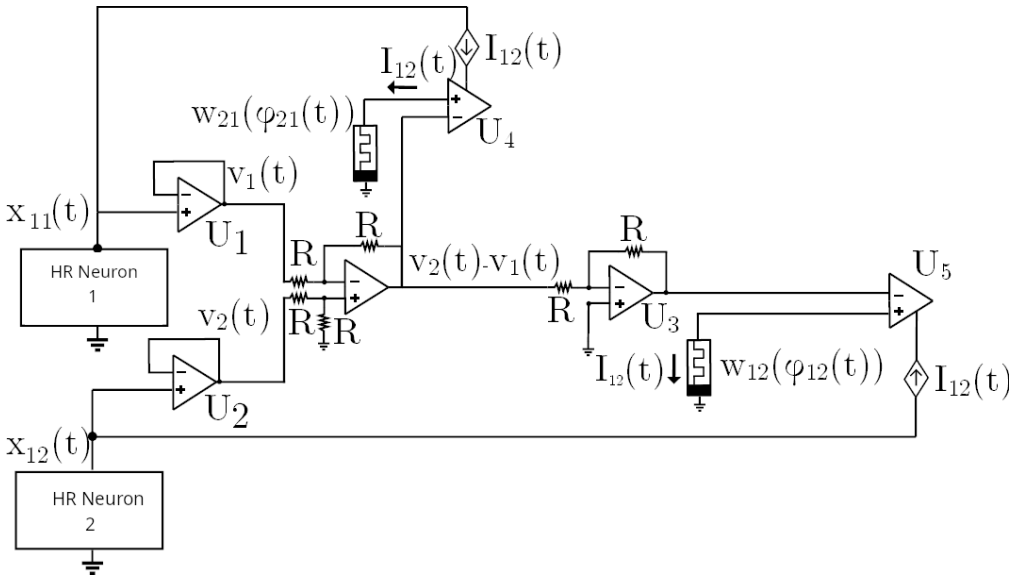

Figure 3.6: Circuit implementation of system (3.27a)-(3.27d). Two Hindmarsh-Rose neurons coupled by memristive synapse

3.2.2 Simulation Examples

Consider two identical HR neurons bidirectionally coupled through memristors M_{21} and M_{12}, the circuit of such system is presented in figure 3.6.

As noticed this circuit is composed of two memristors M_{21} and M_{12} which can be implemented as in [71], four operational amplifiers (OpAmp) U_1-U_4 and two positive second generation current conveyors (CCII+) U_4-U_5 and resistors R. Considering the elements of this circuit are in the ideal region, because the voltages of both neurons are below saturating voltage of OPAM. Its mathematical described by:

$$\dot{\mathbf{x}}_1(t) = f(\mathbf{x}_1(t)) + w_{21}(\varphi_{21}(t))\Gamma(\mathbf{x}_2(t) - \mathbf{x}_1(t)) + \zeta(t) \tag{3.55a}$$
$$\dot{\mathbf{x}}_2(t) = f(\mathbf{x}_2(t)) + w_{12}(\varphi_{12}(t))\Gamma(\mathbf{x}_1(t) - \mathbf{x}_2(t)) \tag{3.55b}$$
$$\dot{\varphi}_{21}(t) = v_2(t) - v_1(t) \tag{3.55c}$$
$$\dot{\varphi}_{12}(t) = v_1(t) - v_2(t) \tag{3.55d}$$

where $\mathbf{x}_1(t) = [x_{11}(t), x_{21}(t), x_{31}(t)]^\top$ is the state of neuron one, and $\mathbf{x}_2(t) = [x_{12}(t), x_{22}(t), x_{32}(t)]^\top$ is that of neuron two, $\Gamma = \text{diag}(1, 0, 0) \in \mathbb{R}^{3\times3}$ is the internal coupling matrix, and the voltage of neurons are $v_1(t) = \gamma\mathbf{x}_1(t), v_2(t) = \gamma\mathbf{x}_2(t)$, where $\gamma = [1, 0, 0]$.

The memristor M_{12}, connects neuron 1 with neuron 2, its magnetic flux is $\varphi_{12}(t)$ described by (3.28a). While M_{21} is the memristor that connects neuron 2 with neuron 1, its magnetic flux is $\varphi_{21}(t)$ given by (3.28b). Here is considered a perturbation signal $\zeta(t) = 0.3e^{-0.005t}$ in the first neuron.

The characteristic function of memristor M_{12} is:

$$g_{12}(\varphi_{12}) = 0.9\varphi_{12} - 0.4(|\varphi_{12} + 140| - |\varphi_{12} - 140|) \tag{3.56}$$

where its parameters are $a_{12} = 0.9$, $b_{12} = 0.1$ and $l_{12} = 140$, the function that describes its memristance is:

$$w_{12}(\varphi_{12}) = \frac{dg_{12}(\varphi_{12})}{d\varphi_{12}} = \begin{cases} 0.9 & , & & \varphi_{12} & < & -140 \\ 0.1 & , & -140 & \leq \varphi_{12} & \leq & 140 \\ 0.9 & , & 140 & < & \varphi_{12} & \end{cases} \tag{3.57}$$

While the characteristic function of memristor M_{21} is:

$$g_{21}(\varphi_{21}) = \varphi_{21} - 0.425(|\varphi_{21} + 120| - |\varphi_{21} - 120|) \tag{3.58}$$

where its parameters are $a_{21} = 1$ and $b_{21} = 0.15$,$l_{21} = 120$, the function that describes its memristance:

$$w_{21}(\varphi_{21}) = \frac{dg_{21}(\varphi_{21})}{d\varphi_{21}} = \begin{cases} 1 & , & & \varphi_{21} & < & -120 \\ 0.15 & , & -120 & \leq \varphi_{21} & \leq & 120 \\ 1 & , & 120 & < & \varphi_{21} & \end{cases} \tag{3.59}$$

the time dependent coupling matrix $W(\varphi(t))$ is piecewise constant, non symmetric and negative semidefinite uniformly in time, therefore condition of Theorem 1 is met, in this case b_{12},b_{21} are chosen big enough so that the conditions of Theorem 1 are satisfied.

The results of simulating numerically the model (3.27a)-(3.27d), with initial conditions $\mathbf{x}_1(0) = [-0.3945, -0.5858, 4.709]^\top$, $\varphi_{21}(0) = 10$,$\mathbf{x}_2(0) = [-1.361, -8.26, 3.11]^\top$, $\varphi_{12}(0) = 50$ and internal connection matrix $\Gamma = \text{diag}(1, 0, 0) \in \mathbb{R}^{3\times3}$, are shown in Figures 3.7-3.8.

Initially the pair of neurons are uncoupled, at $t = 10$ the neurons are coupled, then after $t = 20$ the voltages $x_{11}(t)$, $x_{12}(t)$ converge towards each other in spite of perturbation signal, as shown in Figure 3.7 ; while the error in neurons states (see Figure 3.8) are basically zero. In Figure 3.9 is shown that magnetic flux of memristors $\varphi_{12}(t)$ and $\varphi_{21}(t)$, converge to constant values, notice that their convergence value is different, this is because initial conditions are not equal $\varphi_{12}(0) = 10$,$\varphi_{21}(0) = 50$.

As observed in figure 3.10, the memristor M_{12} reaches high conductance region instantly when $t = 30$, while M_{21} is in low conductance region, having a big enough coupling strength, for neurons to synchronize as observed in Figure 3.7 and 3.8.

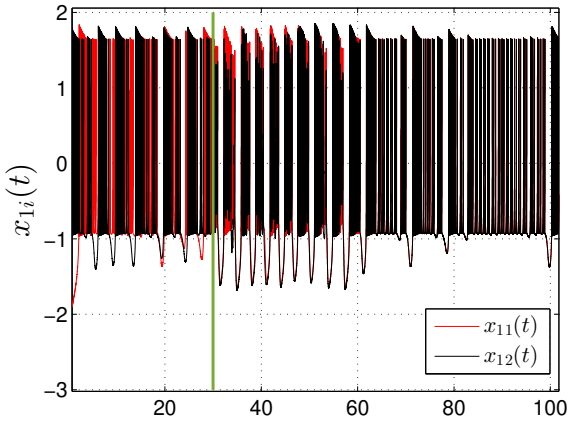

Figure 3.7: (a) Neurons voltages $x_{11}(t)$ and $x_{21}(t)$

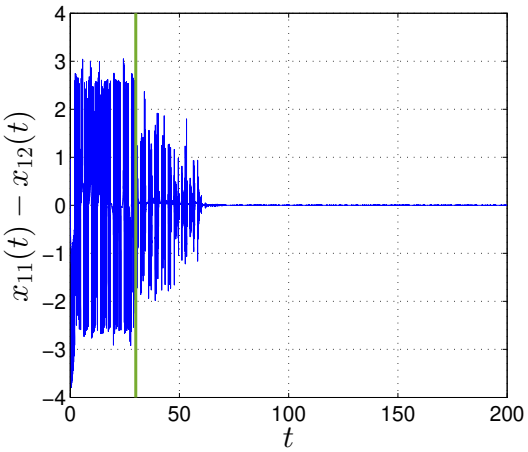

Figure 3.8: Error in neurons voltages

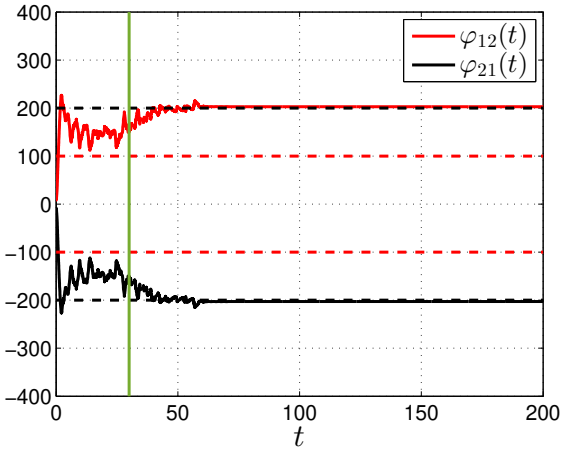

Figure 3.9: Magnetic flux of memristor M_{12} (gray) and memristor M_{21} (black)

Remark 3.6. The emergence of identical synchronization is dependent on the properties of the memristor synapses as long as they have positive memductance, *i.e.* the time dependent connection matrix is negative semidefinite uniformly in time, synchronization is achieved although they are not identical.

Remark 3.7. When a combination of memductances $w_{12}(\cdot)$, $w_{21}(\cdot)$ is not greater than the required coupling strength c to achieve synchronization, the pair of neurons will remain unsynchronized.

Synchronization in a MNN of two HR neurons bidirectionally coupled by nonidentical ideal memristors is investigated, we find sufficient conditions in memristor properties for the identical synchronization, our results show that for memristance sufficiently large and positive definite at all times, the neurons will synchronize with the magnetic flux of the memristors converge to constant values. The analysis of synchronization is based on a linearized error dynamics which restrict our results to a local neighborhood of synchronous state.

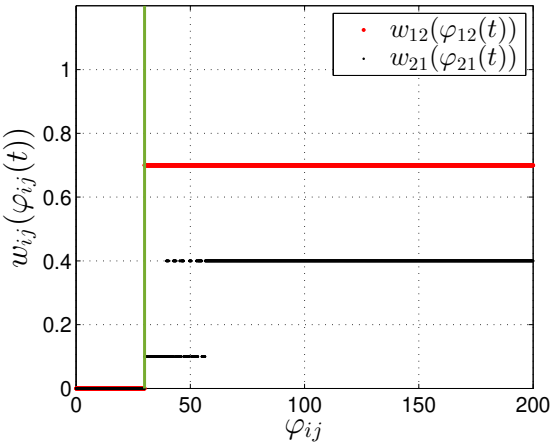

Figure 3.10: Time evolution of memductance values w_{12} (red line) and w_{21} (black line) for coupled memristors M_{12} and M_{21}. Coupling begins at $t = 30$ time units green line

3.3 Generalized synchronization of Hindmarsh-Rose neurons coupled by active memristive synapse

In this work, we consider two Hindmarsh-Rose neurons coupled by active identical memristive synapses, which enable bidirectional weighted coupling between neurons. Utilizing the nearest neighbor methodology proposed, our numerical findings indicate that under memristive active couplings, regimes of identical, phase, and lag synchronization do not manifest; instead, Generalized Synchronization (GS) occurs. The absence of Lag synchronization was confirmed through the similarity function. This indicates that the states of the first neuron are related to the states of the second neuron through a functional relation that holds uniformly over time. We also investigate the influence of memristor parameters on the temporal characteristics of the firing patterns in the two neurons, and our numerical results show that as the memristor strength coefficient increases, the average interburst interval lengthens; conversely, the average interspike interval shortens.

In the following section, we present our MNN model of HR neurons with memristive connections and the description of its synchronization problem.

3.3.1 HR neuron model

Consider a MNN where each node is a HR model describe by:

$$\begin{bmatrix} \dot{x}_1(t) \\ \dot{x}_2(t) \\ \dot{x}_3(t) \end{bmatrix} = \begin{bmatrix} -ax_1(t)^3 + bx_1(t)^2 + x_2(t) - x_3(t) + I_{syn}(t) \\ e - dx_1(t)^2 - x_2(t) \\ \varepsilon(\sigma(x_1(t) - r) - x_3(t)) \end{bmatrix} \tag{3.60}$$

where the variable $x_1(t)$ represents voltage, $x_2(t)$ recuperation, and $x_3(t)$ adaptation of the neural model that captures behaviors of ionic currents through membrane channels, as such, it captures the potassium (K^+) and sodium (Na^+) dynamics which represent the fast subsystem, while the ionic fluxes related to chlorine (Cl^+) and other leaking ions, are related to the slow variable $x_3(t)$. The external input $I_{syn}(t)$ servers to connect neurons. The parameter $0 < \varepsilon \ll 1$ describes the relation of fast-slow time scales in the neural model allowing for periodic currents that trigger the *action potential* displaying different patterns of busting and spiking behavior [72].

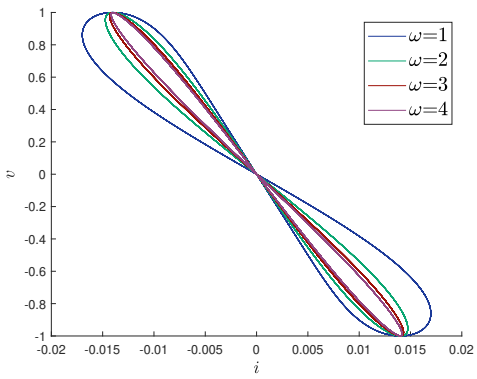

(a) Pinched hysteresis.

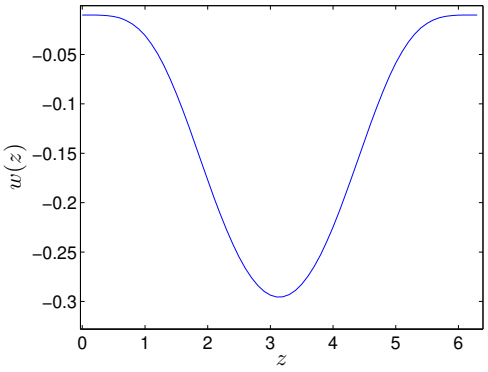

(b) Memductance function.

Figure 3.11: Memristor (3.61)-(3.62). (a) Pinched hysteresis loop of the memristor for $\nu(t) = \sin(\omega t)$, (b) The memductance evaluated for different values of $z(t)$.

The interconnection between neurons is modeled as a current given by memristors of the form:

$$I_{syn}(t) = g(z(t), \nu(t))\nu(t) \tag{3.61a}$$
$$\dot{z}(t) = f(z(t), \nu(t)) \tag{3.61b}$$

where $z(t) \in \mathbb{R}^m$ is the internal state of the memristor, $\nu(t) \in \mathbb{R}$ is the voltage input, and $I_{syn}(t) \in \mathbb{R}$ is the current output of the memristive device; with $f : \mathbb{R}^m \times \mathbb{R} \to \mathbb{R}^m$ and $g : \mathbb{R}^m \times \mathbb{R} \to \mathbb{R}$ are continuous functions describing the internal dynamics and the memductive function, which is zero-at-zero and results as the derivative of characteristic flux-charge relation along the input variable.

In this contribution, we consider that all connections are modeled by memristors with the following memductance function:

$$g(z(t), \nu(t)) = \frac{\beta}{\alpha z^2(t) + 1} - (\beta + \gamma) \tag{3.62}$$

where α, β, and $\gamma > 0$, with β the coupling strength coefficient. As such, the memductance is bounded by:

$$-(\gamma + \beta) \leq g(z(t), \nu(t)) \leq -\gamma \quad \forall z(t) \in \mathbb{R} \tag{3.63}$$

As shown in Figure 3.11, under a periodic input the current-voltage diagram is a frequency-dependent pinch-hysteresis, while the memductance function is quadratic an always negative, therefore the model (3.61)-(3.62) is an active memristor [73].

Using the memristive synapses described above to connect two HR neurons, we have the following MNN:

$$\begin{aligned} \dot{x}_{11}(t) &= x_{12}(t) - x_{13}(t) - ax_{11}^3(t) + bx_{11}^2(t) + I_{ext}(t) + M_{21}(t) \\ \dot{x}_{12}(t) &= c - x_{12}(t) - dx_{11}^2(t) \\ \dot{x}_{13}(t) &= \varepsilon[\sigma(x_{11}(t) - r) - x_{13}(t)] \end{aligned} \tag{3.64}$$

$$\begin{aligned}\dot{x}_{21}(t) &= x_{22}(t) - x_{23}(t) - ax_{21}^3(t) + bx_{21}^2(t) + I_{ext}(t) + M_{12}(t)\\ \dot{x}_{22}(t) &= c - x_{22}(t) - dx_{21}^2(t)\\ \dot{x}_{23}(t) &= \varepsilon[\sigma(x_{21}(t) - r) - x_{23}(t)]\end{aligned} \tag{3.65}$$

$$\begin{aligned}M_{21}(t) &= kg(z_{21}(t), \nu_{21}(t))\nu_{21}(t)\\ \dot{z}_{21}(t) &= \nu_{21}(t)\\ M_{12}(t) &= kg(z_{12}(t), \nu_{12}(t))\nu_{12}(t)\\ \dot{z}_{12}(t) &= \nu_{12}(t)\end{aligned} \tag{3.66}$$

where $x_i(t) = [x_{i1}(t), x_{i2}(t), x_{i3}(t)]^\top \in \mathbb{R}^3$ represents the state of the ith HR neuron; $M_{21}(t)$ represents the memristive synapses from neuron one to neuron two, and M_{12} refers to the connection in the opposite direction. The input to the neurons is their voltage difference $\nu_{21}(t) = x_{11}(t) - x_{21}(t)$ and $\nu_{12}(t) = x_{21}(t) - x_{11}(t)$ with $k > 0$ the network's coupling strength and the memductance function (3.62), which are identical for all connections.

The MNN (3.64)-(3.66) is said to achieve GS if after a transient time $t > t_T$, its states are related through a static function $F(\cdot)$ that holds uniformly in time, such that:

$$x_1(t) = F_{12}(x_2(t)) \tag{3.67}$$

which in implicit form can be written as:

$$F(x_1(t), x_2(t)) = x_1(t) - F_{12}(x_2(t)) = 0, \quad \forall t > t_T \tag{3.68}$$

notice that the functional relation $F(\cdot)$ must be time independent [64].

An alternative way to describe GS is in terms of manifolds. The dynamics of (3.64)-(3.66) evolves in the manifold:

$$M = \{[x_1(t), x_2(t), z_{21}(t), z_{21}(t)]^\top \in \mathbb{R}^8 : \text{ solutions of the system } (3.64) - (3.66)\} \tag{3.69}$$

For MNN (3.64)-(3.66) to achieve GS the manifold $\bar{M}$ must be at least locally asymptotically stable

$$\begin{aligned}\bar{M} = \{&[x_1(t), x_2(t), z_{21}(t), z_{21}(t)]^\top \in \mathbb{R}^8 : F(x_1(t), x_2(t)) = 0,\\ &z_{21}(t) = \bar{c}_1, z_{12}(t) = \bar{c}_2 \text{ with } \bar{c}_1 \text{ and } \bar{c}_2 \text{ constants.}\}\end{aligned} \tag{3.70}$$

Notice that since the states of one system maps on top of another once GS is achieved, the manifold $\bar{M}$ is effectively on the lower dimension $\mathbb{R}^3$, instead of the entire state space $\mathbb{R}^8$. Therefore, GS is achieved if the manifold $\bar{M}$ is locally stable, that is, all transverse directions are contracting. One way to determine the local stability of GS manifold is to characterize all its transversal directions via Lyapunov Exponents (LE), that if all transverse directions have negative LE we have GS [64]. The LEs can be calculated using the well-known algorithm proposed by Wolf [74]. However, since this calculations are complex and demanding, a simplified indicator of GS is the nearest neighbor method [63].

To identify the emergence of GS in our MNN model, we apply the false neighbors approach. To illustrate its calculation we take six points $x_{1,2}^j$ ($j = 1, .., 6$) randomly chosen from the trajectory of each neuron (Figure 3.12a and 3.12b). Then, after sufficient time has

passed (n iteration steps latter) we identify their corresponding neighbors x_1^{jn} (Figure 3.12b). For these points we measure their normalized average distance d as:

$$\begin{aligned} \delta &= (1 - \tfrac{1}{M} \sum_{j=0}^{M-1} \|x_1^j - x_1^{jn}\|) \\ d &= \tfrac{1}{M\delta} \sum_{j=0}^{M-1} \|x_2^j - x_2^{jn}\| \end{aligned} \tag{3.71}$$

where M is the number of randomly chosen points in the trajectory and δ is the average distance between the chosen points and their neighbors for the first neuron.

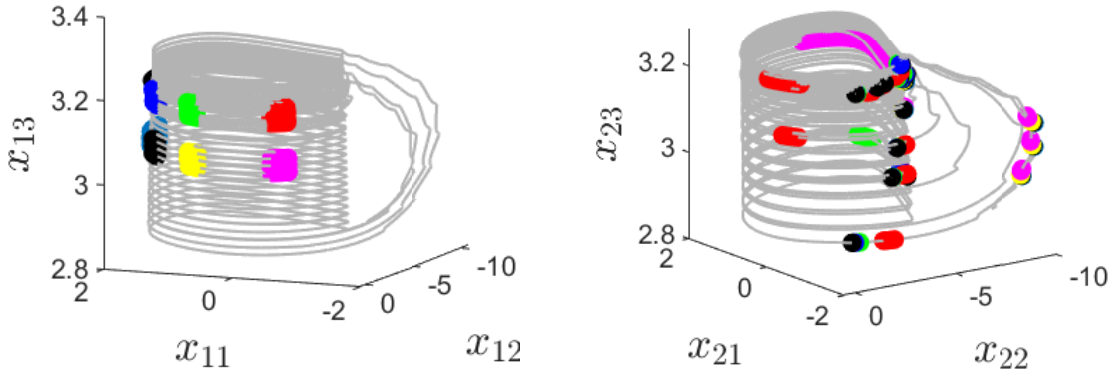

(a) Initial points. (b) Points after transient period.

Figure 3.12: Phase portraits for two HR neurons coupled by memristive synapse (3.64)-(3.66) with $\beta = 0.1$. In this case no GS was detected.

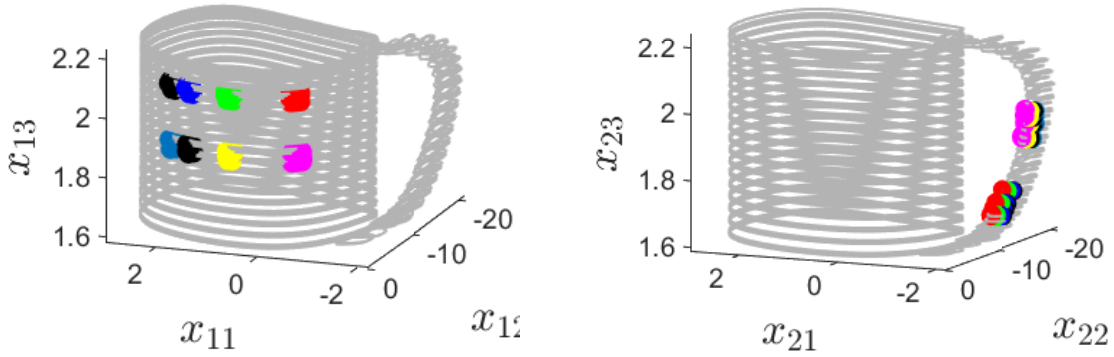

(a) Initial points. (b) Points after transient period.

Figure 3.13: The phase portraits for two HR neurons coupled by memristive synapse (3.64)-(3.66) with $\beta = 1.14$. In this case GS was detected between neuron 1 and 2.

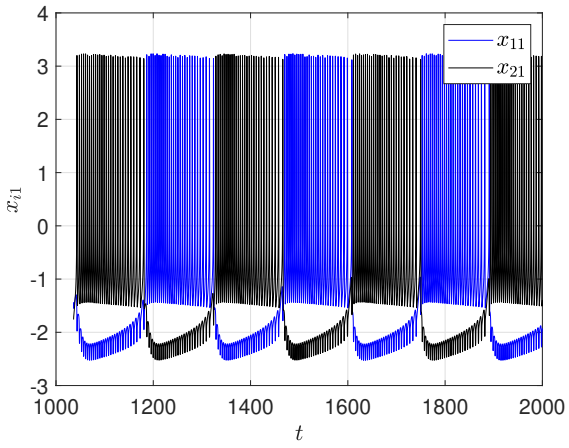

Figure 3.14: Trajectories of HR neuron network with initial condition $(-0.3945, -0.5858, 4.709, -1.361, -8.26, 3.11, 0, 0)$ and $\beta = 1.14$

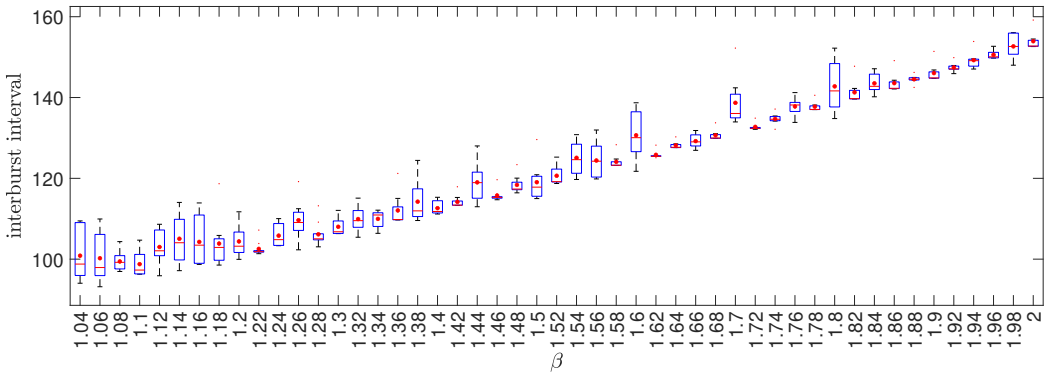

Figure 3.15: Influence of memristor parameter β on IBI of the MNN (3.64)-(3.66).

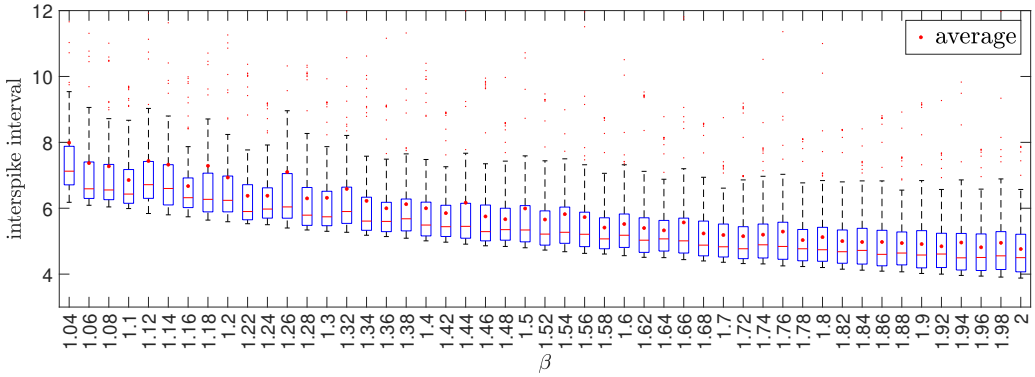

Figure 3.16: Influence of memristor parameter β on the ISI of the MNN (3.64)-(3.66)

As shown in Figure 3.12, when the trajectory moves x_1^j to x_1^{jn} if they are contained in a small vicinity ($\delta \approx 1$). In our illustration, a region of state space with the same color. Then, if in the second neuron our initial points move, after the same amount of time, to places where they are not neighbors. There is no static functional relationship between these systems, in other words, there is no GS in our MNN model. Alternatively, in Figure 3.13, where the coupling memristors have the value $\beta = 1.14$, all neighbors in the second neuron are also in small vicinity ($\delta \approx 1$ and $d \approx 0$). Therefore there is a GS between these neurons.

The MNN model (3.62)-(3.63) with busting HR neuron parameters [72], active memristor synapses ($\beta = 1.14$) [73] and unitary coupling strength ($k = 1$) results on the trajectories shown in Figure 3.14.

Notice that "burstings" appears at regular intervals but at different times for each neuron. This is more clearly shown in their third coordinate where the anti-synchronized nature of the GS generated is easily observed. An alternative way to express this form of GS is the changes in its IBI, if it is periodic with a fixed period, then GS is achieved. In this contribution, we are particularly interested in determining the effect of memristive synapses on the emergence of GS. To this we evaluated the distance d of false neighbors for different values of the parameter β. Notice that for a small β value the distance is to large and therefore no GS is detected.

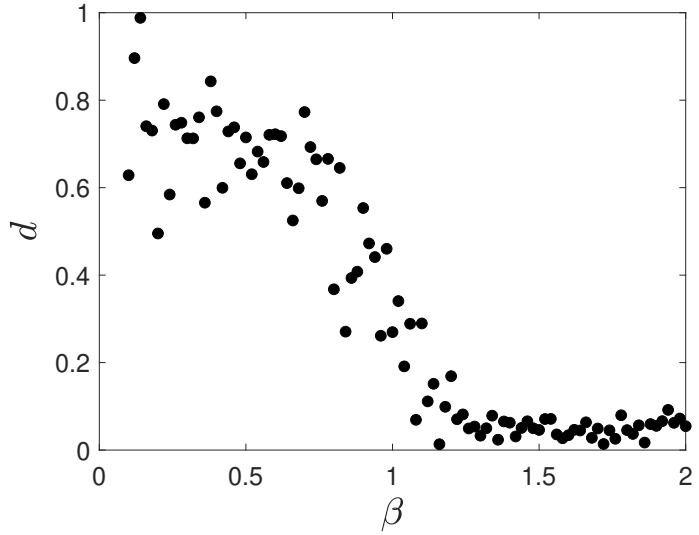

Figure 3.17: The nearest neighbor distance versus the memristor parameter β. For two HR neurons coupled by memristive synapse (3.64)-(3.66).

While for $\beta \leq 1.4$ the neighbors distance is nearly zero, indicating that GS is achieved.

Additionally, we consider the effects of β on the IBI and ISI of the MNN. The interval of time for which these measures are taken is $1000 \geq t \leq 2000$ as shown in figure 3.14. For each value of β, we register maximum, minimum, and average values of IBI for this interval $1000 \geq t \leq 2000$. Figure 3.15 shows that as β increases, the IBI also grows. Conversely, the average ISI decreases linearly as the value of β (see Figure 3.16). Notice that these measures are taken when the neurons are synchronized in the generalized form.

Different approaches can be use to determine the emergence of GS on dynamical networks. In this contribution, for a very small network of HR neurons coupled via active memristive synapse we use the nearest neighbors approach. A particularly significant advantage of this method is that unlike LE is not numerically intensive, with the additional advantage that it can be applied even in the case of large networks and nonidentical nodes. The main concern in this contribution was to identify the effect of parameters in the memristive synapses on the emergence of GS in the resulting MNN. We show that for a pair of HR neurons in a MNN GS is achieve when the memristor parameter β is above a certain threshold value. Furthermore, we identify that the temporal characteristics of their firing patterns are influenced by memristor strength coefficient. Within this operational regime, an increase in the memristor coefficient leads to a proportional increment in the average IBI, while simultaneously resulting in a corresponding decrease in the average ISI. To extend the presented results is necessary to include the effect of larger populations of neurons and the features of their connection structure. Initial efforts in this regard show that additional forms of activations patterns in the MNN that go beyond SG are generated when small-world or scale-free networks are consider, however these results will be reported elsewhere.

Chapter 4

Final comments

Investigate the dynamical behavior of memristive neural networks, with a particular emphasis on the analysis of equilibrium points and synchronization phenomena. Memristive devices lay the foundation for modeling memory-dependent phenomena in neural systems, such as synaptic and neuronal dynamics.

The results presented in this work contribute to understanding how active and passive memristive couplings affect the collective behavior of nonlinear neural models. In particular, the study focused on the stability of equilibrium points in memristive integrate-and-fire neural networks and on the emergence of synchronization phenomena in Hindmarsh-Rose neurons coupled through memristive devices. The main findings of this thesis are summarized in the following.

4.1 Summary of contributions

We addressed the problem of dynamical analysis of memristive neural networks, in which memristive devices are used to model synapses and/or neurons. The main contributions of this work are summarized as follows.

Contribution 1. The first contribution concerns the equilibrium analysis of memristive integrate-and-fire neural networks with time-varying coupling. Sufficient conditions are derived to guarantee the existence of a unique stable equilibrium point for each initial condition, also referred to as the memory state. These conditions are two: the increasing monotonicity of the memristive characteristic function and uniform dissipation of the time-varying Laplacian matrix.

Contribution 2. The second contribution establishes conditions for the synchronization of HR neurons coupled via an ideal memristor. It is shown that when the memristance is sufficiently large and positive definite, the neuronal states synchronize. As a consequence, the magnetic flux associated with the memristor converges to a constant value.

Contribution 3. The third contribution investigates the Generalized synchronization of two Hindmarsh-Rose neurons coupled by an active memristor. The analysis is performed numerically using the nearest-neighbor methodology. It is found that above a certain memristor

strength value, a Generalized Synchronization (GS) regime occurs. The results show that when the memristor strength parameter exceeds a threshold, the system exhibits a generalized synchronization (GS) regime. Furthermore, the results on generalized synchronization highlight the role of memristive parameters in shaping collective neuronal dynamics. These findings contribute to understanding the dynamical properties of MNN with active synapses.

4.2 Scientific significance

This thesis contributes to the understanding of how memristive devices influence the dynamical behavior of neural networks. In particular, for the ideal memristor considered in Contributions 1 and 2, the solution trajectories of the memristive neural network either converge to a stable equilibrium point or evolve toward synchronized motion. These results provide insight into the role of memristive coupling in determining the stability and collective dynamics of neural systems.

In contrast, the use of active memristive synapses allows the emergence of more complex collective phenomena, which can be mathematically characterized through the generalized synchronization regime. This behavior affects not only the collective dynamics of the coupled neurons but also the temporal structure of their firing patterns.

4.3 Future Research directions

One possible direction for future research is the mathematical characterization of more complex collective phenomena, such as regimes of identical, phase, and lag synchronization and Generalized Synchronization (GS) in large memristive neural networks. This could be achieved by considering different network topologies to describe the inter-neuronal connections. In addition, further studies may explore variations of the synaptic models used to represent neuronal coupling, including chemical synapses or coupling mechanisms based on electromagnetic induction effects.

Another possible direction for future research is the incorporation of memristive devices into the neuronal model to characterize the intrinsic dynamics of memristive neurons. This would allow the construction of large networks composed of memristive neurons coupled through active memristive synapses. Such a framework would extend the analysis presented in the first contribution and may provide further insight into the role of memristive dynamics in large-scale neural networks.

In the general case, future research may focus on the study of collective behavior in large memristive neural networks composed of heterogeneous neuron models and heterogeneous synaptic couplings. For instance, the Hindmarsh–Rose neuron model can operate in different dynamical regimes, including chaotic bursting, chaotic firing, or oscillatory behavior. Other neuron models, such as the FitzHugh–Nagumo model, may also be considered to describe oscillatory dynamics, as well as their memristive extensions.

Within such heterogeneous memristive neural networks, it would be of interest to investigate the emergence of complex collective phenomena, including identical synchroniza-

tion, phase synchronization, lag synchronization, and generalized synchronization (GS). The mathematical characterization of these regimes in heterogeneous networks may provide further insight into the role of memristive coupling in shaping large-scale neural dynamics.

Chapter 5

Appendix

Published results

The following publications have been produced as a result of the research presented in this thesis:

Journal Articles

[**J.1**] Carro-Pérez, I., Barajas-Ramírez, J.G. (2025). **Generalized Synchronization of Hindmarsh–Rose Neurons with Memristive Couplings**. *Dynamics*, Vol. 5, Issue 4, pp. 50. DOI: 10.3390/dynamics5040050

Conference Proceedings

[**C.1**] Carro-Perez, I, Barajas-Ramirez, J.G. (2020). **Stability of the Memory State of a Time-Varying Memristive Neural Network Model**. In *Congreso Nacional de Control Automático*, pp. 1-5, ISSN: 2594-24

[**C.2**] Carro-Perez, I, Barajas-Ramirez, J.G.(2022). **Synchronization of memristor based bidirectionally coupled Hindmarsh-Rose neurons**. In *Congreso Nacional de Control Automático*, pp. 516-521. October, ISSN: 2594-2492.

Chapter

[**C.3**] Anzo-Hernández, A., Carro-Pérez, I., Bonilla-Capilla, B., Barajas-Ramírez, J.G. (2024). **Synchronization of Memristive Hindmarsh–Rose Neurons Connected by Memristive Synapses**. In *Complex Systems and Their Applications*, EDIESCA 2023, Campos-Cantón, E., Huerta-Cuellar, G., Zambrano-Serrano, E., Tlelo-Cuautle, E. (eds), Springer, Cham. DOI: 10.1007/978-3-031-51224-7_8

dynamics

MDPI

Article

Generalized Synchronization of Hindmarsh–Rose Neurons with Memristive Couplings

Illiani Carro-Pérez and Juan Gonzalo Barajas-Ramírez *

División de Control y Sistemas Dinámicos, Instituto Potosino de Investigación Científica y Tecnológica A.C. (IPICYT), Camino a la Presa San José 2255, Lomas 4ta. Sección, San Luis Potosí 78216, SLP, Mexico; illiani.carro@ipicyt.edu.mx

* Correspondence: jgbarajas@ipicyt.edu.mx; Tel.: +52-444-834-2000 (ext. 7222)

Abstract

In this study, we explore the emergence of generalized synchronization (GS) in arrays of Hindmarsh–Rose (HR) neurons that are coupled through memristive synapses. We design coupling functions utilizing active memristors to facilitate GS in a bidirectionally coupled two-neuron memristive neural network (MNN). Our analysis employs a nearest neighbor (NN) approach. Our findings indicate that there is a threshold coupling strength for the active memristive synapses required to achieve GS. Additionally, we investigate how memristor parameters affect the temporal characteristics of synchronized neuronal firing patterns. Specifically, we discover that the interburst interval (IBI) is directly proportional to the coupling strength of the memristive synapses, while the interspike interval (ISI) is inversely proportional to this strength.

Keywords: memristors; HR neurons; synchronization; spiking–bursting behavior

1. Introduction

A straightforward way to model brains is to represent them as networks of neurons that communicate via synapses. The collective behavior of these networks is determined by the electrochemical transmission of signals between neurons at synapses [1]. A key dynamical feature of neuron models is the presence of an action potential, which is a spike-shaped output voltage signal. The Hindmarsh–Rose (HR) model is a simplified neuron model that effectively captures the emergence of *action potentials* [2]. Additionally, the HR model can exhibit various types of oscillations, including chaotic behavior, when specific parameter values are chosen [3].

Communication between neurons involves both electrical and chemical components. The electrical aspect describes the ion currents triggered by voltage differences across neuronal membranes. In this context, signals can move through gap junction channels in either direction in accordance with Ohm's law. The chemical part of synaptic transmission involves the *presynaptic* neuron releasing neurotransmitters into the synaptic cleft. When these chemicals bind to receptors on the *postsynaptic* neuron, they generate a signal that modifies the electrical properties of the postsynaptic neuron. As a result, the signal transmission is directed and subject to time-varying parameters, saturating at a constant value as the synaptic cleft becomes filled with neurotransmitters [4].

In recent years, several circuit implementations of neurons and synapses based on memristors have been proposed to emulate neural system behavior, such as channel opening and closing driven by ionic density [5–8]. A generalization of memristors was

check for updates

Academic Editor: Christos Volos

Received: 1 October 2025
Revised: 31 October 2025
Accepted: 1 November 2025
Published: 1 December 2025

Citation: Carro-Pérez, I.; Barajas-Ramírez, J.G. Generalized Synchronization of Hindmarsh–Rose Neurons with Memristive Couplings. *Dynamics* **2025**, *5*, 50. https://doi.org/10.3390/dynamics5040050

introduced in 1976 [9], highlighting a property in which devices can exhibit negative memristance over specific intervals of their internal variable; this phenomenon classifies the device as locally active. These locally active memristors have been utilized to model synaptic behavior [10], capturing nonlinear responses and adaptive plasticity through their internal-state evolution. Several studies [6,8,11,12] have implemented locally active memristors with memductance described by a hyperbolic tangent function, ensuring bounded memristance characteristics. However, the exploration of fully active memristors as synaptic elements remains an open research avenue, particularly regarding their influence on the firing patterns and the synchronization properties of interconnected neural circuits.

In this contribution, we focus on a simplified memristive neural network (MNN) consisting of identical HR neurons that interact through active memristive synapses. Our model comprises two HR neurons bidirectionally coupled via locally active memristors. Although the array is small, it has physical significance since it illustrates the effects of the connection dependency on the memristor's internal state in the emergence of coherent firing patterns in larger arrays. In this regard, previous work has investigated the emergence of identical synchronization between two neurons connected by a locally active memristor [13]. An analytical proof of exponential synchronization in a two-neuron MNN coupled via a locally active memristor was established under suitable conditions on the memristor coupling coefficient and the initial state [11]. Another study explored a network of three HR neurons connected by memristive synapses in a ring topology, revealing that identical synchronization occurs when the coupling strength exceeds a certain threshold [8]. Furthermore, ref. [12] has shown that the transition from synchronization to desynchronization depends on the MNN's connection structure. Notably, in the exponential synchronization approach, analytical criteria provided by the Lyapunov method establish sufficient stability conditions concerning the memristor's initial conditions and coupling strength. These criteria differ from those used in other synchronization regimes, such as generalized synchronization (GS) in mutually coupled systems, where the existence of a synchronization manifold is typically confirmed numerically, e.g., via the nearest-neighbor approach [14].

In this work, we investigate the emergence of coherence in firing patterns of MNNs consisting of identical HR neurons, focusing on the emergence of GS and the dependence of firing patterns, such as interspike interval (ISI) and interburst interval (IBI), on the strength of the memristive connections. We propose a fully active memristive synapse with consistently negative memristance, which was bounded above and below [6,8,11,12]. Taking inspiration from previous research [13,15–19], we proposed quadratic forms for the memristance function. Additionally, we demonstrate the presence of a pinched hysteresis loop (PHL) in the second and fourth quadrants, as in [12]. That remains across various frequency values, while its lobe area decreases as frequency increases.

In the following section, we will present our MNN model of HR neurons with memristive connections and describe its synchronization challenges.

2. Preliminaries

Consider an MNN where the following equations model each node:

$$\begin{bmatrix} \dot{x}_1(t) \\ \dot{x}_2(t) \\ \dot{x}_3(t) \end{bmatrix} = \begin{bmatrix} -ax_1(t)^3 + bx_1(t)^2 + x_2(t) - x_3(t) + I_{syn}(t) \\ e - dx_1(t)^2 - x_2(t) \\ \epsilon(s(x_1(t) + x_0) - x_3(t)) \end{bmatrix} \tag{1}$$

Here, the variable $x_1(t)$ represents voltage, $x_2(t)$ denotes recuperation, and $x_3(t)$ indicates adaptation within the neural model. This model effectively captures the dynamics of ionic currents through membrane channels, specifically potassium K^+ and sodium Na^+ for the fast subsystem. In contrast, the ionic fluxes related to chlorine Cl^- and other

leaking ions pertain to the slow variable $x_3(t)$. The external input $I_{syn}(t)$ facilitates inter-neuronal connections. Notably, the RH model expressed in (1) exhibits chaotic behavior when parameters are set as $a = 1$, $b = 3$, $c = 1$, $d = 5$, $\sigma = 4$, $x_0 = -1.6$, $\varepsilon = 0.0021$, and $I_{ext}(t) = 3.29$ [3].

The parameter $0 < \epsilon \ll 1$ describes the relation of fast–slow time scales in the neural model, allowing for periodic currents that trigger the *action potential* displaying different patterns of bursting and spiking behavior [3].

The interconnection between neurons is modeled as a current given by memristors of the following form:

$$\begin{aligned} I_{syn}(t) &= g(z(t), v(t))v(t) \\ \dot{z}(t) &= f(z(t), v(t)) \end{aligned} \tag{2}$$

where $z(t) \in \mathbb{R}^m$ is the internal state of the memristor, $v(t) \in \mathbb{R}$ is the voltage input, and $I_{syn}(t) \in \mathbb{R}$ is the current output of the memristive device; with $f : \mathbb{R}^m \times \mathbb{R} \to \mathbb{R}^m$ and $g : \mathbb{R}^m \times \mathbb{R} \to \mathbb{R}$ representing continuous functions describing the internal dynamics and the memductive function, which is zero-at-zero and and corresponds to the derivative of the flux–charge characteristic with respect to the input variable.

We simplify the internal dynamics of the memristor:

$$\dot{z}(t) = v(t) \tag{3}$$

In this simplified formulation, the vector field $f(\cdot)$ lacks any leakage term, meaning that no dissipative mechanisms counterbalance the growth of $z(t)$. This implies the absence of processes that would gradually diminish the internal state (memory trace). By neglecting such dissipation, we isolate the intrinsic effect of memristive coupling on neuronal excitability and synchronization.

In this contribution, we consider that all connections are modeled by memristors with the following memductance function:

$$g(z(t), v(t)) = \frac{\beta}{\alpha z^2(t) + 1} - (\beta + \gamma) \tag{4}$$

where α, β, and $\gamma > 0$, with β representing the coupling strength coefficient. As such, the memductance is bounded by the following:

$$-(\gamma + \beta) \leq g(z(t), v(t)) \leq -\gamma \quad \forall z(t) \in \mathbb{R} \tag{5}$$

As shown in Figure 1, under periodic input, the current–voltage diagram is a frequency-dependent pinch hysteresis. At the same time, the memductance function is quadratic and consistently negative; therefore, the model (2)–(4) is an active memristor [8].

It is worth noting that ever since the mathematical generalization of the concept of a memristor in 1976 [9], a more flexible interpretation allows us to consider memristive devices that are not strictly passive; i.e., for some intervals of the memristor's internal variable, its memristance is negative, and it is therefore said to be locally active. This feature is directly related to ionic current channels in physiological models of neuronal membrane electrical activity. Locally active memristors have recently been proposed to model synapse behavior with different memductance functions, including the hyperbolic tangent function [6,8,10–12]. The reason behind modeling memristance this way is to have a bounded memristance value. Taking inspiration from these works, a memductance function that saturates as a function of the memristor's locally active internal variable can be proposed in the form (4), as shown in (5). In addition to the saturation of the memristive function, the proposed quadratic memductance function in the current–voltage variables

follows the reasoning of [13,15–19], which implies a cubic relation in the charge–flux interpretation of the memristor. That results in the preservation of the pinched hysteresis loop (PHL) in the second and fourth quadrants, as observed in Figure 1.

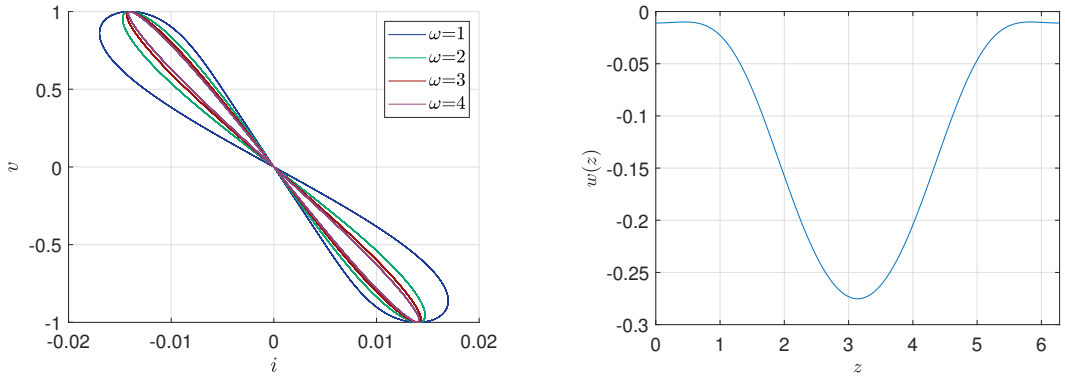

(**a**) Pinched hysteresis. (**b**) Memductance function.

Figure 1. Memristor (2)–(4). (**a**) Pinched hysteresis loop of the memristor for $v(t) = \sin(\omega t)$, (**b**) the memductance evaluated for different values of $z(t)$.

Using the memristive synapses described above to connect two HR neurons, we have the following MNN:

$$\begin{aligned}
\dot{x}_{11}(t) &= x_{12}(t) - x_{13}(t) - ax_{11}^3(t) + bx_{11}^2(t) + I_{ext}(t) + M_{21}(t) \\
\dot{x}_{12}(t) &= c - x_{12}(t) - dx_{11}^2(t) \\
\dot{x}_{13}(t) &= \varepsilon[\sigma(x_{11}(t) - x_0) - x_{13}(t)] \\
\dot{x}_{21}(t) &= x_{22}(t) - x_{23}(t) - ax_{21}^3(t) + bx_{21}^2(t) + I_{ext}(t) + M_{12}(t) \\
\dot{x}_{22}(t) &= c - x_{22}(t) - dx_{21}^2(t) \\
\dot{x}_{23}(t) &= \varepsilon[\sigma(x_{21}(t) - x_0) - x_{23}(t)]
\end{aligned} \tag{6}$$

$$\begin{aligned}
M_{21}(t) &= kg(z_{21}(t), \nu_{21}(t))\nu_{21}(t) \\
\dot{z}_{21}(t) &= \nu_{21}(t) \\
M_{12}(t) &= kg(z_{12}(t), \nu_{12}(t))\nu_{12}(t) \\
\dot{z}_{12}(t) &= \nu_{12}(t)
\end{aligned} \tag{7}$$

where $x_i(t) = [x_{i1}(t), x_{i2}(t), x_{i3}(t)]^\top \in \mathbb{R}^3$ represents the state of the ith HR neuron; $M_{21}(t)$ represents the memristive synapses from neuron one to neuron two, and M_{12} refers to the connection in the opposite direction. The input to the neurons is their voltage difference $\nu_{21}(t) = x_{11}(t) - x_{21}(t)$ and $\nu_{12}(t) = x_{21}(t) - x_{11}(t)$ with $k > 0$ the network's coupling strength and the memductance function (4), which are identical for all connections.

The MNN (6) and (7) is said to achieve GS if after a transient time $t > t_T$, its states are related through a static function $F(\cdot)$ that holds uniformly in time, such that

$$x_1(t) = F_{12}(x_2(t)) \tag{8}$$

In implicit form, this can be written as

$$F(x_1(t), x_2(t)) = x_1(t) - F_{12}(x_2(t)) = 0, \quad \forall t > t_T \tag{9}$$

Notice that the functional relation $F(\cdot)$ must be independent of time and state variables.

The main difference between generalized and identical synchronization is that in GS, the relationship between states is not the identity. That is, their temporal coordination follows a more general relation that must be static and independent of the systems' states. As such, the stability conditions are essentially the same but in a different error dynamics:

instead of the difference between states, it is the difference between the state of one system and the image of the static function that describes the relationship between the states. A simple physical interpretation is that GS appears when a system, instead of exactly copying the motion of a system, does the exact opposite. This phenomenon, sometimes called antisynchronization, is in fact one form of GS [14].

An alternative way to describe GS is in terms of manifolds. The dynamics of (6) and (7) evolves in the manifold:

$$M = \{[x_1(t), x_2(t), z_{21}(t), z_{21}(t)]^\top \in \mathbb{R}^8 : \text{ solutions of the system (6) and (7)}\} \tag{10}$$

For MNN (6) and (7) to achieve GS, the manifold $\bar{M}$ must be at least locally asymptotically stable:

$$\begin{aligned} \bar{M} \quad = \quad & \{[x_1(t), x_2(t), z_{21}(t), z_{21}(t)]^\top \in \mathbb{R}^8 : F(x_1(t), x_2(t)) = 0, \\ & z_{21}(t) = \bar{c}_1, z_{12}(t) = \bar{c}_2 \text{ with } \bar{c}_1 \text{ and } \bar{c}_2 \text{ constants.}\} \end{aligned} \tag{11}$$

Notice that since the states of one system map on top of another once GS is achieved, the manifold $\bar{M}$ is effectively on the lower dimension $\mathbb{R}^3$ instead of the entire state space $\mathbb{R}^8$. Therefore, GS is achieved if the manifold $\bar{M}$ is locally stable, that is, all transverse directions are contracting. One way to determine the local stability of the GS manifold is to characterize all its transverse directions via Lyapunov exponents (LEs). If all transverse directions have negative LEs, then the GS manifold is locally stable [14]. The LEs can be calculated using the well-known algorithm proposed by Wolf [20]. However, since these calculations are complex and demanding, a simplified indicator of GS is the nearest neighbor method [21]. The nearest-neighbor method measures the distance between M points on the solution trajectories of the systems as they evolve in time; if this distance remains approximately constant, the systems are coordinated in time. A significant advantage of this method is that the number of distances to calculate scales linearly with the number of nodes in the network, unlike Lyapunov-based methods, which require evaluating variational equations and Jacobian matrices. The nearest neighbor method is computationally efficient, as it only involves storing and comparing state vectors, which are operations that are considerably faster and more amenable to parallelization. Consequently, the method is well-suited for the analysis of large and even heterogeneous networks.

3. Numerical Results

To identify the emergence of GS in our MNN model, we apply the false neighbors approach. To illustrate its calculation, we take six points $x^j_{1,2}$ ($j = 1, \ldots, 8$) randomly chosen from the trajectory of each neuron (Figure 2a,b). Then, after sufficient time has passed such that a full oscillation has been completed (n iteration steps later), we identify their corresponding neighbors x^{jn}_1 (Figure 2b). For these points, we measure their normalized average distance d as

$$d \;=\; \tfrac{1}{\delta \bar{K}} \sum_{j=0}^{M-1} \sum_{n=0}^{K_j - 1} \left\| x_2^j - x_2^{jn} \right\|_2 \qquad \bar{K} = \sum_{j=0}^{M-1} K_j \tag{12}$$

where M is the number of randomly chosen points in the trajectory and δ is the average distance between the chosen points and their neighbors for the first neuron, while K_j is the number of nearest neighbors for point j. On average, we use $N = 153$ points across all experiments. Allowing K_j to vary has practical advantages: it provides a more reliable estimate of local distances.

As shown in Figure 2, the trajectory moves from x_1^j to x_1^{jn} if they are contained in a small vicinity ($\rho \ll 1$). In our illustration, a region of state space is represented with the same color. Then, in the second neuron, our initial points move, after the same amount of time, to places where they are no longer neighbors. Then, there is no static functional relationship between these systems; in other words, there is no GS in our MNN model. Alternatively, in Figure 3, where the coupling memristors have the value $\beta = 1.14$, all neighbors in the second neuron are also in a small vicinity ($\delta \approx 1$ and $d \approx 0$). Therefore, there is GS between these neurons.

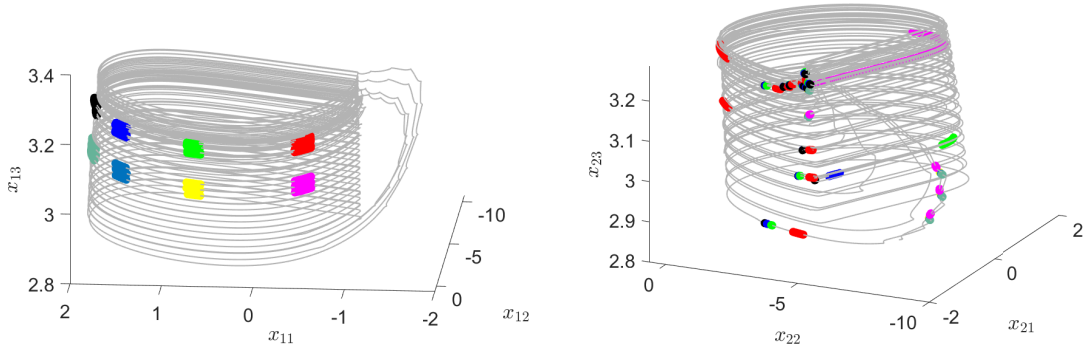

(**a**) Initial points. (**b**) Points after transient period.

Figure 2. Phase portraits for two HR neurons coupled by a memristive synapse (6) and (7) with $\beta = 0.1$. In this case, since neighbors are mostly false, no GS was detected.

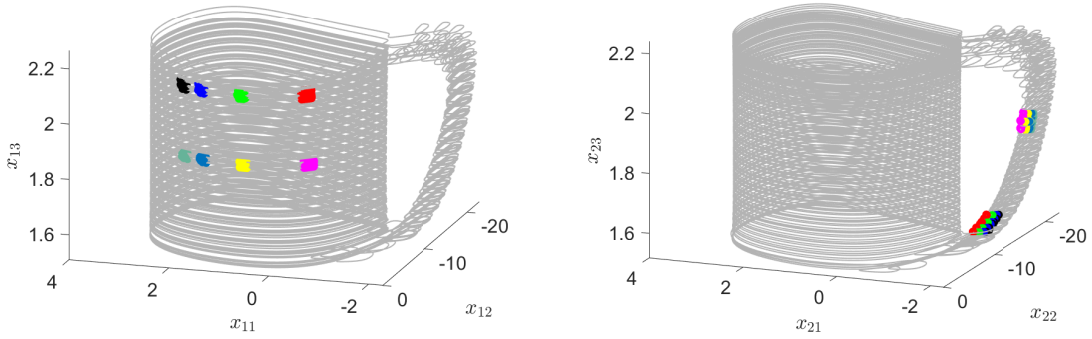

(**a**) Initial points. (**b**) Points after transient period.

Figure 3. The phase portraits for two HR neurons coupled by a memristive synapse (6) and (7) with $\beta = 1.5$. In this case, GS was detected between neurons 1 and 2.

The MNN model (4) and (5) with busting HR neuron parameters [3], active memristor synapses ($\beta = 1.14$) [8] and unitary coupling strength ($k = 1$) results in the trajectories shown in Figure 4.

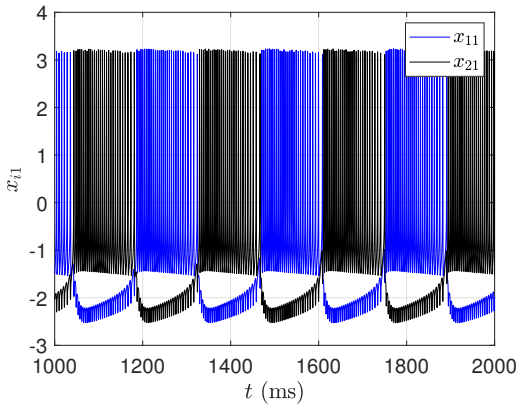

(**a**) $x_{11}(t)$ and $x_{21}(t)$.

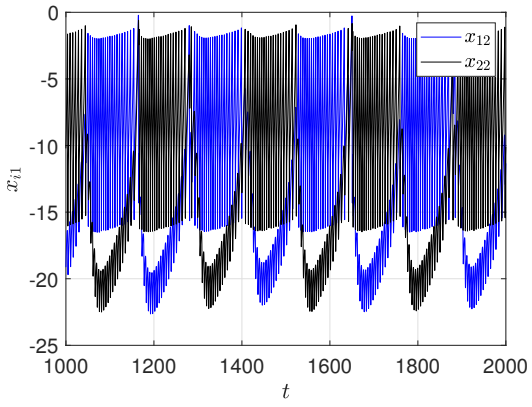

(**b**) $x_{12}(t)$ and $x_{22}(t)$.

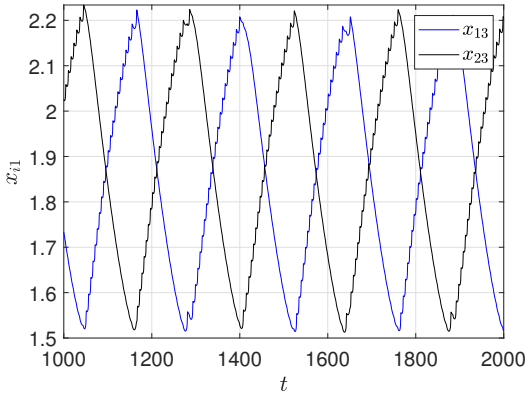

(**c**) $x_{13}(t)$ and $x_{23}(t)$.

Figure 4. Trajectories of two HR neuron networks coupled via memristor synapses (6)–(9) with the initial condition to $(-0.3945, -0.5858, 4.709, -1.361, -8.26, 3.11, 0, 0)$ and $\beta = 1.5$.

Notice that "burstings" appear at regular intervals but at different times for each neuron. This is more clearly shown in their third coordinate, where the anti-synchronized nature of the GS generated is easily observed. An alternative way to express this form of GS is the changes in its IBI; if it is periodic with a fixed period, then GS is achieved. In this contribution, we are particularly interested in determining the effect of memristive synapses on the emergence of GS. To this end, we evaluated the distance d to false neighbors for different values of the parameter β.

Notice that for a small β value, the distance is too considerable and therefore no GS is detected. For $beta \leq 1.4$, the neighbors' distance is nearly zero, indicating that GS is achieved.

Additionally, we consider the effects of β on the MNN's IBI and ISI. For each value of β, we register maximum, minimum, and average values. Figure 5 shows that as β increases, the IBI also grows. Conversely, the average ISI decreases linearly as the value of β decreases (see Figure 6).

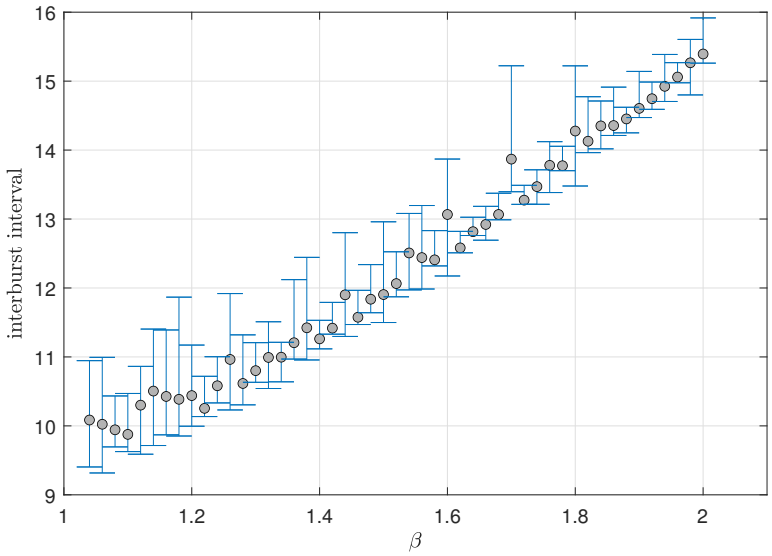

Figure 5. Influence of memristor parameter β on the IBI of the MNN (6) and (7).

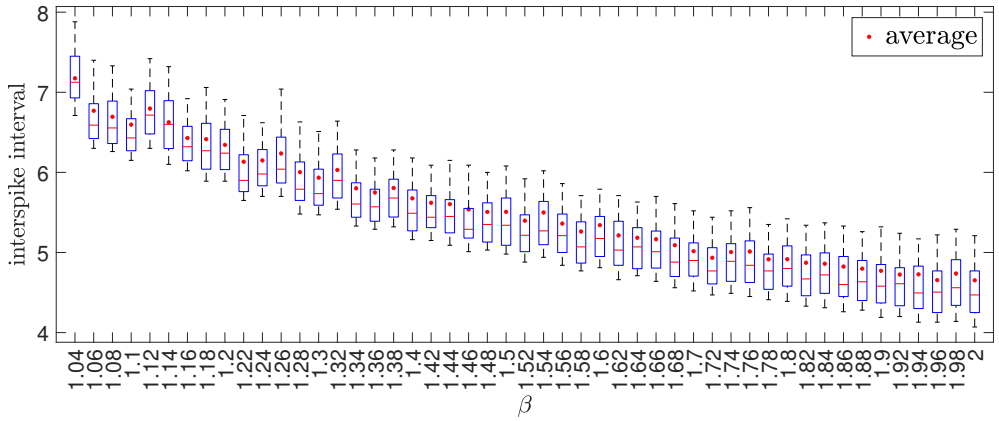

Figure 6. Influence of memristor parameter β on the ISI of the MNN (6) and (7).

4. Discussion of Results

Different approaches can be used to determine the emergence of GS on dynamical networks. In this contribution, we use the nearest neighbor approach for a small network of HR neurons coupled via an active memristive synapse. A significant advantage of the nearest neighbor approach is that unlike Lyapunov-based methods, it does not require the evaluation of variational equations or Jacobian matrices. This makes it computationally efficient, as it only involves storing and comparing state vectors—operations that are considerably faster and more amenable to parallelization. Consequently, the method is well suited for the analysis of large or heterogeneous networks composed of nonidentical nodes. The primary concern in this contribution was to identify the effects of memristive synapse parameters on the emergence of GS in the resulting MNN. We show that for a pair of HR neurons in an MNN, GS is achieved when the memristor parameter β is above a particular threshold value (see Figure 7). Furthermore, we identify that the memristor strength coefficient influences the temporal characteristics of their firing patterns. Within this operational regime, an increase in the memristor coefficient leads to a proportional increment in the average IBI while simultaneously resulting in a corresponding decrease in the average ISI. To extend the presented results, it is necessary to include the effects of larger populations of neurons and the features of their connection structure. Initial efforts in this regard indicate that additional activation patterns in the MNN beyond SG emerge

when small-world or scale-free networks are considered; however, these results will be reported elsewhere.

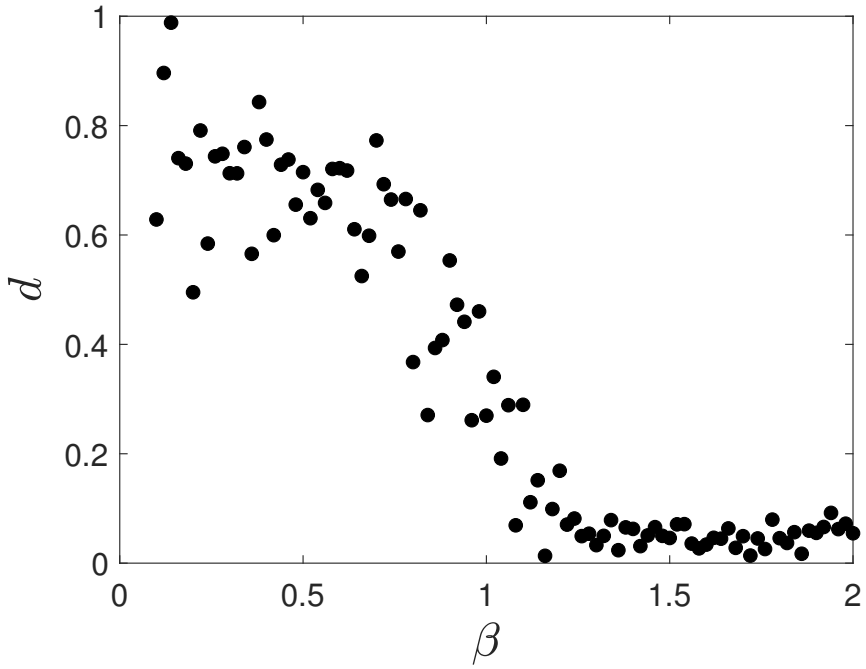

Figure 7. The nearest neighbor distance versus the memristor parameter β for two HR neurons coupled by memristive synapse (6) and (7).

Author Contributions: Conceptualization, analysis and validation I.C.-P. and J.G.B.-R. Original draft preparation J.G.B.-R. All authors have read and agreed to the published version of the manuscript.

Funding: This research was funded by the SECIHTI of Mexico under the 968050 grant for doctoral studies.

Data Availability Statement: Programs and simulation data are available via direct contact with the authors.

Conflicts of Interest: The authors declare no conflicts of interest.

References

1. Rabinovich, M.I.; Varona, P.; Selverson, A.I.; Abarbanel, H.D.I. Dynamical principles in neuroscience. *Rev. Mod. Phys.* **2006**, *78*, 1213–1265. [CrossRef]
2. Hindmarsh, J.L.; Rose, R.M. A model of neuronal bursting using three coupled first order differential equations. *Proc. R. Soc. Lond. Ser. B Biol. Sci.* **1984**, *221*, 87–102. [CrossRef]
3. Innocenti, G.; Morelli, A.; Genesio, R.; Torcini, A. Dynamical phases of the Hindmarsh-Rose neuronal model: Studies of the transition from bursting to spiking chaos. *Chaos Interdiscip. Nonlinear Sci.* **2007**, *17*, 043128. [CrossRef] [PubMed]
4. Sterratt, D.; Graham, B.; Gillies, A.; Willshaw, D. *Principles of Computational Modeling in Neuroscience*; Cambridge University Press: Cambridge, UK, 2011. [CrossRef]
5. Chua, L.O. Memristor-The missing circuit element. *IEEE Trans. Circuit Theory* **1971**, *18*, 507–519. [CrossRef]
6. Wu, J.; Li, Z.; Lan, Y. Coexistence and control of firing patterns in a heterogeneous neuron-coupled network by memristive synapses. *Nonlinear Dyn.* **2025**, *113*, 13715–13726. [CrossRef]
7. Mannan, Z.I.; Kim, H.; Chua, L.O. Implementation of Neuro-Memristive Synapse for Long- and Short-Term Bio-Synaptic Plasticity. *Sensors* **2021**, *21*, 644. [CrossRef] [PubMed]
8. Hu, X.; Jiang, B.; Chen, J.; Liu, C. Synchronization behavior in a memristive synapse-connected neuronal network. *Eur. Phys. J. Plus* **2022**, *137*, 895. [CrossRef]
9. Chua, L.O.; Kang, S.M. Memristive devices and systems. *Proc. IEEE* **1976**, *64*, 209–223. [CrossRef]

10. Li, R.; Wang, Z.; Dong, E. A new locally active memristive synapse-coupled neuron model. *Nonlinear Dyn.* **2021**, *104*, 4459–4475. [CrossRef]
11. Bao, H.; Zhang, Y.; Lu, W.; Bao, B. Memristor synapse-coupled memristive neuron network: Synchronization transition and occurrence of chimera. *Nonlinear Dyn.* **2020**, *100*, 937–950. [CrossRef]
12. Kanagaraj, S.; Durairaj, P.; Sampath, S.; Karthikeyan, A.; Rajagopal, K. Collective dynamics of a coupled Hindmarsh–Rose neurons with locally active memristor. *Biosystems* **2023**, *232*, 105010. [CrossRef] [PubMed]
13. Xu, F.; Zhang, J.; Fang, T.; Huang, S.; Wang, M. Synchronous dynamics in neural system coupled with memristive synapse. *Nonlinear Dyn.* **2018**, *92*, 1395–1402. [CrossRef]
14. Moskalenko, O.I.; Koronovskii, A.A.; Hramov, A.E.; Boccaletti, S. Generalized synchronization in mutually coupled oscillators and complex networks. *Phys. Rev. E* **2012**, *86*, 036216. [CrossRef] [PubMed]
15. Ma, J.; Lv, M.; Zhou, P.; Xu, Y.; Hayat, T. Phase synchronization between two neurons induced by coupling of electromagnetic field. *Appl. Math. Comput.* **2017**, *307*, 321–328. [CrossRef]
16. Cheng, X.; Song, X.; Wang, R. Self-organization collective dynamics of heterogeneous neurons with memristive and plastic chemical synapses. *Int. J. Mod. Phys. B* **2022**, *36*, 2250030. [CrossRef]
17. Zandi-Mehran, N.; Jafari, S.; Hashemi, G.S.; Nazarimehr, F.; Perc, M. Different synaptic connections evoke different firing patterns in neurons subject to an electromagnetic field. *Nonlinear Dyn.* **2020**, *100*, 1809–1824. [CrossRef]
18. Usha, K.; Subha, P.A. Hindmarsh-Rose neuron model with memristors. *Biosystems* **2019**, *178*, 1–9. [CrossRef] [PubMed]
19. Xu, Y.; Xia, Y.; Ma, J.; Alsaedi, A.; Ahmad, B. Synchronization between neurons coupled by memristor. *Chaos Solitons Fractals* **2017**, *104*, 435–442. [CrossRef]
20. Wolf, A.; Swift, J.B.; Swinney, H.L.; Vastano, J.A. Determining Lyapunov exponents from a time series. *Phys. D Nonlinear Phenom.* **1985**, *16*, 285–317. [CrossRef]
21. Rulkov, N.F.; Sushchik, M.M.; Tsimring, L.S.; Abarbanel, H.D.I. Generalized synchronization of chaos in directionally coupled chaotic systems. *Phys. Rev. E* **1995**, *51*, 980–994. [CrossRef] [PubMed]

Memorias del 2022 Congreso Nacional de Control Automático
12-14 de Octubre, 2022. Tuxtla Gutiérrez, México.

Synchronization of memristor based bidirectionally coupled Hindmarsh-Rose neurons ⋆

Illiani Carro-Pérez * **Juan Gonzalo, Barajas-Ramírez** *

* *IPICYT, División de Control y Sistemas Dinámicos, Camino a la Presa San José 2055, Col. Lomas 4a CP. 78216, San Luis Potosí, S.L.P., México. (E-mail: illiani.carro,jgbarajas@ipicyt.edu.mx).*

Abstract: An ideal memristor is a device whose resistive memory value is determine by its initial conditions and the voltage that has been applied across its terminals. As such, it is a good candidate to model the *synaptic plasticity* of neural systems. When memristors are included in neural models, they are called memristive neural networks. In this contribution, we investigate the emergence of synchronization in an array of two identical Hindmarsh-Rose neurons bidirectionally coupled through their voltage variables via memristors. We show that, for a sufficiently large positive memductance, synchronization emerges between neurons while the memristors converge to constant synaptic weight values. We illustrate our results with numerical simulations.

Keywords: Memristor, Synapse, Hindmarsh-Rose Neuron, Synchronization

1. INTRODUCTION

Neurons are the basic processing units of neural systems. In [Hodgkin & Huxley (1949)] (HH) an electric-physiological model of its behavior was proposed where voltage-dependent conductances were used to approximate the effects of ionic currents and contraregulatory effects of their concentrations on the neuron's membrane potential. The main dynamical feature of these model is the emergence of an action potential. Latter, in [Hindmarsh & Rose (1984)] (HR) a simplified model was proposed to capture the dynamical features of HH model. In particular, the bursting of spikes (action potentials) observed in real-world neurons. Under an appropriate choice of parameters the HR model can produce diverse firing patterns including single spiking, square bursting, chaotic bursting, and periodic firing [Innocenti (2007)].

A synapse is the extracellular space between neurons where electro-chemical transmission takes place [Kandel (2013)]. A transmitting neuron is called the *presynaptic* neuron while the receiving neuron is called *postsynaptic*. The action potential associated with the transmission of information is caused by an electrical current and the release of specialized molecules (neurotransmitters) by the dendrites on the synaptic space. Next, they bind to receptors on the postsynaptic neuron, that allow the opening of ion channels and therefore modify the electrical response in the postsynaptic neuron. One property of synapses is *plasticity* [Serrat (2011)], which consists in the variation of synaptic conductance, as a result of this property the inhibition or excitation of postsynaptic neuron can be achieved.

An alternative way to have an electrical representation of neurons and synapses is using circuits with memristors [Amirsoleimani (2016)]. The memristor [Chua (1971)] is a theoretical electronic device with resistive memory, characterized by a function that relates its electric charge with its magnetic flux. It is called an *ideal*-memristor because the current and voltage in the device correspond exactly with the derivatives of its charge and magnetic flux, respectively. From these relationships, the resistivity value of a flux-controlled memristor depends on the history of its voltage. Furthermore, once its voltage becomes zero, the resistance value of the memristor remains fixed. As a result, memristors have potential applications [Sanchez-Lopez (2019)][Carro-Perez (2018)] as non-volatile memories. When memristors are used in models of neurons and synapses, they are called memristive neural networks (MNN).

There are several applications of MNN such as pattern classification [Amirsoleimani (2016)], experimental demonstration of associative memory PershinVentra (2009), supervised learning [Nishitani (2015)] and secure communication[Li (2021)]. Among the different dynamical behaviors that neuron models coupled by memristive synapse can present we are interested in the synchronization of their firing patterns, our approach is analytical and does not involve a physical implementation. In this

⋆ I. Carro-Pérez received a scholarship from Consejo Nacional de Ciencia y Tecnológica -CONACYT- under grand number 968050.

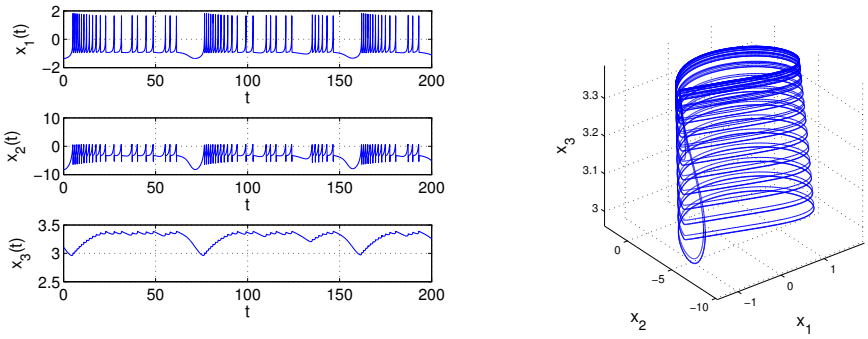

(a) (b)

Fig. 1. HR model with chaotic bursting behavior where (a) states vs time (b) chaotic spiking attractor

paper, we focus on the synchronization in two identical HR neurons bidirectionally coupled by ideal memristors, we determine that for a sufficient large memristance value identical synchronization is achieved even though the memory states of the synapses may not be identical but fixed.

In Section 2, we present the neuron and memristor models used to construct our proposed MNN model. In Section 3, we state the synchronization problem and present our main result. While in Section 4 we illustrate our results with numerical simulations and close the contribution with some final comments and remarks.

2. PRELIMINARIES

The HR neuron model is described by:

$$\begin{aligned}\dot{x}_1(t) &= -ax_1^3(t) + bx_1^2(t) + x_2(t) - x_3(t) + I(t)\\ \dot{x}_2(t) &= c - dx_1^2(t) - x_2(t)\\ \dot{x}_3(t) &= \epsilon\left[\omega\left(x_1(t) - x_0\right) - x_3(t)\right]\end{aligned} \tag{1}$$

where $x_1(t)$ is related to the neuron voltage, $x_2(t)$ to the recuperation variable, $x_3(t)$ to the adaptation variable, and $I(t)$ is the excitation current. With the following parameters $a = 1, b = 3, c = 1, d = 5, \omega = 4, x_0 = -1.6$,$I(t) = 5$,$\epsilon = 0.0021$ a chaotic bursting behavior as observed as shown in Figures 1(a)-1(b).

Rewriting (1) is in vector form one gets:

$$\dot{\mathbf{x}}(t) = f(\mathbf{x}(t)) \tag{2}$$

where $\mathbf{x}(t) = [x_1(t), x_2(t), x_3(t)]^\top$ and $f(\cdot)$ is the vector field described by equation (1), $f : \mathbb{R}^3 \to \mathbb{R}^3$, where $f(\cdot)$ is locally Lipschitz in $\mathbb{R}^3$.

Biological neural systems can be characterized through memristors. An ideal memristor is defined in [Chua (1971)] as theoretically being a basic electronic passive two terminal device that relates electric charge to magnetic flux, such that the following relationship is found:

$$q_w(t) = g(\varphi_w(t)) \tag{3}$$

where $q_w(t) \in \mathbb{R}$ is the electric charge, and $\varphi_w(t) \in \mathbb{R}$ is the magnetic flux, $g : \mathbb{R} \to \mathbb{R}$ is its characteristic function, that satisfies the conditions: (i) $g(0) = 0$, $g(\cdot) \in C^1$; and (ii) $g(\cdot)$ is strictly monotonic increasing. The electrical representation of such device is shown in Figure 2.

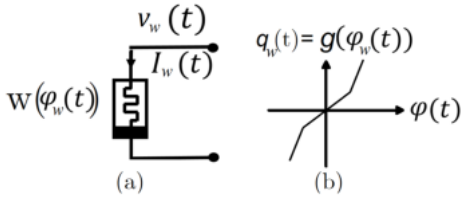

Fig. 2. (a) electric representation (b) memristive characteristic function [Itoh (2008)]

For the ideal memristor a current-voltage relation is given by:

$$i_w(t) = w(\varphi_w)v_w(t) \tag{4}$$

where $v_w(t) = \dot{\varphi}_w(t)$ and $i_w(t) = \dot{q}_w(t)$ are the voltage and current of the memristor, respectively; with its memductance given by:

$$w(\varphi_w) = \frac{dg(\varphi_w)}{d\varphi_w} \tag{5}$$

where $w(\varphi_w) > 0, \forall\varphi_w$, $w(\cdot)$ is a bounded function.

By integrating the voltage variable with respect to time, the magnetic flux $\varphi_w(t)$ is found to be:

$$\varphi_w(t) = \int_0^t v_w(\tau)d\tau + \varphi_w(0) \tag{6}$$

where $\varphi_w(t_0)$ is the initial magnetic flux. Therefore, the magnetic flux described by (6) depends on the *history* of the memristor voltage $v_w(t)$.

3. PROBLEM STATEMENT

Consider a MNN consisting of two identical HR neurons bidirectionally coupled by two ideal memristors, let $\mathbf{x}_1(t)$ the state of neuron 1 and $\mathbf{x}_2(t)$ the state of neuron 2. One says that the MNN achieves identical synchronization when the states of each nodes move at unison, *i.e.*,

$$\mathbf{x}_1(t) = \mathbf{x}_2(t) = s(t).$$

Where $s(t)$ is called synchronization solution of the network.

The dynamics of MNN are described by:

$$\dot{\mathbf{x}}_1(t) = f(\mathbf{x}_1(t)) + w_{21}(\varphi_{21}(t))\Gamma(\mathbf{x}_2(t) - \mathbf{x}_1(t)) \quad (7a)$$
$$\dot{\mathbf{x}}_2(t) = f(\mathbf{x}_2(t)) + w_{12}(\varphi_{12}(t))\Gamma(\mathbf{x}_1(t) - \mathbf{x}_2(t)) \quad (7b)$$
$$\dot{\varphi}_{21}(t) = v_2(t) - v_1(t) \quad (7c)$$
$$\dot{\varphi}_{12}(t) = v_1(t) - v_2(t) \quad (7d)$$

where $\mathbf{x}_1(t) = [x_{11}(t), x_{21}(t), x_{31}(t)]^\top$ is the state of neuron one, and $\mathbf{x}_2(t) = [x_{12}(t), x_{22}(t), x_{32}(t)]^\top$ is that of neuron two, $\Gamma = \text{diag}(1, 0, 0) \in \mathbb{R}^{3\times3}$ is the internal coupling matrix, and the voltage of neurons are $v_1(t) = \gamma\mathbf{x}_1(t), v_2(t) = \gamma\mathbf{x}_2(t)$, where $\gamma = [1, 0, 0]$. In this example is considered a perturbation signal in the first neuron. The memristor that connects neuron 1 with neuron 2 is M_{12} with $\varphi_{12}(t)$ its magnetic flux (8a). While M_{21} is the memristor that connects neuron 2 with neuron 1, with its magnetic flux $\varphi_{21}(t)$ given by (8b).

$$\varphi_{12}(t) = \int_0^t (v_1(\tau) - v_2(\tau))d\tau + \varphi_{12}(0) \quad (8a)$$
$$\varphi_{21}(t) = \int_0^t (v_2(\tau) - v_1(\tau))d\tau + \varphi_{21}(0) \quad (8b)$$

the memristive characteristic function of M_{12} is:

$$\begin{aligned} g_{12}(\varphi_{12}) &= a_{12}\varphi_{12} + \frac{1}{2}(b_{12} - a_{12})(|\varphi_{12} + l_{12}|) \\ &\quad -\frac{1}{2}(b_{12} - a_{12})(|\varphi_{12} - l_{12}|) \end{aligned} \quad (9)$$

where a_{12},$b_{12}, l_{12} > 0$ are constants, $b_{12} < a_{12}$, taking the derivative of (9) is obtained its memristance function:

$$w_{12}(\varphi_{12}) = \frac{dg_{12}(\varphi_{12})}{d\varphi_{12}} = \begin{cases} a_{12}\ , & \varphi_{12} < -l_{12} \\ b_{12}\ , & -l_{12} \le \varphi_{12} \le l_{12} \\ a_{12}\ , & l_{12} < \varphi_{12} \end{cases} \quad (10)$$

On the other hand, the memristive characteristic function of M_{21} is:

$$\begin{aligned} g_{21}(\varphi_{21}) &= a_{21}\varphi_{21} + \frac{1}{2}(b_{21} - a_{21})(|\varphi_{21} + l_{21}|) \\ &\quad -\frac{1}{2}(b_{21} - a_{21})(|\varphi_{21} - l_{21}|) \end{aligned} \quad (11)$$

where a_{21},$b_{21}, l_{21} > 0$ are constants, $b_{21} < a_{21}$, taking the derivative of (11) is obtained its memristance function:

$$w_{21}(\varphi_{21}) = \frac{dg_{21}(\varphi_{21})}{d\varphi_{21}} = \begin{cases} a_{21}\ , & \varphi_{21} < -l_{21} \\ b_{21}\ , & -l_{21} \le \varphi_{21} \le l_{21} \\ a_{21}\ , & l_{21} < \varphi_{21} \end{cases} \quad (12)$$

as consequence of identical synchronization, $\varphi_{12}(t) = \bar{\varphi}_{12}$ and $\varphi_{21}(t) = \bar{\varphi}_{21}$, where:

$$\begin{aligned} \bar{\varphi}_{12} &= \lim_{t\to\infty} \int_0^t (v_1(\tau) - v_2(\tau))d\tau + \varphi_{12}(0) \\ \bar{\varphi}_{21} &= \lim_{t\to\infty} \int_0^t (v_2(\tau) - v_1(\tau))d\tau + \varphi_{21}(0) \end{aligned}$$

At the synchronized state $s(t)$ the coupling term in the MNN goes to zero, therefore one has that its behavior is that of an isolated node:

$$\dot{s}(t) = f(s(t)) \quad (13)$$

Lets define the synchronization error as

$$\mathbf{e}_1(t) = \mathbf{x}_1(t) - s(t) \quad (14a)$$
$$\mathbf{e}_2(t) = \mathbf{x}_2(t) - s(t) \quad (14b)$$

where $\mathbf{e}_1(t) = [e_{11}(t), e_{21}(t), e_{31}(t)] \in \mathbb{R}^3$, and $\mathbf{e}_2(t) = [e_{12}(t), e_{22}(t), e_{32}(t)] \in \mathbb{R}^3$. Therefore, identical synchronization in the MNN is equivalent to the stability of the zero solution of the synchronization error dynamics.

Notice that when identical synchronization occurs $\mathbf{e}_1(t) = \mathbf{e}_2(t) = 0$, therefore $s(t) = \mathbf{x}_1(t) = \mathbf{x}_2(t)$. The error dynamics is obtained by taking the derivative of (14a)-(14b)

$$\dot{\mathbf{e}}_1(t) = \dot{\mathbf{x}}_1(t) - \dot{s}(t) \quad (15a)$$
$$\dot{\mathbf{e}}_2(t) = \dot{\mathbf{x}}_2(t) - \dot{s}(t) \quad (15b)$$

substituting $\mathbf{x}_1(t) = \mathbf{e}_1(t) + s(t)$ in (15a), and $\mathbf{x}_2(t) = \mathbf{e}_2(t) + s(t)$ (15b) one obtains:

$$\begin{aligned} \dot{\mathbf{e}}_1(t) &= f(\mathbf{x}_1(t)) - \dot{s}(t) \\ &\quad + w_{21}(\varphi_{21}(t))\Gamma(\mathbf{e}_2(t) + s(t) - \mathbf{e}_1(t) - s(t)) \end{aligned} \quad (16a)$$
$$\begin{aligned} \dot{\mathbf{e}}_2(t) &= f(\mathbf{x}_2(t)) - \dot{s}(t) \\ &\quad + w_{12}(\varphi_{12}(t))\Gamma(\mathbf{e}_1(t) + s(t) - \mathbf{e}_2(t) - s(t)) \end{aligned} \quad (16b)$$

substituting (13) in (16a),(16b) and rearranging:

$$\begin{aligned} \dot{\mathbf{e}}_1(t) &= f(\mathbf{x}_1(t)) - f(s(t)) \\ &\quad + w_{21}(\varphi_{21}(t))\Gamma(\mathbf{e}_2(t) - \mathbf{e}_1(t)) \end{aligned} \quad (17a)$$
$$\begin{aligned} \dot{\mathbf{e}}_2(t) &= f(\mathbf{x}_2(t)) - f(s(t)) \\ &\quad + w_{12}(\varphi_{12}(t))\Gamma(\mathbf{e}_1(t) - \mathbf{e}_2(t)) \end{aligned} \quad (17b)$$

where $f(\cdot)$ is described by (2), expressing (17a) in vector form becomes:

$$\dot{\mathbf{e}}(t) = F(\mathbf{X}(t)) - F(\mathbf{S}(t)) + W(\varphi(t)) \otimes \Gamma\mathbf{e}(t) \quad (18a)$$
$$\dot{\varphi}(t) = G \otimes \gamma\mathbf{e}(t) \quad (18b)$$

where $\mathbf{e}(t) = [\mathbf{e}_1^\top(t), \mathbf{e}_2^\top(t)]^\top \in \mathbb{R}^6$, $F(\cdot) = [f^\top(\cdot), f^\top(\cdot)]^\top \in \mathbb{R}^6$, $\mathbf{X}(t) = [\mathbf{x}_1^\top(t), \mathbf{x}_2^\top(t)]^\top \in \mathbb{R}^6$, $\mathbf{S}(t) = [s^\top(t), s^\top(t)]^\top \in \mathbb{R}^6$ is the synchronous solution, $\varphi(t) = [\varphi_{12}(t), \varphi_{21}(t)]^\top \in \mathbb{R}^2$, $\Gamma = \text{diag}(\gamma) \in \mathbb{R}^{3\times3}$, $\gamma = [1, 0, 0]$, and $\otimes$ is the Kronecker product.

Assuming the existence of a bounded solution to magnetic flux equation (18b) on $\mathbb{R}^2$, the time dependent connection matrix is given by:

$$W(\varphi(t)) = \begin{bmatrix} -w_{21}(\varphi_{21}(t)) & w_{21}(\varphi_{21}(t)) \\ w_{12}(\varphi_{12}(t)) & -w_{12}(\varphi_{12}(t)) \end{bmatrix} \quad (19)$$

where $W(\varphi(t))$ is a continuous piecewise linear matrix

$$W(\varphi(t)) = \begin{cases} W_1(\varphi(t)), & \varphi_{12}(t) < l_{12}\ , & \varphi_{21}(t) < -l_{21} \\ W_2(\varphi(t)), & \varphi_{12}(t) < -l_{12}\ , & -l_{21} \le \varphi_{21}(t) < l_{21} \\ W_3(\varphi(t)), & \varphi_{12}(t) < -l_{12}\ , & 21 \le \varphi_{21}(t) \\ W_4(\varphi(t)), & -l_{12} \le \varphi_{12}(t) < l_{12}\ , & \varphi_{21}(t) < -l_{21} \\ W_5(\varphi(t)), & -l_{12} \le \varphi_{12}(t) < l_{12}\ , & -l_{21} \le \varphi_{21}(t) < -l_{21} \\ W_6(\varphi(t)), & -l_{12} \le \varphi_{12}(t) < l_{12}\ , & l_{21} \le \varphi_{21}(t) \\ W_7(\varphi(t)), & l_{12} \le \varphi_{12}(t)\ , & \varphi_{21}(t) < -l_{21} \\ W_8(\varphi(t)), & l_{12} \le \varphi_{12}(t)\ , & -l_{21} \le \varphi_{21}(t) < l_{21} \\ W_9(\varphi(t)), & l_{12} \le \varphi_{12}(t)\ , & l_{21} \le \varphi_{21}(t) \end{cases}$$

where:

$$W_1(\varphi(t)) = \begin{bmatrix} -a_{12}\ , & a_{12} \\ a_{21}\ , & -a_{21} \end{bmatrix}, W_2(\varphi(t)) = \begin{bmatrix} -b_{12}\ , & b_{12} \\ a_{21}\ , & -a_{21} \end{bmatrix},$$
$$W_3(\varphi(t)) = \begin{bmatrix} -a_{12}\ , & a_{12} \\ a_{21}\ , & -a_{21} \end{bmatrix}, W_4(\varphi(t)) = \begin{bmatrix} -a_{12}\ , & a_{12} \\ b_{21}\ , & -b_{21} \end{bmatrix},$$

$$W_5(\varphi(t)) = \begin{bmatrix} -a_{12} & a_{12} \\ b_{21} & -b_{21} \end{bmatrix}, W_6(\varphi(t)) = \begin{bmatrix} -a_{12} & a_{12} \\ b_{21} & -b_{21} \end{bmatrix},$$
$$W_7(\varphi(t)) = \begin{bmatrix} -a_{12} & a_{12} \\ a_{21} & -a_{21} \end{bmatrix}, W_8(\varphi(t)) = \begin{bmatrix} -b_{12} & b_{12} \\ a_{21} & -a_{21} \end{bmatrix},$$
$$W_9(\varphi(t)) = \begin{bmatrix} -a_{12} & a_{12} \\ a_{21} & -a_{21} \end{bmatrix}.$$

$$G = \begin{bmatrix} -1 & 1 \\ 1 & -1 \end{bmatrix} \tag{20}$$

where $W(\varphi(t))$ is non-symmetric and the sum of its rows is zero uniformly in time, therefore it is negative semidefinite uniformly in time, furthermore its eigenvalues are $\lambda_{1,2}(W(\varphi(t)))$, where $\lambda_1(W(\varphi(t))) = 0, \forall\varphi \in \mathbb{R}^2$ and $\lambda_2(W(\varphi))$ is given by (21).

Equation (18a) is rewritten:

$$\dot{\mathbf{e}}(t) = \hat{F}(t, \mathbf{e}(t)) \tag{22}$$

where $\hat{F}(t, \mathbf{e}(t)) = F(\mathbf{X}(t)) - F(\mathbf{S}(t)) - W(\varphi(t)) \otimes \Gamma\mathbf{e}(t)$.

We aim to determine if $\mathbf{e}(t) \to 0$ exponentially in time at lest locally, which means that $\mathbf{S}(t)$ is a solution exponentially stable of (18a) and consequently $\varphi(t) \to \bar{\varphi}$ in (18b), where $\bar{\varphi} = [\bar{\varphi}_{12}, \bar{\varphi}_{21}]^\top$ is a constant value denominated the memory states of the memristive synapses.

Let $\|\cdot\|$ be the euclidean norm, with $B_r = \{\mathbf{e} \in \mathbb{R}^6 : \|\mathbf{e}\| < r\}$ the following properties of $\hat{F}(\cdot)$ are satisfied: (I) $\hat{F}(t, \mathbf{e})$ is Locally Lipschitz on B_r and piecewise continuous with respect to t. (II) Linearizing (22) around the origin we obtain:

$$\dot{\mathbf{e}}(t) = A(\mathbf{S}(t))\mathbf{e}(t) + W(\varphi(t)) \otimes \Gamma\mathbf{e}(t) \tag{23}$$

where $A(\mathbf{S}(t))$ is black diagonal matrix:

$$A(\mathbf{S}(t)) = \begin{bmatrix} Df(s(t)) & 0 \\ 0 & Df(s(t)) \end{bmatrix} \in \mathbb{R}^{6\times 6}$$

which is locally Lipschitz in B_r uniformly in t and $Df(s(t)) \in \mathbb{R}^{3\times 3}$ is the Jacobian of $f(\cdot)$.

Theorem 1. Assume:
(**A1**) $s(t)$ is an exponentially stable solution of single node dynamics (2), and
(**A2**) $||D(f(s(t)))|| < \alpha$, where $||\cdot||$ is a matrix induced norm and $\alpha > 0$ a positive constant.
If the memductance matrix $W(\cdot)$ is negative semidefinite uniformly in time, then the linearized error dynamics (23) are exponentially in time ($\mathbf{e}(t) \to 0$). Furthermore, since the origin is a locally exponentially stable solution of the nonlinear system (22) identical synchronization between the neurons is achieved.

Proof. The system (23) is rewritten:

$$\dot{\nu}(t) = Df(s(t))\nu(t) + \Gamma\nu(t)(W\varphi(t))^\top \tag{24}$$

where $\nu(t) = [\mathbf{e}_1(t), \mathbf{e}_2(t)] \in \mathbb{R}^{3\times 2}$ for the given $W(\varphi(t))$ there exists a non singular matrix $Z(t) \in \mathbb{R}^{2\times 2}$ such that:

$$\Lambda(t) = Z^{-1}(\varphi(t))W(\varphi(t))Z(\varphi(t))$$

where $\Lambda(t) = \text{diag}(\lambda_1(t), \lambda_2(t)) \in \mathbb{R}^{2\times 2}$ and

$$Z(\varphi(t)) = \begin{bmatrix} -\dfrac{w_{12}(\varphi_{12}(t))}{w_{21}(\varphi_{21}(t))} & 1 \\ 1 & 1 \end{bmatrix}$$

a change of base is considered:

$$\eta(t) = \nu(t)Z^{-1}(\varphi(t)) \tag{25}$$

taking the derivative of (25) is obtained:

$$\dot{\eta}(t) = \dot{\nu}(t)Z(\varphi(t)) + \nu(t)\dot{Z}(\varphi(t)) \tag{26}$$

substituting (23) in (26):

$$\dot{\eta}(t) = Df(s(t))\eta(t) + \Gamma\eta(t)\Lambda(t) - \eta(t)\dot{Z}^{-1}(\varphi(t))Z(\varphi(t)) \tag{27}$$

given that $Z(\varphi(t))$ is a piece-wise constant matrix $\dot{Z}(\varphi(t)) = \text{diag}(0, 0) \in \mathbb{R}^{2\times 2}$, then equation (27) becomes:

$$\dot{\eta}(t) = Df(s(t))\eta(t) + \Gamma\eta(t)\Lambda(t) \tag{28}$$

expanding (28) by columns and considering $\lambda_1(t) = 0\ \forall t$ is obtained:

$$\dot{\eta}_1(t) = Df(s(t))\eta_1(t) \tag{29a}$$
$$\dot{\eta}_2(t) = Df(s(t))\eta_2(t) + \lambda_2(t)\Gamma\eta_2(t) \tag{29b}$$

given that $s(t)$ is a exponentially stable solution of (2) by converse Lyapunov theorem $\eta_1(t) \to 0$ exponentially in (29a), to determine if $\eta_2(t)$ converges exponentially to the origin, we propose a Lyapunov candidate function:

$$V(\eta_2(t)) = \frac{1}{2}\eta_2^\top(t)\eta_2(t) \tag{30}$$

taking the derivative of (30) is obtained:

$$\dot{V}(\eta_2(t)) = \eta_2^\top(t)\dot{\eta}_2(t) \tag{31}$$

substituting (29b) in (31) is obtained:

$$\dot{V}(\eta_2(t)) = \eta_2^\top(t)D(f(s(t)))\eta_2(t) + \lambda_2(t)\eta_2^\top(t)\Gamma\eta_2(t) \tag{32}$$

given that $Df(s(t))$ is bounded and $\Gamma = \text{diag}(1, 0, 0) \in \mathbb{R}^{3\times 3}$, equation (32) becomes

$$\dot{V}(\eta_2(t)) = c\|\eta_2(t)\|^2 + \lambda_2(t)\eta_{12}^2(t) \tag{33}$$

we know $\eta_{12}^2(t) < \|\eta_2(t)\|^2, \forall\eta_2(t) \neq 0$, therefore (33) becomes:

$$\begin{aligned} \dot{V}(\eta_2(t)) &< c\|\eta_2(t)\|^2 + \lambda_2(t)\|\eta_2(t)\|^2 \\ \dot{V}(\eta_2(t)) &< (c + \lambda_2(t))\|\eta_2(t)\|^2 \end{aligned} \tag{34}$$

considering $-(b_{12} + b_{21}) \leq \lambda_2(t) \leq -(a_{12} + a_{21})$, if $a_{12} + a_{21} > c$, then $\dot{V}(\eta_2(t)) < 0\ \forall\eta_2 \neq 0$. We conclude that $\eta_2(t) = 0$ is an exponential solution (29b), therefore $\mathbf{e}(t)$ converge exponentially in time to zero solution in the linearized error dynamics (23); by converse Lyapunov theorem $\mathbf{e} = 0$ is an exponentially stable equilibrium point of nonlinear dynamics (22). □

4. SIMULATION EXAMPLES

Consider two identical HR neurons bidirectionally coupled through memristors M_{21} and M_{12}, the circuit of such system is presented in figure 3. As noticed this circuit is composed of two memristors M_{21} and M_{12} which can be implemented as in [Sanchez-Lopez (2014)], four operational amplifiers (OPAM) U_1-U_4 and two positive second generation current conveyors (CCII+) U_4-U_5 and resistors R. Considering the elements of this circuit are

$$\lambda_2(W(\varphi(t))) = \begin{cases} -(a_{12}+a_{21}), & \varphi_{12}(t) < -l_{12}\ , & \varphi_{21}(t) < -l_{21} \\ -(a_{12}+b_{21}), & \varphi_{12}(t) < -l_{12}\ , & -l_{21} \le \varphi_{21}(t) < l_{21} \\ -(a_{12}+a_{21}), & \varphi_{12}(t) < -l_{12}\ , & l_{21} \le \varphi_{21}(t) \\ -(b_{12}+a_{21}), & -l_{12} \le \varphi_{12}(t) < l_{12}\ , & \varphi_{21}(t) < -l_{21} \\ -(b_{12}+b_{21}), & -l_{12} \le \varphi_{12}(t) < l_{12}\ , & -l_{21} \le \varphi_{21}(t) < -l_{21} \\ -(b_{12}+a_{21}), & -l_{12} \le \varphi_{12}(t) < l_{12}\ , & l_{21} \le \varphi_{21}(t) \\ -(a_{12}+a_{21}), & l_{12} \le \varphi_{12}(t)\ , & \varphi_{21}(t) < -l_{21} \\ -(a_{12}+b_{21}), & l_{12} \le \varphi_{12}(t)\ , & -l_{21} \le \varphi_{21}(t) < l_{21} \\ -(a_{12}+a_{21}), & l_{12} \le \varphi_{12}(t)\ , & l_{21} \le \varphi_{21}(t) \end{cases} \tag{21}$$

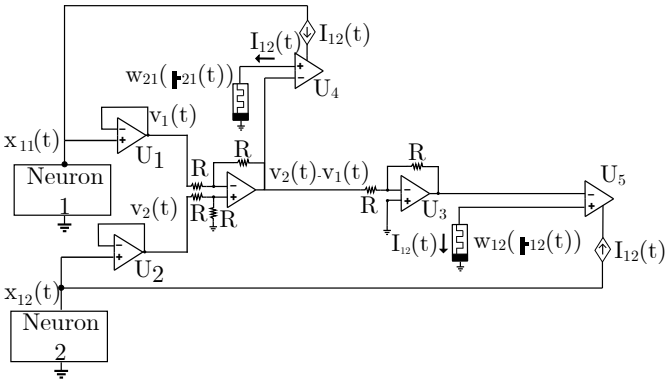

Fig. 3. Circuit implementation

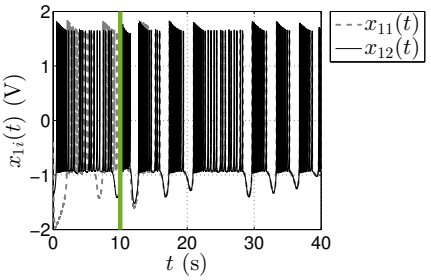

Fig. 4. (a) Neurons voltages $x_{11}(t)$ and $x_{21}(t)$

in the ideal region, because the voltages of both neurons are below saturating voltage of OPAM. Its mathematical described by:

$$\dot{\mathbf{x}}_1(t) = f(\mathbf{x}_1(t)) + w_{21}(\varphi_{21}(t))\Gamma(\mathbf{x}_2(t) - \mathbf{x}_1(t)) + \zeta(t) \tag{35a}$$

$$\dot{\mathbf{x}}_2(t) = f(\mathbf{x}_2(t)) + w_{12}(\varphi_{12}(t))\Gamma(\mathbf{x}_1(t) - \mathbf{x}_2(t)) \tag{35b}$$

$$\dot{\varphi}_{21}(t) = v_2(t) - v_1(t) \tag{35c}$$

$$\dot{\varphi}_{12}(t) = v_1(t) - v_2(t) \tag{35d}$$

where $\mathbf{x}_1(t) = [x_{11}(t), x_{21}(t), x_{31}(t)]^\top$ is the state of neuron one, and $\mathbf{x}_2(t) = [x_{12}(t), x_{22}(t), x_{32}(t)]^\top$ is that of neuron two, $\Gamma = \text{diag}(1,0,0) \in \mathbb{R}^{3\times3}$ is the internal coupling matrix, and the voltage of neurons are $v_1(t) = \gamma\mathbf{x}_1(t), v_2(t) = \gamma\mathbf{x}_2(t)$, where $\gamma = [1,0,0]$.

The memristor M_{12}, connects neuron 1 with neuron 2, its magnetic flux is $\varphi_{12}(t)$ described by (8a). While M_{21} is the memristor that connects neuron 2 with neuron 1, its magnetic flux is $\varphi_{21}(t)$ given by (8b). Here is considered a perturbation signal $\zeta(t) = 0.3e^{-0.005t}$ in the first neuron.

The characteristic function of memristor M_{12} is:

$$g_{12}(\varphi_{12}) = 0.9\varphi_{12} - 0.4(|\varphi_{12}+140| - |\varphi_{12}-140|) \tag{36}$$

where its parameters are $a_{12} = 0.9$, $b_{12} = 0.1$ and $l_{12} = 140$, the function that describes its memristance is:

$$w_{12}(\varphi_{12}) = \frac{dg_{12}(\varphi_{12})}{d\varphi_{12}} = \begin{cases} 0.9\ , & \varphi_{12} < -140 \\ 0.1\ , & -140 \le \varphi_{12} \le 140 \\ 0.9\ , & 140 < \varphi_{12} \end{cases} \tag{37}$$

While the characteristic function of memristor M_{21} is:

$$g_{21}(\varphi_{21}) = \varphi_{21} - 0.425(|\varphi_{21}+120| - |\varphi_{21}-120|) \tag{38}$$

where its parameters are $a_{21} = 1$ and $b_{21} = 0.15$,$l_{21} = 120$, the function that describes its memristance:

$$w_{21}(\varphi_{21}) = \frac{dg_{21}(\varphi_{21})}{d\varphi_{21}} = \begin{cases} 1\ , & \varphi_{21} < -120 \\ 0.15\ , & -120 \le \varphi_{21} \le 120 \\ 1\ , & 120 < \varphi_{21} \end{cases} \tag{39}$$

the time dependent coupling matrix $W(\varphi(t))$ is piecewise constant, non symmetric and negative semidefinite uniformly in time, therefore condition of Theorem 1 is met, in this case b_{12},b_{21} are chosen big enough so that the conditions of Theorem 1 are satisfied.

The results of simulating numerically the model (7a)-(7d), with initial conditions $\mathbf{x}_1(0) = [-0.3945, -0.5858, 4.709]^\top$, $\varphi_{21}(0) = 10$,$\mathbf{x}_2(0) = [-1.361, -8.26, 3.11]^\top$, $\varphi_{12}(0) = 50$ and internal connection matrix $\Gamma = \text{diag}(1,0,0) \in \mathbb{R}^{3\times3}$, are shown in Figures 4-5.

Initially the pair of neurons are uncoupled, at $t = 10$ the neurons are coupled, then after $t = 20$ the voltages $x_{11}(t)$, $x_{12}(t)$ converge towards each other in spite of perturbation signal, as shown in Figure 4 ; while the error in neurons states (see Figure 5) are basically zero. In Figure 6 is shown that magnetic flux of memristors $\varphi_{12}(t)$ and $\varphi_{21}(t)$, converge to constant values, notice that their convergence value is different, this is because initial conditions are not equal $\varphi_{12}(0) = 10$,$\varphi_{21}(0) = 50$.

As observed in figure 7, the memristor M_{12} reaches high conductance region instantly when $t = 30$, while M_{21} is in low conductance region, having a big enough coupling strength, for neurons to synchronize as observed in Figure 4 and 5.

Remark 1. The emergence of identical synchronization is dependent on the properties of the memristor synapses as long as they have positive memductance, *i.e.* the

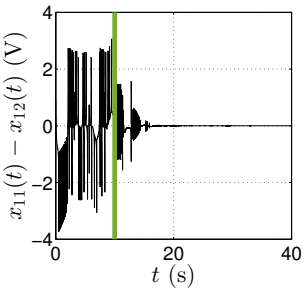

Fig. 5. Error in neurons voltages

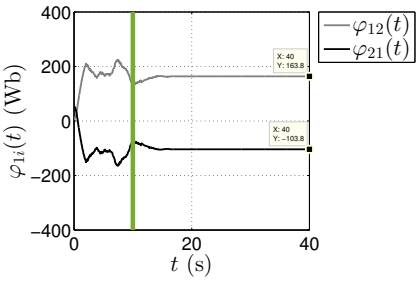

Fig. 6. Magnetic flux of memristor M_{12} (gray) and memristor M_{21} (black)

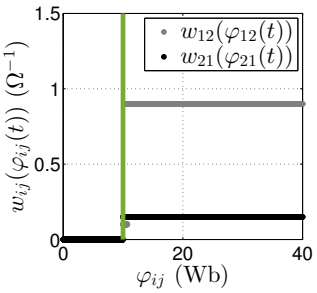

Fig. 7. Memductance

time dependent connection matrix is negative semidefinite uniformly in time, synchronization is achieved although they are not identical.

Remark 2. When a combination of memductances $w_{12}(\cdot)$, $w_{21}(\cdot)$ is not greater than the required coupling strength c to achieve synchronization, the pair of neurons will remain unsynchronized. All code scripts are available upon reasonable request.

Remark 3. All code scripts are available upon reasonable request.

5. CONCLUSION

In this paper, synchronization in a MNN of two HR neurons bidirectionally coupled by nonidentical ideal memristors is investigated, we find sufficient conditions in memristor properties for the identical synchronization, our results show that for memristance sufficiently large and positive definite at all times, the neurons will synchronize with the magnetic flux of the memristors converge to constant values. The analysis of synchronization is based on a linearized error dynamics which restrict our results to a local neighborhood of synchronous state.

REFERENCES

A. L. Hodgkin, A. F. Huxley, B. Katz "Ionic currents underlying activity in the giant axon of the squid," Arch. Sci. Physiologiques, 3, 129–150, 1949.

J.L. Hindmarsh, R.M. Rose. A model of neunoral bursting using 3 coupled 1st order differential-equations, Proc. R. Soc. Lond. B, 221(1222),87-102,1984.

E.R. Kandel, T.M. Jessell, J.H. Schwartz, S.A. Siegelbaum, A.J. Hudspeth Principles of Neural Science,, McGraw-Hill, 2013.

D. Serrat, B. Graham, A. Gillies, D. Willshaw Principles of Computational Modeling in Neuroscience Cambridge University Press, 2011.

A. Amirsoleimani, M. Ahmadi, A. Ahmadi, M. Boukadoum. Pattern classification with memristive neural network using the Hodgkin-Huxley neuron IEEE Int. Conf. on Electron. Circuits and Syst. ICECS, 81-84,2016.

Y. Pershin, M. Di Ventra. Experimental demonstration of associative memory with memristive neural networks Nat Prec, 2009.

Y. Nishitani, Y. Kaneko, M. Ueda. Supervised Learning Using Spike-Timing-Dependent Plasticity of Memristive Synapses IEEE Trans Neural Netw Learn Syst,26(12),2999-3008, 2015.

Y. Li, B. Luo, D. Liu, Y. Yang and Z. Yang. Robust Exponential Synchronization for Memristor Neural Networks With Nonidentical Characteristics by Pinning Control IEEE Trans. Syst. Man Cybern.: Syst.,51(3),1966-1980, 2021.

C. Sánchez-López, V.H. Carbajal-Gómez, M.A. Carrasco-Aguilar PID controller design based on memductor AEU - Int. J. Electron, 101,9-11, 2019.

I. Carro-Perez ,C. Sánchez-López, H.G. Gonzalez-Hernandez, PID controller design based on memductor AEU - Int. J. Electron, 101,9-11, 2019.

G. Innocenti, A. Morelli, R. Genesio, A. Torcini Dynamical phases of the Hindmarsh-Rose neuronal model: Studies of the transition from bursting to spiking chaos, Chaos,17(4), 2007.

L. O. Chua Memristor-The missing circuit element, IEEE Trans. Circuits Theo., 18(5), 507-519, 1971.

M. Itoh , L. O. Chua Memristor Oscillators, Int. J. Bifurc. Chaos, 18(5), 18(11),3183-3206.

D. Purves, G. Augustine, D. Fitzpatrick, W. C. Hall, A. LaMantia, R. Mooney ,L. E White. Neuroscience, Sinauer, EE. UU.,2018

H.K. Khalil. Nonlinear Systems, Prentice Hall, 2002.

C. Sanchez-Lopez, J. Mendoza-Lopez, M.A. Carrasco-Aguilar, C. Muñiz-Montero A Floating Analog Memristor Emulator Circuit, IEEE Trans. Circuits Sys. II: Express Br., 61(5), 309-313, 2014.

Memorias del Congreso Nacional de Control Automático ISSN: 2594-2492

Stability of the memory state of a time-varying memristive neural network model ⋆

Illiani Carro-Pérez * **Juan Gonzalo, Barajas-Ramírez** *

* *IPICYT, División de Control y Sistemas Dinámicos, Camino a la Presa San José 2055, Col. Lomas 4 Sección CP. 78216, San Luis Potosí, S.L.P., México. (E-mail: illiani.carro, jgbarajas@ipicyt.edu.mx).*

Abstract: Memristors are resistive memory devices, where the resistive memory state is a function of the memristor's initial conditions and the history of the voltage across its terminals. Applications of these devices are in neuromorphic circuits. In particular, as representations of the open-close dynamics of the ionic channels in neurophysiological models. We use a memristive version of the Integrate and Fire neuron to construct a time-varying memristive neural network. In this model, a memory state is a stable unique equilibrium point. We show that the existence of a memory state depends uniformly on properties of the network topology and description of the memristive characteristic function. We illustrate our results using numerical simulations.

Keywords: Memristors, Neural network models, Neuron models, Resistive memory.

1. INTRODUCTION

The brain is capable of information integration and processing incoming from several different organs resulting in capabilities like memory and reasoning. The neuron is the basic processing unit of the brain, its behavior, and emergent properties as they are connected into networks are studied in many different ways. The neuron's electrical behavior is captured by the Hodgkin and Huxley model (HH) (Hodgkin & Huxley, 1949). In particular, the action potential phenomenon is the result of the physiological excitability of the ionic currents in the neuron's membrane. The so-called *Integrate and Fire* (IF) neural model is a simplified model that captures this phenomenon as a charge and discharge of a capacitor (Lapique, 1971).

The electrical representation of neural models required the use of time-varying conductance to model the opening and closing of ion channels in the membrane. No basic discrete electronic component had these features until in 1971 L. O. Chua theorized the existence of a fourth electric basic element called Memristor (Chua, 1971). That name is a contraction of words: resistance and memory.

The memristor is an electronic device characterized by a relation between its electric charge and its magnetic flux. Since these variables are related to the current and voltage across the device via its derivative, the resistance value of the memristor depends on the *history* of the voltage that passed through it, furthermore as the derivative goes to zero the resistance value is maintained in the device without new current been needed. As a result, *non-volatility* is a property of this resistive memory (Chua, 2011).

As presented in (Sah *et.al*, 2016), the memristor is a candidate to represent the time-varying conductances of the neural model (Hodgkin & Huxley, 1949). The possibility of implementing memristive circuits as a representation of biological neurons gives the interest in them as neuromorphic circuits (Chua *et.al*, 2012; Yang *et.al*, 2019). In particular, (Di Marco *et.al*, 2018) proposes a memristive version of the IF neural model.

As biological neurons communicate with each other through synapses, several memristive neurons can be coupled together into networks where dynamical phenomena can emerge. Yet, the dynamical behavior of memristive neurons, in particular Memristive IF neurons (MIFN), needs to be studied further.

An important feature of the MIFN model is that it has a continuum of equilibrium points. However, for a given fixed initial condition there exists only an equilibrium point and further this unique equilibrium point is stable, as such, in the sense of a memristor resistance, this unique stable equilibrium point is the memory state of the MIFN model (Di Marco *et.al*, 2018).

⋆ I. Carro-Pérez received a scholarship from Consejo Nacional de Ciencia y Tecnológica -CONACYT- under grand number 968050.

This contribution aims to establish under what conditions a network on identical MIFN models with a time-varying coupling structure has a memory state. In other words, under what conditions, both in terms of the memristor description and the coupling structure of time-varying connections, of a memristor IF neural network (MIFNN) has a unique stable fixed point for a given fixed initial condition.

The remainder of the contribution is organized as follows: In Section 2, the basic aspects of memristor theory, and the memristive version of the IF neuron model are presented. In Section 3, the memory state problem for the time-varying MIFNN model is described in detail. Section 4 presents our main result, in the form of conditions for existence, uniqueness, and stability of an equilibrium point for the time-varying MIFNN. In Section 5 our results are illustrated with numerical simulations, then the contribution is finished with closing remarks.

2. PRELIMINARIES

2.1 Memristor

In (Chua, 1971) a memristor is defined as a basic electronic element that relates electric charge with magnetic flux, and represented as shown in Fig. 1.

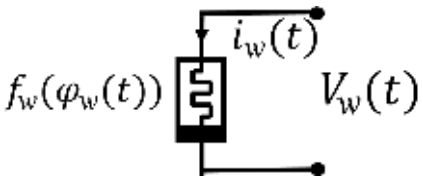

Fig. 1. Memristor's electronic symbol

The memristor fundamental function is defined as:

$$Q_w(t) = f_w(\varphi_w(t)) \tag{1}$$

where $Q_w(t) \in \mathbb{R}$ is the electric charge, and $\varphi_w(t) \in \mathbb{R}$ is the magnetic flux of the memristor. $f_w : \mathbb{R} \to \mathbb{R}$, $f_w(\cdot) \in C^1$ is the memristive characteristic function, it usually considered to be a monotonic increasing function.

We have voltage $V_w(t)$ and current $I_w(t)$ in the memristor are expressed as:

$$V_w(t) = \dot{\varphi}_w(t) \tag{2a}$$

$$I_w(t) = \dot{Q}_w(t) \tag{2b}$$

From the above, the current-voltage relation on the memristor is:

$$I_w(t) = w(\varphi_w)V_w(t) \tag{3}$$

where $w(\varphi_w) = \frac{df_w(\varphi_w)}{d\varphi_w}$ is the memductance of the memristor in Ω^{-1}. By integrating (2a) with respect to time, the magnetic flux $\varphi_w(t)$ is found to be:

$$\varphi_w(t) = \int_{t_0}^{t} V_w(\tau)d\tau + \varphi_w(t_0) \tag{4}$$

where $\varphi_w(t_0)$ is the initial magnetic flux.The magnetic flux described by (4) depends on the *history* of the memristor voltage $V_w(t)$, for this reason if the dynamics of the voltage and magnetic flux converge to a fixed value (Q_w^*, φ_w^*), furthermore if it is stable, one can call (Q_w^*, φ_w^*), the *memory state* of the memristor and $w(\varphi_w^*)$ its memductance.

In (Chua & Kang, 1976) is proposed a general mathematical description called *memristive system* described by:

$$\begin{aligned} \dot{\mathbf{x}}(t) &= \mathbf{f}(\mathbf{x}(t), v(t)) \\ i(t) &= h(\mathbf{x}(t))v(t) \end{aligned} \tag{5}$$

where $\mathbf{x}(t) \in \mathbb{R}^n$ is vector of state variables of the memristive system, $v(t) \in \mathbb{R}$ is the input associated to the electrical variable voltage, $i(t) \in \mathbb{R}$ is the output associated to the electrical variable current, $\mathbf{f} : \mathbb{R}^n \times \mathbb{R} \to \mathbb{R}$ is locally Lipschitz in $\mathbb{R}^n \times \mathbb{R}$, $h : \mathbb{R}^n \to \mathbb{R}$ is a continuous function.

Memristive systems have been used to characterize the behavior of biological systems, in particular the behavior of time-varying conductances on neuron membrane models as can been seen in (Chua *et.al*, 2012).

2.2 Simplified neural models

There are several reduced models of the HH model (Hodgkin & Huxley, 1949). One of them is the IF (Lapique, 1971), in which electrical circuit representation is depicted in Fig. 2.

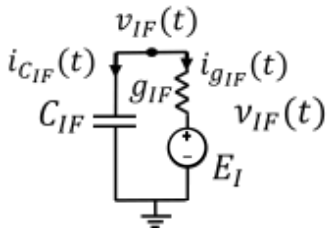

Fig. 2. IF neuron model

From Fig.2, the current $i_{C_{IF}}(t) \in \mathbb{R}$ of the capacitor is defined by:

$$i_{C_{IF}}(t) = C_{IF}\dot{v}_{IF}(t) \tag{6}$$

where $v_{IF}(t) \in \mathbb{R}$ is the voltage across the capacitor and C_{IF} is its capacitance, the current $i_{g_{IF}}(t)$ of the conductance g_{IF} is defined by:

$$i_{g_{IF}}(t) = g_{IF}(v_{IF}(t) - E_I) \tag{7}$$

The dynamical model of the circuit in Fig. 2 is obtained by the Kirchoff's Currents Law.

$$i_{C_{IF}}(t) + i_{g_{IF}}(t) = 0 \tag{8}$$

Substituting equations (6) and (7) in (8) is obtained:

$$C\dot{v}_{IF}(t) = -g_{IF}(v_{IF}(t) - E_I). \tag{9}$$

The IF neuron model is modified by including memristive elements in its description to generate the so-called MIFN

model. In the following subsection, its electrical circuit and dynamical model are presented.

2.3 Memristive Integrate and Fire Neuron Model

Consider the Memristive Integrate and Fire neuron model as proposed in (Di Marco *et.al*, 2018) consisting of a memristor M connected in parallel to a capacitor C as represented in Fig. 3.

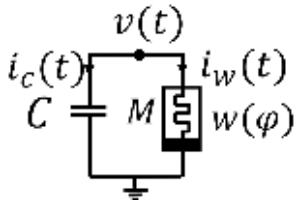

Fig. 3. Electrical circuit of the MIFN model

From Fig. 3, the current $i_c(t) \in \mathbb{R}$ of the capacitor is defined by:

$$i_c(t) = C\dot{v_C}(t) \tag{10}$$

where $v_C(t) \in \mathbb{R}$ is the capacitor voltage and C is its capacitance. The memristor current $i_w(t)$ is defined by:

$$i_w(t) = w(\varphi(t))v_M(t) \tag{11}$$

as before $w(\varphi)$ is the memductance of the memristor. According to Kirchhoff's Voltage Law $v_C(t) - v_M(t) = 0$, therefore $v_C(t) = v_M(t) = v(t)$. The dynamical model of the circuit in Fig. 3 is obtained by the Kirchhoff's Current Law.

$$i_c(t) + i_w(t) = 0 \tag{12}$$

Substituting equations (10) and (11) in (12) and recalling (2a), the following MIFN model equations are obtained:

$$C\dot{v}(t) = -w(\varphi(t))v(t) \tag{13a}$$

$$\dot{\varphi}(t) = v(t) \tag{13b}$$

with initial conditions $\varphi(t_0) = \varphi_0$ and $v(t_0) = v_0$.

The equilibrium points of (13a)-(13b) are a continuum given by

$$\pi_e = \{[0, \varphi]^\top \in \mathbb{R}^2 : \varphi \in \mathbb{R}\}. \tag{14}$$

Is important to note that for a given fixed initial condition there exits a unique equilibrium point $(0, \varphi_e) \in \mathbb{R}^2$ for (13). Furthermore, this equilibrium point if stable, is the *memory state* of the MIFN model.

In the following section, the MIFNN model is presented and investigated under the consideration of time-varying couplings.

3. TIME-VARYING MIFNN MODEL

Consider a set of N identical MIFN (13a-b) called *nodes* $\mathcal{M} = \{m_1, ..., m_N\}$. Where each node has unitary capacitances $C_1 = .. = C_N = 1$ and identical characteristic memristive functions $f_{w_1}(\cdot) = ... = f_{w_N}(\cdot) = f_w(\cdot)$. Therefore, all nodes have identical memductance $w(\cdot) = w_1(\cdot) = ... = w_N(\cdot)$.

If node m_i is connected to node m_j by a *fixed* edge $s_{ij} \in \mathcal{S} \subset \mathcal{M} \times \mathcal{M}$ where $i \neq j$, then $a_{ij} = 1$. Alternatively, if these nodes are not connected $a_{ij} = 0$. Since the edges are undirected, $a_{ij} = a_{ji}\ \forall i, j$ and there are no isolated nodes in the network. The coupling structure is given by the adjacency matrix $A = \{a_{ij}\} \in \mathbb{R}^{N\times N}$.

Let every edge has an associated *time-dependent* connection weight given by a function $c_{ij} : \mathbb{R}_+ \to \mathbb{R}_{>0}$ locally Lipschitz in $\mathbb{R}_+$. The time-varying Laplacian matrix $\mathcal{L}(t) = (\ell_{ij}(t))_{N\times N}$ associated to this connection topology is given by:

$$\ell_{ij}(t) = \begin{cases} \sum\limits_{k=1,k\neq i}^{N} a_{ik}c_{ik}(t), & i = j \\ -a_{ij}c_{ij}(t), & i \neq j \end{cases} \tag{15}$$

The dynamics of the $i-$th node is given by:

$$\dot{v_i}(t) = -w(\varphi_i(t))v_i(t) - \sum_{j=1}^{N} \ell_{ij}(t)v_j(t) \tag{16a}$$

$$\dot{\varphi}_i(t) = v_i(t) \tag{16b}$$

for $i = 1, 2, \cdots, N$.

A vectorial form of (16) is:

$$\dot{V}(t) = -W(\phi(t))V(t) - \mathcal{L}(t)V(t) \tag{17a}$$

$$\dot{\phi}(t) = V(t) \tag{17b}$$

where $V(t) = [v_1(t), ..., v_N(t)]^\top \in \mathbb{R}^N$ and $\phi(t) = [\varphi_1(t), ..., \varphi_N(t)]^\top \in \mathbb{R}^N$ are the voltage and magnetic flux vectors, respectively. With the memductance matrix $W(\phi(t)) = \text{diag}(w(\varphi_1(t)), .., w(\varphi_N(t))) \in \mathbb{R}^{N\times N}$.

From (15) we have that the time-varying Laplacian matrix of the MIFNN is uniformly diffusive, that is, the sum by row and by columns is zero at all times. As a consequence the eigenvalues of $\mathcal{L}(t)$, denoted as $\lambda_i(t)$ $(i = 1, \cdots, N)$ can be arrange as (Lü & Chen, 2005):

$$\lambda_N(t) \geq \cdots \lambda_2(t) \geq \lambda_1 = 0 \tag{18}$$

In other words, the coupling of the MIFNN is captured by a Laplacian matrix that is semipossitive at each time instant.

As before, for (16a)-(16b) there is a continuum of the equilibrium points defined by the set

$$\beta_e = \{[0, \phi]^\top \in \mathbb{R}^{2N} : \phi \in \mathbb{R}^N\}. \tag{19}$$

The equilibrium point $[0, \phi^*]^\top \in \beta_e$ is a memory state of the MIFNN model, if for a given fixed initial condition $[V_0, \phi_0]^\top \in \mathbb{R}^{2N}$, $[0, \phi^*]^\top$ is unique and stable equilibrium point to which the network model converges, as shown in the following section, where we determine the conditions for the existence and stability of a unique equilibrium point of (16a-b) for a given fixed initial condition.

$$\mathcal{L}(t) = \begin{pmatrix} \ell_{11}(t) & -1.5 & -6 & -0.5+\exp(2-0.1t) & -0.5-t\exp(-0.1t) & -0.1t^2 \\ -1.5 & \ell_{22}(t) & -\exp(0.1t-6) & -6\cos^2(t)\sin(0.1\pi t)-7 & -\exp(-0.5t) & -\exp(0.1t) \\ -6 & -\exp(0.1t-6) & \ell_{33}(t) & -0.1t & -\cos(t)-1.1 & -\arctan(t) \\ -0.5-\exp(2-0.1t) & -6\cos^2(t)\sin(0.1\pi t)-7 & -0.1t & \ell_{44}(t) & -10 & -3 \\ -0.5-t\exp(-0.1t) & -\exp(-0.5t) & -\cos(t)-1.1 & -10 & \ell_{55}(t) & -\sin(\pi t)-1.1 \\ -0.1t^2 & -\exp(0.1t) & -\arctan(t) & -3 & -\sin(\pi t)-1.1 & \ell_{66}(t) \end{pmatrix} \tag{20}$$

$$\begin{aligned} \ell_{11}(t) &= 1.5+6+0.5+\exp(2-0.1t)+0.5+t\exp(-0.1t)+0.1t^2 \\ \ell_{22}(t) &= 1.5+6\cos^2(t)\sin(0.1\pi t)+\exp(0.1t-6)+7+\exp(-0.5t)+\exp(0.1t) \\ \ell_{33}(t) &= 6+\exp(0.1t-6)+0.1t+\cos(t)+1.1+\arctan(t) \\ \ell_{44}(t) &= 0.5+\exp(2-0.1t)+6\cos^2(t)\sin(0.1\pi t)+7+0.1t+10+3 \\ \ell_{55}(t) &= 0.5+t\exp(-0.1t)+\exp(-0.5t)+\cos(t)+1.1+10+\sin(\pi t)+1.1 \\ \ell_{66}(t) &= 0.1t^2+\exp(0.1t)+\arctan(t)+3+\sin(\pi t)-1.1 \end{aligned} \tag{21}$$

4. MAIN RESULTS

To establish the existence and stability of a unique equilibrium point for the MIFNN model given a fixed initial condition $[V_0, \phi_0]^\top$, we start considering the voltage equation (16a).

Assuming:

(1) There exists a solution to the magnetic flux equation (16b) which is unique and continuous on $\mathbb{R}$ for each node i.
(2) The memristive characteristic $f_w(\cdot)$ of the neurons is a monotonic and strictly increasing function.

The voltage equation of the MIFNN model (17a) can be written as

$$\dot{V}(t) = -B(t)V(t) \tag{22}$$

where $B(t) = W(\phi(t)) + \mathcal{L}(t)$,

We have the following results:

Theorem 1. The voltage equation (22) has a unique equilibrium point given by

$$V^* = 0 \in \mathbb{R}^N \tag{23}$$

Proof 1. Given that the $\mathcal{L}(t)$ is a positive semidefinite matrix for all time instants, and $W(\phi(t))$ is positive definite due to assumption (2). Their sum is positive definite $\forall t$, and as a consequence $B(t)$ is a non-singular matrix $\forall t$, therefore get that $V^* = 0$ is the only solution to its equilibrium point algebraic equation. □

From the above result we can derive the following:

Theorem 2. Under assumptions (1) and (2) the unique equilibrium point $V^* = 0 \in \mathbb{R}^N$ is uniformly asymptotically stable.

Proof 2. To establish the stability of $V^* = 0$ consider the Lyapunov candidate function, $\dot{E}(V(t)) = \frac{1}{2}V^\top(t)PV(t)$ with P a constant symmetric and positive definite matrix of appropriate dimensions. Its derivative on the trajectories of (22) is given by

$$\dot{E}(V(t)) = -V^\top(t)\left[PB(t)\right]V(t) \tag{24}$$

If $\exists Q \in \mathbb{R}^{N\times N}$ definite positive for all time, such that $PB(t) > -Q$, would imply that $\dot{E}(V(t)) < 0$, $\forall t$, that is, $V^* = 0$ is uniformly asymptotically stable equilibrium point of (17a). □

As a consequence of Theorem 2 we know that the right side of (17b) will converge to zero. Then, we have the following result:

Corollary 2.1. Under assumptions of theorem 2. If $B(t)$ is positive definite $\forall t$, then the solution of the magnetic flux equation of the MIFNN model (17b) will converge asymptotically to a fixed value $\phi^* \in \mathbb{R}^N$. Furthermore,

$$\phi^* = \lim_{t\to\infty}\int_{t_0}^{t} V(\tau)d\tau + \phi_0 \tag{25}$$

Proof 3. Integrating both sides of (17b) we have

$$\phi(t) = \int_{t_0}^{t} V(\tau)d\tau + \phi_0$$

From the result in Theorem 2 we have that for a sufficiently large T, $V(T) = 0$, regardless of the initial condition $[V_0, \phi_0]^\top \in \mathbb{R}^{2N}$, and given that $V(t)$ is a unique and continuous function, the limit in (25) exists and is a unique fixed value that depends on the history of the voltage across the memristive neurons and the initial conditions.

Finally, combining the above results we have

Theorem 3. Under assumptions of theorem 2, for a given fixed initial condition the time-varying MIFNN model (17a-b) has a unique equilibrium point $[0, \phi^*]^\top \in \mathbb{R}^{2N}$ and it is uniformly asymptotically stable.

Proof 4. It follows from the previous results.

5. SIMULATION EXAMPLE

In this numerical analysis, we illustrate Theorems 2 and 3, by constructing six node network as described in (17a)-(17b), where every node is connected to its five neighbor nodes, the network topology consists of a six-node fully connected network, where its time-varying Laplacian is described in equation (20). Let the initial conditions be:

$$V_0 = [-5.5, 4.5, -3.1, 6.3, -2.2, 5.2]^\top \tag{26}$$

$$\phi_0 = [1, -1, -2, -1.4, -1.6, 3]^\top \tag{27}$$

Let the memductance matrix be:
$W(\phi) = \mathrm{diag}(w(\varphi_1), \cdots, w(\varphi_6)) \in \mathbb{R}^{6\times 6}$, where $w(\varphi_i) = \frac{df_w(\varphi_i)}{d\varphi_i}$ is the memductance function and $f_w(\varphi_i)$ the memristive characteristic function described by:

$$f_w(\varphi_i) = \begin{cases} 0.1\varphi_i - 4, & \varphi_i \leq -2 \\ 2.1\varphi_i, & -2 < \varphi_i < 2 \\ 0.1\varphi_i + 4, & \varphi_i \leq 2 \end{cases} \tag{28}$$

Therefore, assumption (2) is satisfied, and we proceed to solve the system of the six node network, described above via numerical integration using Matlab® software, through *Runge-Kutta* method. First is verified Theorem 2, that is, asymptotic convergence of nodes voltages towards zero solution as shown in Fig. 4.

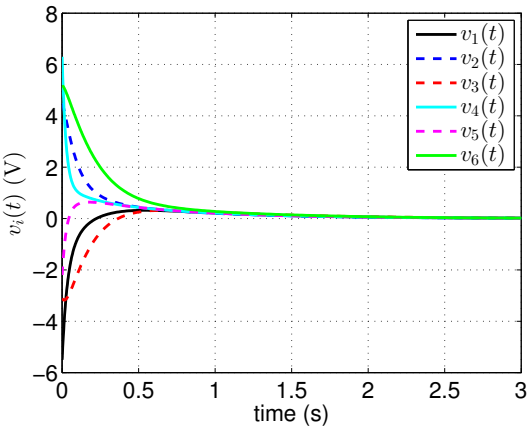

Fig. 4. Numerical integration of the MIFNN network described by (17a-b). Plot of node voltages $V(t) = [v_1(t), v_2(t), v_3(t), v_4(t), v_5(t), v_6(t)]$

Subsequently, to verify the results of Corollary 2.1, that is, the asymptotic convergence of nodes magnetic fluxes towards different constant values, dependent on the initial conditions $[V_0, \phi_0]^\top \in \mathbb{R}^{12}$, as shown in Fig. 5.

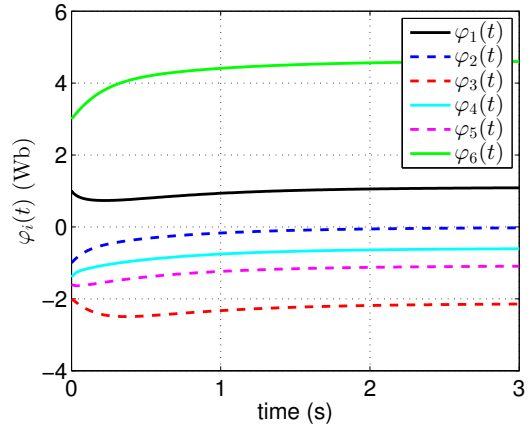

Fig. 5. Numerical integration of the six nodes network described by (17a-b). Plot of nodes magnetic fluxes $\phi(t) = [\varphi_1(t), \varphi_2(t), \varphi_3(t), \varphi_4(t), \varphi_5(t), \varphi_6(t)]$

As shown in Fig. 5 the corresponding equilibrium point ϕ^* as described in equation (25) in Corollary 2.1 is:

$$\phi^* = [1.1002, -0.0152, -2.1316, -0.5967, -1.0827, 4.6169]^\top \tag{29}$$

As a result of the numerical analysis performed in Fig. 4 and Fig.5 is verified Theorem 3, in which is shown that for the initial condition (26), the equilibrium point $[0, \phi^*]^\top$, where ϕ^* is given in (29), is an asymptotic stable equilibrium point of (17a-b).

6. DISCUSSION OF RESULTS

In this contribution, we proposed a time-varying MIFNN model and derived simple conditions to establish the existence of a memory state, e.g. a unique stable equilibrium point for each initial condition. The conditions for the existence of a memory state are the increasing monotonicity of the memristive characteristic function and uniform dissipation of the time-varying Laplacian matrix to describe the neuron connections. Further, we show using the Lyapunov approach that the voltage equation of the MIFNN model converges to the zero solution as its only equilibrium point and that is uniformly asymptotically stable. As a consequence of this, for a given initial condition the entire time-varying network has a unique stable equilibrium point, which represents the network's memory of its initial conditions.

REFERENCES

Hodgkin, A. L., Huxley, A. F., Katz, B. "Ionic currents underlying activity in the giant axon of the squid," Arch. Sci. Physiologiques, 3, 129–150, 1949.

Lapique, L. "Recherches Quantitatives Sur l'excitation Electrique Des Nerfs Traitee Comme Une Polarization," J. de Physiologie Path. Gen., 22(1), 620–635, 1907.

Chua, L. O. "Memristor-The missing circuit element," IEEE Trans. Circuits Theo., 18(5), 507–519, 1971.

Chua, L. O. "Resistance switching memories are memristors," Appl. Phys. A, 102(51), 102–783, 2011.

Chua, L.O., Sbitnev, V., Kim, H. "Hodgkin–Huxley Axon Is Made Of Memristors," Int. J. Bifur. Chaos, 22(3), 1230011 1–48, 2012.

Sah, M., Kim, H., Eroglu, A., Chua, L.O., "Memristive Model of the Barnacle Giant," Int. J. Bifur. Chaos, 26(1), 1630001 1–40, 2016.

Di Marco, M., Forti, M., Pancioni, L. "New Conditions for Global Asymptotic Stability of Memristor Neural Networks," IEEE Trans. Neur. Net. Lear. Syst., 28(5), 1822–1834, 2018.

Yang, L., Zeng, Z., Shi, X., "A memristor-based neural network circuit with synchronous weight adjustment," Neurocomputing, 363, 114–124, 2019.

Chua, L. O., Kang, S. M. "Memristive Devices and Systems," Proc. of the IEEE, 64(2), 209–223, 1976.

Lü, J., Chen, G. "A time-varying complex dynamical network model and its controlled synchronization criteria," IEEE Trans. on Automatic Control,50(6), 841–846, 2005.

Bibliography

[1] M. Di Marco, M. Forti, and L. Pancioni. New conditions for global asymptotic stability of memristor neural networks. *IEEE Transactions on Neural Networks and Learning Systems*, 28(5):1822–1834, 2018.

[2] F. Xu, J. Zhang, T. Fang, S. Huang, and M. Wang. Synchronous dynamics in neural system coupled with memristive synapse. *Nonlinear Dyn*, 92:1395–1402, 2018.

[3] H. Bao, Y. Zhang, W. Lu, and B. Bao. Memristor synapse-coupled memristive neuron network: synchronization transition and occurrence of chimera. *Nonlinear Dyn*, 100:937–950, 2020.

[4] S.H. Thompson and S.J. Smith. Depolarizing afterpotentials and burst production in molluscan pacemaker neurons. *Journal of Neurophysiology*, 39(1):153–161, 1976.

[5] M. Gola. Neurones à ondes-salves des mollusques. *Pflugers Archiv*, 352:17–36, 1974.

[6] J. L. Hindmarsh and R. M. Rose. A model of neunoral bursting using 3 coupled 1st order differential-equations. *Proc. R. Soc. Lond. B*, 221(1222):87–102, 1984.

[7] L. O. Chua and S. M. Kang. Memristive devices and systems. *Proceedings of the IEEE*, 64(2):209–223, 1976.

[8] S. Kanagaraj, P. Durairaj, S. Sampath, A. Karthikeyan, and K. Rajagopal. Collective dynamics of coupled hindmarsh–rose neurons with a locally active memristor. *Biosystems*, 232:105010, 2023.

[9] Y. Xu, Ya Xia, J. Ma, A. Alsaedi, and B. Ahmad. Synchronization between neurons coupled by memristor. *Chaos Solit.*, 104:435–442, 2017.

[10] K. Usha and P.A. Subha. Hindmarsh-rose neuron model with memristors. *Biosystems*, 178:1–9, 2019.

[11] J. Ma, M. Lv, P. Zhou, Y. Xu, and T. Hayat. Phase synchronization between two neurons induced by coupling of electromagnetic field. *Applied Mathematics and Computation*, 307:321–328, 2017.

[12] Z. Li, H. Zhou, M. Wang, and M. Ma. Coexisting firing patterns and phase synchronization in locally active memristor coupled neurons with hr and fn models. *Nonlinear Dynamics*, 104:1455–1473, 2021.

[13] S. Mostaghimi, F. Nazarimehr, S. Jafari, and J. Ma. Chemical and electrical synapse-modulated dynamical properties of coupled neurons under magnetic flow. *Applied Mathematics and Computation*, 348:42–56, 2019.

[14] E.R. Kandel, T.M. Jessell, J.H. Schwartz, S.A. Siegelbaum, and J.A. Hudspeth. *Principles of Neural Science*. McGraw-Hill, EE. UU., 5th edition, 2013.

[15] L. Galvani. Commentarius. *Bon. Sci. Art. Inst. Acad. Comm.*, 1791.

[16] G. Finkelstein. *Emil du Bois-Reymond: Neuroscience, Self, and Society in Nineteenth-Century Germany*. The MIT Press, Cambridge; London.

[17] W. Nernst and J.O.W. Barratt. Zur kinetik der lösung befindlichen körper: theorie der diffusion. *Z Phys Chem.*, 2:613–637, 1888.

[18] L. Lapique. Recherches quantitatives sur l'excitation electrique des nerfs traitée comme une polarization. *Journal de Physiologie et de Pathologie Generale*, 9:620–635, 1907.

[19] K. S. Cole. Dynamic electrical characteristics of the squid axon membrane. *Arch. Sci. Physiol.*, 3:253–258, 1949.

[20] C.M. Armstrong. Inactivation of the potassium conductance and related phenomena caused by quaternary ammonium ion injection in squid axons. *J. Gen. Physiol.*, 54(5):553–575, 1969.

[21] W. Nernst and J.O.W. Barratt. Über die elektrische nervenreizung durch. *Zeitschr Elektrochem.*, 10(35):664–668, 1904.

[22] F. Gabbiani and S. Cox. *Mathematics for Neuroscientists, 2nd Edition*. Elsevier, 2017.

[23] A. L. Hodgkin and A. F. Huxley. A quantitative description of membrane current and its application to conduction and excitation in nerve. *The Journal of Physiology*, 114(4):500–544, 1952.

[24] V.I. Krinskii and Y.M. Kokoz. Analysis of equations of excitable membranes-i. reduction of the hodgkin-huxley equations to a second-order system. *Biophysics*, 18(3):533–539, 1973.

[25] R.A. FitzHugh. Impulses and physiological states in theoretical models of nerve membrane. *Journal of Biophysics*, 1:445–466, 1961.

[26] J. Nagumo, S. Arimoto, and S. Yoshizawa. An active pulse transmission line simulating nerve axon. *Proc IRE*, 50(10):2061–2070, 1962.

[27] D. Purves, G. Augustine, D. Fitzpatrick, W. C. Hall, A. LaMantia, R. Mooney, and L. E. White. *Neuroscience*. Sinauer, EE. UU., 2018.

[28] W. Rall. Distinguishing theoretical synaptic potentials computed for different soma-dendritic distributions of synaptic input. *Journal of Neurophysiology*, 30(5):1138–1168, 1967.

[29] D. Serrat, B. Graham, A. Gillies, and D. Willshaw. *Principles of Computational Modelling in Neuroscience*. Cambridge University Press, Cambridge, 2011.

[30] L. O. Chua, C. A. Desoer, and E. S. Kuh. *Linear and Nonlinear Circuits*. McGraw-Hill, New York, USA, 1987.

[31] L. O. Chua. Resistance switching memories are memristors. *Applied Physics A*, 102(4):765–783, 2011.

[32] L. O. Chua. Memristor—the missing circuit element. *IEEE Transactions on Circuit Theory*, 18(5):507–519, 1971.

[33] D. Lin, R. Hui, and L. O. Chua. Gas discharge lamps are volatile memristors. *IEEE Transactions on Circuits and Systems*, 61(7):2066–2073, 2014.

[34] T.W. Hickmott. Low-frequency negative resistance in thin anodic oxide films. *Journal of Applied Physics*, 33(9):2669–2682, 1962.

[35] L. O. Chua. *If It's Pinched It's a Memristor*, pages 15–88. Springer International Publishing, Cham, 2019.

[36] A. Beck, J. G. Bednorz, Ch. Gerber, C. Rossel, and D. Widmer. Reproducible switching effect in thin oxide films for memory applications. *Applied Physics Letters*, 77(1):139–141, 07 2000.

[37] S. L. Johnson, A. Sundararajan, D.P. Hunley, and D.R. Strachan. Memristive switching of single-component metallic nanowires. *Nanotechnology*, 21(12):125204, mar 2010.

[38] R. Waser. Resistive non-volatile memory devices. 86(7–9):1925–1928, July 2009.

[39] A. Chanthbouala, V. Garcia, R. Cherifi, K. Bouzehouane, S. Fusil, X. Moya, S. Xavier, H. Yamada, C. Deranlot, N. D. Mathur, M. Bibes, and A. Barthélémy. A ferroelectric memristor. *Nature Materials*, 11:860–864, 2012.

[40] Ø. Martinsen, S. Grimnes, L. Carsten, and G. Johnsen. Memristance in human skin. *Journal of Physics: Conference Series*, 224:012071, 05 2010.

[41] G. K. Johnsen, C. A. Lütken, Ø. G. Martinsen, and S. Grimnes. Memristive model of electro-osmosis in skin. *Phys. Rev. E*, 83:031916, Mar 2011.

[42] E. Gale, R. Mayne, A. Adamatzky, and B. de Lacy Costello. Drop-coated titanium dioxide memristors. *Materials Chemistry and Physics*, 143(2):524–529, 2014.

[43] A. G. Volkov, C. Tucket, J. Reedus, M. I. Volkova, V. S. Markin, and L.O. Chua. Memristors in plants. *Plant Signaling & Behavior*, 9(3):e28152, 2014.

[44] L.O. Chua, V. Sbitnev, and H. Kim. Hodgkin–huxley axon is made of memristors. *International Journal of Bifurcation and Chaos*, 22(03):1230011, 2012.

[45] M. Lv, C. Wang, G. Ren, J. Ma, and X. Song. Model of electrical activity in a neuron under magnetic flow effect. *Nonlinear Dyn*, 85:1479–1490, 2016.

[46] L. Xu, G. Qi, and J. Ma. Modeling of memristor-based hindmarsh-rose neuron and its dynamical analyses using energy method. *J. Appl. Math. Model.*, 101:503–516, 2022.

[47] I. Carro-Pérez, C. Sánchez-López, and H.G. González-Hernández. Experimental verification of a memristive neural network. *Nonlinear Dyn*, 93:1823–1840, 2018.

[48] F. Corinto, A. Ascoli, V. Lanza, and M. Gilli. Memristor synaptic dynamics' influence on synchronous behavior of two hindmarsh-rose neurons. In *The 2011 Int. Joint Conference on Neural Networks (IJCNN)*, pages 2403–2408, 2011.

[49] C.K. Volos, I.M. Kyprianidis, and I.N. Stouboulos. The memristor as an electric synapse - synchronization phenomena. In *17th Int. Conf. on Digit. Signal Processing (DSP)*, pages 1–6, 2011.

[50] H. Bao, W. Liu, and A. Hu. Coexisting multiple firing patterns in two adjacent neurons coupled by memristive electromagnetic induction. *Nonlinear Dynamics*, 95:43–56, 2019.

[51] K. Ikeda and J. M. Bekkers. Autapses. *Current Biology*, 16(9):R308, 2006.

[52] H. Bao, A. Hu, W. Liu, and B. Bao. Hidden bursting firings and bifurcation mechanisms in memristive neuron model with threshold electromagnetic induction. *IEEE Transactions on Neural Networks and Learning Systems*, 31(2):502–511, 2020.

[53] K.M. Wouapi, B.H. Fotsin, F.P. Louodop, K.F. Feudjio, Z.T. Njitacke, and T.H. Djeudjo. Various firing activities and finite-time synchronization of an improved hindmarsh–rose neuron model under electric field effect. *Cogn Neurodyn*, 14:375–397, 2020.

[54] N. Zandi, S. Jafari, S. Hashemi Golpayegani, F. Nazarimehr, and M. Perc. Different synaptic connections evoke different firing patterns in neurons subject to an electromagnetic field. *Nonlinear Dynamics*, 100, April 2020.

[55] X. Cheng, X. Song, and R. Wang. Self-organization collective dynamics of heterogeneous neurons with memristive and plastic chemical synapses. *International Journal of Modern Physics B*, 36(3):2250030, 2022.

[56] X. Hu, B. Jiang, J. Chen, and C. Liu. Synchronization behavior in a memristive synapse-connected neuronal network. *European Physical Journal Plus*, 137(8):895, 2022.

[57] L. Euler. *Mechanica sive motus scientia analytice exposita*, volume 2. Ex Typographia Academiae Scientiarum, Petropoli, 1736.

[58] J. L. Lagrange. *Mécanique analytique*. Chez la Veuve Desaint, Paris, 1788.

[59] H. K. Khalil. *Nonlinear Systems*. Prentice Hall, Upper Saddle River, NJ, 3rd edition, 2002.

[60] A. S. Hornby. *Oxford Advanced Learner's Dictionary of Current English*. Oxford University Press, Oxford, 1974.

[61] S. Boccaletti. *The Synchronized Dynamics of Complex Systems*, volume 6 of *Monograph Series on Nonlinear Science and Complexity*. Elsevier, 2008.

[62] S. Boccaletti, J. Kurths, G. Osipov, D.L. Valladares, and C.S. Zhou. The synchronization of chaotic systems. *Physics Reports*, 366(1):1–101, 2002.

[63] N.F. Rulkov, M.M. Sushchik, L.S. Tsimring, and H. D. I. Abarbanel. Generalized synchronization of chaos in directionally coupled chaotic systems. *Physical Review E*, 51(2):980–994, 1995.

[64] O. I. Moskalenko, A. A. Koronovskii, A. E. Hramov, and Stefano Boccaletti. Generalized synchronization in mutually coupled oscillators and complex networks. *Physical Review E*, 86:036216, 2012.

[65] A. L. Hodgkin, A. F. Huxley, and B. Katz. Ionic currents underlying activity in the giant axon of the squid. *Arch. Sci. Physiol.*, 3:129–150, 1949.

[66] L. Lapique. Recherches quantitatives sur l'excitation electrique des nerfs traitee comme une polarization. *Journal de Physiologie et de Pathologie Generale*, 9:620–635, 1907.

[67] M. Sah, H. Kim, A. Eroglu, and L. O. Chua. Memristive model of the barnacle giant synapse. *International Journal of Bifurcation and Chaos*, 26(1):1630001, 2016.

[68] L. O. Chua, V. Sbitnev, and H. Kim. Hodgkin–huxley axon is made of memristors. *International Journal of Bifurcation and Chaos*, 22(3):1230011, 2012.

[69] J. Lü and G. Chen. A time-varying complex dynamical network model and its controlled synchronization criteria. *IEEE Transactions on Automatic Control*, 50(6):841–846, 2005.

[70] M. Itoh and L. O. Chua. Memristor oscillators. *International Journal of Bifurcation and Chaos*, 18(11):3183–3206, 2008.

[71] C. Sánchez-López, J. Mendoza-López, M.A. Carrasco-Aguilar, and C. Muñiz-Montero. A floating analog memristor emulator circuit. *IEEE Transactions on Circuits and Systems II: Express Briefs*, 61(5):309–313, 2014.

[72] G. Innocenti, A. Morelli, R. Genesio, and A. Torcini. Dynamical phases of the Hindmarsh–Rose neuronal model: Studies of the transition from bursting to spiking chaos. *Chaos: An Interdisciplinary Journal of Nonlinear Science*, 17(4):043128, 2007.

[73] M. I. Rabinovich, P. Varona, A. I. Selverston, and H. D. I. Abarbanel. Dynamical principles in neuroscience. *Reviews of Modern Physics*, 78:1213–1265, 2006.

[74] A. Wolf, J. B. Swift, H. L. Swinney, and J. A. Vastano. Determining lyapunov exponents from a time series. *Physica D: Nonlinear Phenomena*, 16(3):285–317, 1985.